



POLITECNICO DI MILANO
DEPARTMENT OF PHYSICS
PhD in Physics

**Photons quantum interference induced by
space-time curvature: a possible verification
method based on a space platform**

PhD Doctoral Thesis of:
Piergiovanni Magnani
Matricola 880144
C.P. 10096147

Supervisor: Prof. Paolo Villoresi (Università di Padova)
Tutor: Prof. Roberta Ramponi (Politecnico di Milano)
PhD coordinator: Prof. Marco Finazzi (Politecnico di Milano)

PHD CYCLE XXXII

2020

(Page Intentionally Left Blank)

Table of contents

ABSTRACT	1
1 INTRODUCTION.....	3
2 CURVED SPACETIME	5
2.1 Reference curved spacetime.....	5
2.2 Photon propagation frequency related effects in curved spacetime .	6
2.3 Some considerations on photon state superposition spontaneous collapse.....	8
3 EVALUATION OF CONFIGURATIONS	11
3.1 Oneway configuration	14
3.1.1 <i>Interferometric scheme</i>	<i>15</i>
3.1.2 <i>General considerations on classical Doppler compensation</i>	<i>21</i>
3.1.3 <i>Detail evaluation of the Doppler compensation approach proposed (based on interferometer length real-time control).....</i>	<i>23</i>
3.1.4 <i>Nominal expected performances on a test trajectory T2.....</i>	<i>34</i>
3.2 Twoways configuration S/C-GS-S/C.....	36
3.2.1 <i>General.....</i>	<i>36</i>
3.2.2 <i>Nominal expected performances on test trajectory T2.....</i>	<i>42</i>
3.3 Twoways configuration GS-S/C-GS.....	44
3.3.1 <i>General and expected performance on test trajectory T2</i>	<i>44</i>
3.3.2 <i>Previous utilization of Twoways GS-S/C-GS like configuration.....</i>	<i>48</i>
3.4 Selection of configuration.....	49
4 ONEWAY CONFIGURATION: ANALYSIS OF PERFORMANCE IN A REFERENCE EXPERIMENTAL SCHEME.....	51
4.1 Reference orbit (R1), reference GS and reference Interferometer length	51
4.2 Nominal performances under reference conditions	52
4.3 Sensitivity analysis	55
4.3.1 <i>Sensitivity to each of the parameters.....</i>	<i>55</i>
4.3.2 <i>Sensitivity to all parameters superimposed and tentative requirements</i>	<i>58</i>

5	TECHNOLOGY AND IMPLEMENTATION ISSUES.....	63
5.1	Spacecraft speed predictor	63
5.1.1	<i>Development needs</i>	69
5.2	Prism positioner for Doppler effects compensation.....	70
5.2.1	<i>General considerations</i>	70
5.2.2	<i>The 'Modulus $N \cdot \lambda$' compensation</i>	71
5.2.3	<i>Candidate nano-positioner</i>	73
5.2.4	<i>Development needs</i>	77
5.3	Interferometers calibration.....	77
5.3.1	<i>General considerations</i>	77
5.3.2	<i>Requirements on frequencies overall accuracy</i>	79
5.3.3	<i>Frequency Initial Matching</i>	81
5.3.4	<i>Cavity Frequency Drift: ultra-stable optical cavities and temperature stability</i>	82
5.3.5	<i>Frequency stabilization and first and second order PDH compensation</i>	87
5.3.6	<i>Development needs</i>	90
5.4	Fibre optic thermal stability and attenuation.....	91
5.4.1	<i>Development needs</i>	93
5.5	Single Photon Detectors	94
5.5.1	<i>Development needs</i>	95
5.6	Some issues on Corner Cube Retro-Reflectors	95
5.6.1	<i>Development needs</i>	95
6	OVERAL EXPECTED PERFORMANCES	97
6.1	Model updating based on photon counting.....	97
6.1.1	<i>Photon pulses repetition rate</i>	98
6.1.2	<i>Attenuations</i>	98
6.1.3	<i>Single Photon detectors (features and gating)</i>	101
6.2	Revised reference requirements.....	103
6.3	Expected performance in selected orbital cases	103
6.3.1	<i>Simulated cases</i>	103
6.3.2	<i>Simulation results</i>	106
6.3.3	<i>Considerations on obtained results</i>	111
7	SUMMARY AND CONCLUSIONS	115
8	ANNEXES.....	119
8.1	Annex-A: Estimation of frequency perturbations caused by light trajectory bending.....	119
8.2	Annex-B: Coordinate speeds vs. physical speeds: effects on frequency perturbations	122
9	REFERENCES.....	123
10	LIST OF ACRONYMS	127

ABSTRACT

The main subject of this PhD research has been to discuss the effects played by gravity on single photon interference in cases where photon propagation is over long distances (thousands or tens of thousands kilometres) with large variation of General Relativistic (GR) metric. Indeed space-time metric theoretically affects phase coherence of photons wave packets propagating in quantum superposition along trajectories at different gravitational potential; measurable interferometric effects should therefore arise with fringes and visibility characteristics depending on the specific experimental conditions.

A possible experimental configuration involving Ground based elements and Space based elements, which potentially allows for this type of experimentation, has been identified in which photon states superposition and recombination are obtained using beam splitters appropriately arranged in two Mach-Zender like interferometers (one at Ground Station and one on-board a Spacecraft).

Interferometric effects resulted strongly related to frequency variations induced by the experimental conditions and space-time curvature. Specifically frequency variation caused by the so-called 'gravitational red-shift (GR time dilation)' and 'photon trajectory bending' can be derived in curved space time by considering the assumed metric tensor. It is however noted that this effect could also be explained in a semi-classical approach; for photons this imply assuming a 'gravitational mass' equal to the photon energy divided by the square of the speed of light. As far as 'time dilation' effects, involved by Special Relativistic like signature (pseudo Euclidean), they cannot be explained semi-classically and the metric embedded in the fundamental tensor is definitely necessary.

Frequency variations caused by classical 'observer-source relative motion' generates very large frequency Doppler effects and wave packets phase variations which mask and 'confuse' the relativistic effects: *the classical Doppler effect has to be removed to a high degree of precision* in order to get the ones related to metric only.

It is evidenced that the first measurements related to gravity induced quantum interference has been performed by Colella-Overhauser-Werner (COW) in 1975 utilizing a Neutron Interferometer implementing quantum superposition along separate trajectories in a laboratory set-up; indeed it was a phase shift measurement on matter-waves. The experiment has been subsequently repeated always utilizing Neutrons.

As stated above, in this Research Thesis has been studied the detection of gravity induced quantum interference directly employing photons in schematics utilizing both ground elements and space platform: this approach is sometimes named 'optical COW' and has already been suggested by other researchers.

The single photon conditions at the detecting interferometer are approximated, in the considered cases, by means of laser short pulses duly attenuated along the optical link (crossing the atmosphere and propagating over a long free-space distance).

The simulated single photon counting at two detectors placed on the on-board interferometer allows then to extract the photon arrival probabilities (at the detectors) and the de-phasing associated to the space-time metric effects.

The Spacecraft orbits considered in the analysis are in general compatible with the ones achievable with small class launchers and small mass satellites payload.

During the research the following main areas have been specifically investigated:

- frequency related effects for photon propagating in General Relativistic space-time (assuming Schwarzschild metric) between a source and a target;
- photon states superposition realization and recombination and interference effects for the indistinguishable superposed states;
- evaluation of experiment configurations and selection of the most performing one;
- selection of a candidate 'classical Doppler' compensation scheme;
- evaluation (by simulation) of the expected experiment performance for the selected configuration in terms of interferometric effects and de-phasing (on the superposed indistinguishable photon states) caused by space-time metric effects only;
- sensitivity analysis as support to technological needs and evaluation of some key technology areas (e.g., calibration of interferometers, speed projector, positioner for Doppler compensation, Single Photon Detectors).

1 INTRODUCTION

Space-time curvature theoretically affects the phase coherence of photons wave packets propagating in quantum superposition along trajectories at different gravitational potential. Measurable interferometric effects should therefore arise with fringes and visibility characteristics depending on the specific experimental conditions. *Gravitational 'red-shift'* and *'time dilation'* as well as *observer-source 'relative motion'* all contribute, to a different degree, to phase shift accumulation and interference visibility ('which-way' information) building-up shaping the measured interferograms.

The first measurements of gravity induced quantum interference has been performed by Colella-Overhauser-Werner (COW) in 1975 utilizing a Neutron Interferometer implementing quantum superposition along separate trajectories. The trajectories could be repositioned in the lab, at different heights, in order to scan different levels of relative gravity; indeed it was a phase shift measurement on Neutron De Broglie waves. The experiment has been subsequently repeated several times during the years, always utilizing Neutrons, achieving progressively better agreement with the theory. A schematics of the initial COW apparatus and of achieved interferogram is shown in Figure 1-1 (pictures taken from Ref.[1] and Ref.[2]).

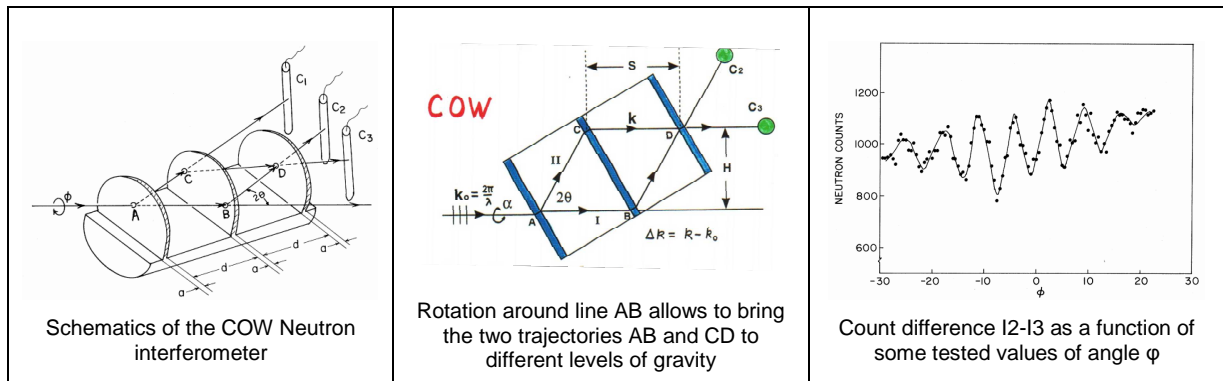


Figure 1-1 Schematics of COW experiment and example of achieved interferogram (Ref.[1] and Ref.[2])

This type of experiment, when performed in laboratory, poses constraints on the maximum achievable difference of gravity together with side effects due to structure residual nano-deformations (bending) arising during repositioning which need be duly taken into account in data interpretation.

An alternative approach in the detection of gravity induced quantum interference would be, as proposed in Ref.[3] to directly employ photons and utilize a ground station and a space platform as schematized in Figure 1-2 (picture derived from Ref.[3]); this type of configuration is named optical COW. This scheme foresees the use of two separate Mach Zender Interferometers and the photon states arrival time profile (at detectors) will be of the 'multi peaks time tagged type'. In practice the gravity separation between the two interferometers would be obtained and scanned by the movement of the spacecraft itself. The ground interferometer being always at the same gravity level while the second interferometer being carried around by the Satellite movement and not any more by a physical rotation of the instrument as in the original COW experiment. Much larger gravitational variations (indeed metric variations) can be achieved w.r.t. the ones achievable in laboratory.

The measured interferometric behaviour would therefore depend not only on the phase variations caused by the metric effects at the two interferometers but also on phase modulations caused by the relative speed between the Spacecraft (S/C) and the Ground Station (GS). These 'relative motion type disturbances', absent in the laboratory based

experiments, are in general very large and therefore precise extraction of the metric related effects from an overall interferogram would need careful attention.

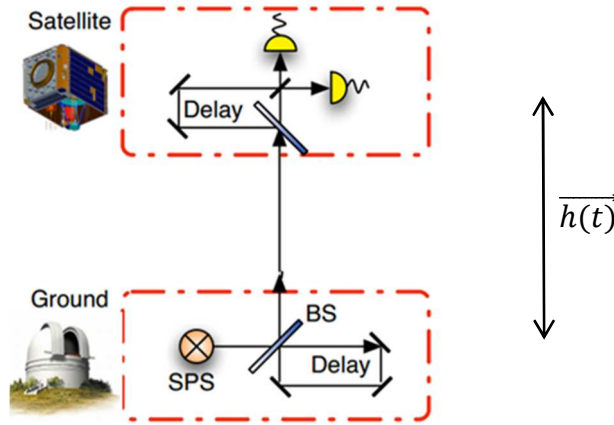


Figure 1-2 General schematics of ‘optical COW experiment’ making use of a Ground Station and a Space Platform (picture derived from Ref.[3])

In general ‘the photon’ launched from the ground interferometer to the space based one is in a superposition of two time separated states. As far as presently hypotised, the superposition is expected to be maintained across the space distance separating the ground station to the spacecraft; if this were not true for any reason then interferogram shapes would modify and depart from the expected ones.

This experimentation is complex since it involves the availability and utilization of ground and space elements. In this respect advantages could be taken from the ongoing ASI (Italian Space Agency) development program activity on small satellites and on the availability of the Matera Laser Ranging facility run by ASI/Telespazio already used for some quantum interference experiments (see Ref. [5]).

The main interest of this PhD research is to study/discuss the relation between single photon quantum interference and space-time curvature over distances where GR metric tensor variations become relevant; in particular the main foreseen activities are related to the assessment of the configuration and expected performances of an ‘optical COW’ like experiment and specifically the evaluation of:

- frequency related effects for photon propagating in General Relativistic space-time (assuming Schwarzschild metric) between a source and a target;
- photon states superposition realization and recombination and interference effects for the indistinguishable superposed states;
- evaluation of experiment configurations and selection of the most performing one;
- selection of a candidate ‘classical Doppler’ compensation scheme;
- evaluation (by simulation) of the expected experiment performance for the selected configuration in terms of interferometric effects and de-phasing (on the superposed indistinguishable photon states) caused by space-time metric effects only;
- sensitivity analysis as support to technological needs and evaluation of some key technology areas (e.g., calibration of interferometers, speed projector, positioner for Doppler compensation, Single Photon Detectors).

As far as known, single photon quantum interference experiment, with interference caused and modulated by metric effects only, has not yet been performed in space over the large distances and time separation here considered.

2 CURVED SPACETIME

2.1 Reference curved spacetime

The curved space-time considered in this analysis is based on Schwarzschild metric which present a differential 'line' element in the exterior of a spherical Earth of the following form (see e.g. Ref. [6]):

$$ds^2 = (1 - \xi) \cdot (cdt)^2 - \frac{1}{(1-\xi)} (dr)^2 - r^2 (d\vartheta)^2 - r \cdot \cos\vartheta (d\varphi)^2 \quad (2.1)$$

$$\xi(r) = \frac{2GM}{c^2 r} = \text{Dimensionless quantity}$$

$$G = \text{Gravitational constant} \sim 6.67408 \cdot 10^{-11} \frac{m^3}{kg \ s^2}$$

$$M = \text{Earth mass} \sim 5.97219 \cdot 10^{24} \text{ kg}$$

$$c = \text{Speed of light in vacuum} \text{ m/s}$$

The coordinates $ct, r, \vartheta, \varphi$ represents Schwarzschild coordinates (Earth centered and non rotating) and defined as:

$ct \rightarrow$ time evaluated by a distant observer

$r \rightarrow$ radius defined as circumference value divided by 2π

$\vartheta \rightarrow$ colatitude

$\varphi \rightarrow$ longitude

The differential 'line' element, written as above, can be of three types:

$ds > 0 \rightarrow$ time-like separated events (events accessible by moving physical particles)

$ds = 0 \rightarrow$ null separated events (photons free trajectory)

$ds < 0 \rightarrow$ space-like separated events (there exist a local frame transformation judging the event as simultaneous-belonging to a 'present')

In this space-time the fundamental metric tensor takes, with the signature $+- --$ considered, the following form (see e.g. Ref. [6] and Ref. [7]):

$$g_{\alpha\beta} = \begin{bmatrix} (1-\xi) & 0 & 0 & 0 \\ 0 & -\frac{1}{(1-\xi)} & 0 & 0 \\ 0 & 0 & -r^2 & 0 \\ 0 & 0 & 0 & -r^2 \sin^2\vartheta \end{bmatrix} \quad (2.2)$$

The photon trajectory is described by a null geodesics which utilizes the definition of the Christoffel symbols and taking the following form (where the general tensor calculus conventions and rulings are assumed as per the references):

$$\left\{ \begin{array}{l} \frac{d^2 x^\mu}{d\lambda^2} + \left\{ \begin{array}{c} \mu \\ \alpha \beta \end{array} \right\} \frac{dx^\alpha}{d\lambda} \frac{dx^\beta}{d\lambda} = 0 \\ g_{\alpha\beta} \frac{dx^\alpha}{d\lambda} \frac{dx^\beta}{d\lambda} = 0 \\ \lambda = \text{Parameter} \\ \left\{ \begin{array}{c} \mu \\ \alpha \beta \end{array} \right\} = \frac{1}{2} (g_{\alpha\beta,\gamma} + g_{\gamma\beta,\alpha} - g_{\alpha\gamma,\beta}) g^{\mu\gamma} = \text{Christoffel symbols of second kind} \end{array} \right. \quad (2.3)$$

In case of events, differentially spaced, occurring at the same r ($dr=0$), the differential line form can be written as:

$$ds^2 = (1 - \xi) \cdot (cdt)^2 - r^2(d\vartheta)^2 - r \cdot \cos\vartheta(d\varphi)^2 = (1 - \xi) \cdot (cdt)^2 - (dl)^2 \quad (2.4)$$

in this case the quantity:

$$\frac{dl}{dt} = c \sqrt{1 - \xi} = V$$

can be interpreted as the 'local speed of light' when evaluated by a 'distant observer'.

2.2 Photon propagation frequency related effects in curved spacetime

A photon propagating in a curved space-time (typically over long distances) is measured by different observers to be at different frequencies primarily due to:

- velocities of the observers causing primary **classical like Doppler effects**
- **GR red/blue-shift type effects** caused by General Relativistic time dilation (mainly time-time metric coefficient depending on gravitational potentials)
- Time dilation associated to **Relativistic signature** of the fundamental tensor
- **'bending' of photon trajectory** (null geodesic of the General Relativistic curved of space-time)

For a generic Source and a generic Observer in orbit, the schematics shown in Figure 2-1 can be considered.

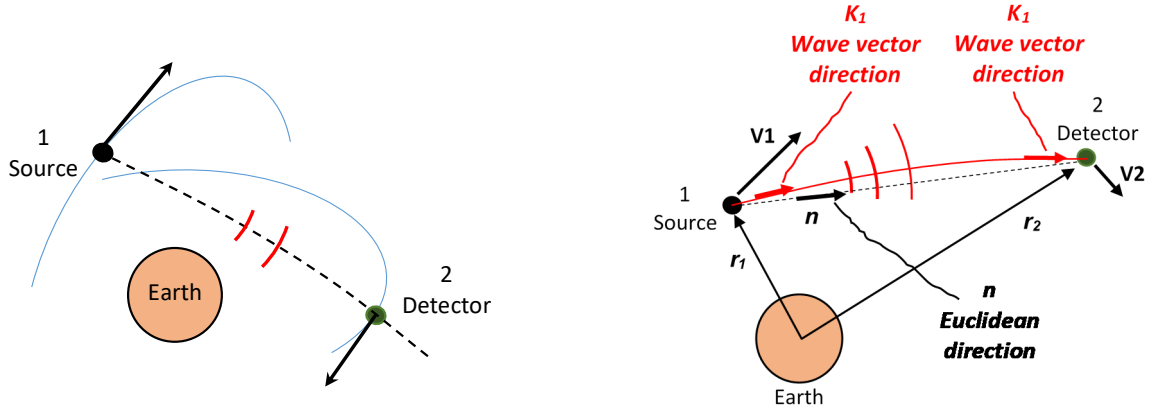


Figure 2-1 Schematics for a generic Source and generic Detector in orbit

The relation between the transmitted frequency as judged by the Source observer and the received frequency as judged by the Detector observer has the following structure (see e.g. Ref.[8] as far as the topic related to frequencies relation and Ref.[9]):

$$\omega_2 = \omega_1 \frac{\sqrt{\left(1 - \frac{2MG}{c^2 r_1}\right) - \frac{1}{\left(1 - \frac{2MG}{c^2 r_1}\right)} \left(\frac{V_{1r}}{c}\right)^2 - \left(\frac{V_{1\vartheta}}{c}\right)^2 - \left(\frac{V_{1\varphi}}{c}\right)^2}}{\sqrt{\left(1 - \frac{2MG}{c^2 r_2}\right) - \frac{1}{\left(1 - \frac{2MG}{c^2 r_2}\right)} \left(\frac{V_{2r}}{c}\right)^2 - \left(\frac{V_{2\vartheta}}{c}\right)^2 - \left(\frac{V_{2\varphi}}{c}\right)^2}} \cdot \frac{1 - \frac{V_2 \cdot \mathbf{k}_2}{c}}{1 - \frac{V_1 \cdot \mathbf{k}_1}{c}} \quad (2.5)$$

where V_r , V_ϑ , V_φ are here coordinate speeds ($V_r = dr/dt$, $V_\vartheta = r \cdot d\vartheta/dt$, $V_\varphi = r \cdot \sin\vartheta \cdot d\varphi/dt$).

The vectors \mathbf{k} and \mathbf{n} are slightly different and so it is convenient to re-write above expression in the following way where the source of frequency variations are evidenced:

$$\omega_2 = \omega_1 \frac{\sqrt{\left(1 - \frac{2MG_1}{c^2 r_1}\right) - \frac{1}{\left(1 - \frac{2MG}{c^2 r_1}\right)} \left(\frac{V_{r1}}{c}\right)^2 - \left(\frac{V_{\vartheta1}}{c}\right)^2 - \left(\frac{V_{\varphi1}}{c}\right)^2}}{\sqrt{\left(1 - \frac{2MG}{c^2 r_2}\right) - \frac{1}{\left(1 - \frac{2MG}{c^2 r_2}\right)} \left(\frac{V_{r2}}{c}\right)^2 - \left(\frac{V_{\vartheta2}}{c}\right)^2 - \left(\frac{V_{\varphi2}}{c}\right)^2}} \cdot \frac{1 + \frac{V_2 \cdot \mathbf{n}}{c} + \frac{V_2 \cdot (\mathbf{k}_2 - \mathbf{n})}{c}}{1 - \frac{V_1 \cdot \mathbf{n}}{c} - \frac{V_1 \cdot (\mathbf{k}_1 - \mathbf{n})}{c}} \quad (2.6)$$

GR red/blue-shift type effect (still observers) Metric related signature GR-SR

Classical like Doppler effect 'Bending' of photon trajectory

The different causes affect the photon frequency during propagation to various degrees depending on the overall experiment characteristics and the time evolution of the system. The rough orders of magnitude of the different effects are hereafter given with reference to specific conditions.

Classical like Doppler effect

Its order of magnitude is proportional to the source-detector relative speed and for experiments based on LEO (Low Earth Orbit) or MEO (Medium Earth Orbit) spacecrafts and a Ground Station this relative speed is limited and will be more than e.g. 6000 m/s leading to a maximum frequency perturbation contribution in the order of:

$$\left| \frac{\delta\omega}{\omega} \right| \approx \left| \frac{V_{//}}{c} \right| \approx 2 \cdot 10^{-5}$$

GR red/blue-shift type effects

The order of magnitude for this effect depend on the distance of the Source and Detector from the Earth centre. For experiment based on MEO spacecrafts and a Ground Station the maximum frequency perturbation contribution is in the order of:

$$\left| \frac{\delta\omega}{\omega} \right| \approx \left| \frac{MG}{c^2} \left(-\frac{1}{r_1} + \frac{1}{r_2} \right) \right| \approx 6 \cdot 10^{-10}$$

with $r_1 \sim 6500$ km and r_2 very high (e.g. ~ 40000 km)

Time dilation associated to Relativistic signature (SR-GR)

Its order of magnitude depend on the source and detector absolute speeds. For experiments based on LEO (Low Earth Orbit) platform and a Ground Station the maximum speed of the spacecraft can be around 7800 m/s; the maximum frequency perturbation contribution would be in the order of:

$$\left| \frac{\delta\omega}{\omega} \right| \approx \left| \frac{1}{2} \cdot \frac{V_{//}^2}{c^2} \right| \approx 4 \cdot 10^{-10}$$

'Bending' of photon trajectory

This effect is more complex to be estimated than the previous three and in annex-A is reported an example of estimation based on the photon null geodesic trajectory in accordance to Ref.[10]. In general the bending related effects are higher for low observation elevations w.r.t. the local horizon (maximum at 0° null at 90° elevations) and increases as the S/C – GS separation becomes larger. With reference to annex-A, an estimate of such frequency perturbation for a spacecraft placed in a MEO orbit is in the order of:

$$\left| \frac{\delta\omega}{\omega} \right| \approx \left| \frac{-V_{\perp}}{c} \right| |k_2 \times n| \longrightarrow \begin{cases} \approx 10^{-15} & \text{for } ELV = 30^\circ \\ \approx 10^{-16} & \text{for } ELV = 60^\circ \\ \approx 0 & \text{for } ELV \rightarrow 90^\circ \end{cases}$$

2.3 Some considerations on photon state superposition spontaneous collapse

One of condition to be able to observe single photon quantum interference in experiments involving 'large' space/time separation between sources and detectors is that the photon travelling such distance remain in superposition of states without incurring in states (spontaneous) collapse along its travel. Consider for example the scheme reported in Figure 2-2 constituted by a MZI interferometer (Mach Zender Interferometer).

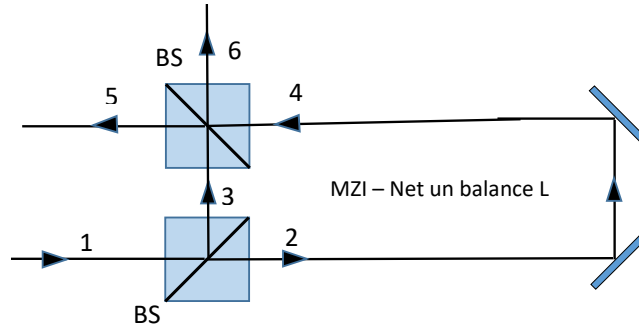


Figure 2-2 General scheme for creating photon state superposition

A (one) photon entering the MZI in space mode 1, will be placed in a superposition of states along space modes 5 and 6 according to (see also para. 3.1.1 for a brief note on used formalism):

$$\begin{aligned}
 |\psi_{in}\rangle &= |1\rangle \Rightarrow \frac{1}{\sqrt{2}} (|2\rangle + i|3\rangle) \Rightarrow \frac{1}{\sqrt{2}} (e^{i\Phi}|4\rangle + i|3\rangle) \Rightarrow \\
 &\Rightarrow \frac{1}{\sqrt{2}} (e^{i\Phi} \frac{1}{\sqrt{2}} (|5\rangle + i|6\rangle) + i \frac{1}{\sqrt{2}} (|6\rangle + i|5\rangle)) \Rightarrow \frac{1}{2} (e^{i\Phi} - 1)|5\rangle + i \frac{1}{2} (e^{i\Phi} + 1)|6\rangle
 \end{aligned}
 \tag{2.7}$$

where:

- the general term $e^{i\alpha}$ is here intended as a 'phase/time tag' symbol
- Φ = Total phase 'delay' accumulated in MZI = $L \cdot \frac{2\pi}{\lambda} = L \cdot k$
- $k = \frac{2\pi}{\lambda} = \text{Wave number}$

If the unbalance L of the interferometer is sufficiently large ($L \gg$ photon coherence length, as discussed in the initial part of paragraph 3) the photon (the system) will end up in four distinguishable states: two of them along space mode 5 and two of them along space mode 6.

Considering for example space mode 6, assumed as the output of the interferometer, the question is if the time distinguishable states $\frac{1}{2}e^{i\Phi}|6\rangle$ and $+\frac{1}{2}|6\rangle$ remains persistent or after some distance or permanence time can undergo states superposition modifications. These may in principle result from the interaction between system superposed states and an environment (thermal bath) leading to what is sometimes called in on going researches 'spontaneous' collapse (see for example Ref.[11] and Ref.[12] and hereafter discussion). At global product level (system and environment) the overall state still evolve unitary but seen at lower system level only, the evolution may not be any more unitary indicating irreversibility.

In the experimental conditions here considered the environment would be constituted by the gravitational field that from a GR point of view is, externally to the planetary body, a four dimensional curved continuum and in such conditions is not easy to find reasons for spontaneous collapse.

On the other hand the gravitational field may result being quantized and states products between the quantum systems and the environment quantized field would follow. This is exploited in spontaneous collapse researches to describe the 'non quantum behaviour' of macroscopic bodies (ensembles of an enormous amount of microscopic quantum systems). According to Ref.[11] and Ref.[12] the time required for a single quantum *particle* to enter state collapse depends on the mass and size of the particle as compared to the size characteristics of the quantized environment (e.g. correlation length of the environment noise bath, quantum imprecision of spacetime,...).

Utilizing formulas 200 and 201 of Ref.[12] which relate to a single quantum particle and assimilating (may be erroneously) a photon to a quantum particle of mass $m=h\nu/c^2$ the probable order of magnitude for time for collapse can be estimated in:

$$\tau_c = \frac{\bar{h}^3}{m^5 \cdot G^2}$$

$$m = \frac{h \cdot \nu}{c^2} \quad \longrightarrow \quad \tau_c \approx 10^{62} \text{ s} !!!$$

$$h = \bar{h} \cdot 2\pi = 6.62607004 \cdot 10^{-34} \text{ m}^2 \text{ kg/s} \quad \text{Planck constant}$$

basically no single specific photon spontaneous collapse are ever expected to be observed (especially in the timespan of the possible LEO/MEO experiments which is at most in the rough order of < 0.1 - 0.2 seconds for a Ground Station to Spacecraft link, or even solar system size experiment).

The studied experiment is therefore expected to measure the presence of states interference over the foreseen distances.

3 EVALUATION OF CONFIGURATIONS

In this chapter three configurations are evaluated from a nominal point of view in order to assess their relative performance level in terms of capability to *detect and quantify single photon interference*. Before introducing the configurations, some clarifications are given:

- the assessment of single photon interference is implemented by physically counting each single photon arriving at counting detectors;
- the counting scheme and the counted photons will be as such to be able to reconstruct the (measured) arrival probabilities and de-phasing between the indistinguishable interfering states at detectors;
- the reconstructed (measured) arrival probabilities and reconstructed de-phasing can then be compared with the theoretically foreseen ones to verify the *existence of interference* and its *matching or deviations from expectations*.

The design of the experiment shall therefore assure that the interferences observed are occurring at single photon level.

Three configurations will be presented and discussed and all of them makes use of one S/C (Spacecraft) and one GS (Ground Station):

- Oneway
- Twoways S/C-GS-S/C
- Twoways GS-S/C-GS

The experiment consider the launching of photons from either the GS or the S/C as regularly spaced short laser pulses (each pulse of a given optical energy with associated an expected average number of photons $\bar{N}_{emitted}$). During the long trip, a very large attenuation will occur and, by design, upon arrival the average number of photons characterizing the received pulse, $\bar{N}_{received}$, will be expected much less than the transmitted. Assuming the pulses be characterized by a Poissonian photon number N distribution, the following is expected at pulse reception:

$$\left\{ \begin{array}{l} \bar{N}_{received} = T \cdot \bar{N}_{emitted} \\ T = \text{Overall link transmissibility (in number of photons or energy)} \\ P(N) = \frac{(\bar{N}_{received})^N}{N!} e^{-\bar{N}_{received}} \quad \text{for } N=0, 1, 2, 3, \dots \end{array} \right. \quad (3.1)$$

If the conditions $\bar{N}_{received} \ll 1$ (for example 0.01) is realized, then the following happen:

- the majority of the pulses will carry no photons;
- with a small probability *one* photon only is present;
- with a much smaller probability *two* photons only are present;
- etc.

Therefore the nominal ‘single photon’ conditions are *approximated via a very large attenuation of the emitted laser pulses*. When these conditions are achieved if something is observed it is, with large probability, at ‘single photon level’. The ‘*single photon*’ so generated is characterized by a coherence time related to the time length of the generating short laser pulse. In general

the field time profile, for ultra-short pulses (e.g. some tens of femtoseconds), is of the form shown in Figure 3-1 (e.g. Ref.[13] and Ref.[5]).

For laser pulses of some tens of picoseconds width (utilized in this analysis), the field profile is more uniform and could resemble as schematically shown in Figure 3-2 (pulse duration not to scale). In these cases the coherence time has been considered to be the pulse time width.

The **Oneway configuration** is sketched in Figure 3-3 and utilizes two interferometers, one on board the S/C one on ground at the GS. The photon is launched from ground in state superposition and detected on board the S/C.

The **Twoways S/C-GS-S/C configuration** is sketched in Figure 3-4 and utilizes one interferometer on board the S/C; at the GS is implemented the reflection. Therefore a double trip is present: from S/C to GS and back to S/C. The photon is launched from the S/C in state superposition and detected again on board the S/C upon return.

The **Twoways GS-S/C-GS configuration** is sketched in Figure 3-5 and utilizes one interferometer at the GS; the S/C implements the reflection. Therefore a double trip is present: from GS to S/C and back to GS. The photon is launched from GS in state superposition and detected again at the GS upon return.

The three configurations will be compared in terms on nominal performance with the spacecraft assumed in an 'evaluation trajectory'.

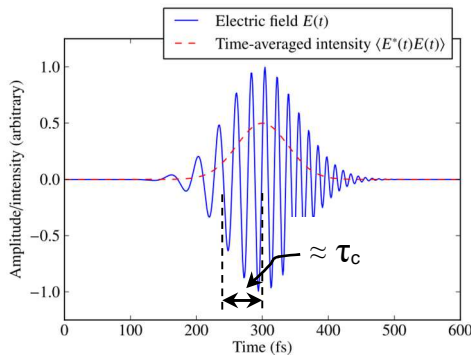


Figure 3-1 General schematics of an ultra-short pulse
(<https://commons.wikimedia.org/wiki>)

$$\left\{ \begin{array}{l} \psi(t) \sim \frac{1}{(2\pi\tau_c^2)^{\frac{1}{4}}} \cdot e^{-\frac{t^2}{4\tau_c^2}} \cdot e^{i\omega t} \\ \tau_c = \text{Coherence time} \sim \tau_{FWHM} \\ l_c = \text{Coherence length} \sim \tau_c \cdot c \end{array} \right. \quad (3.2)$$

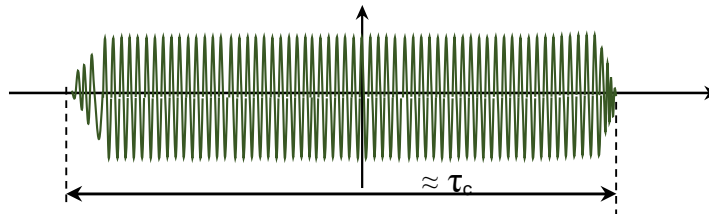


Figure 3-2 Field profile in a short laser pulse (schematics only-pulse duration not to scale)

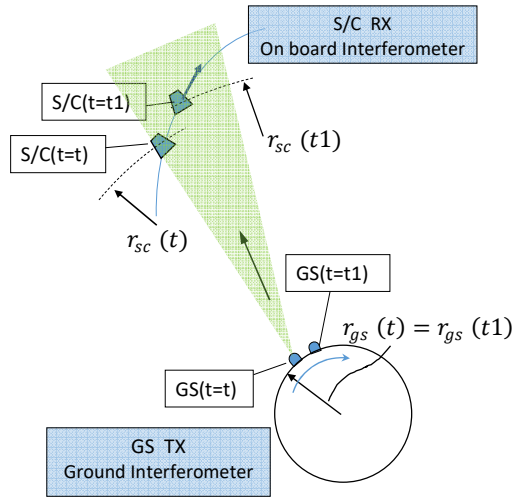


Figure 3-3 Schematics of the Oneway configuration

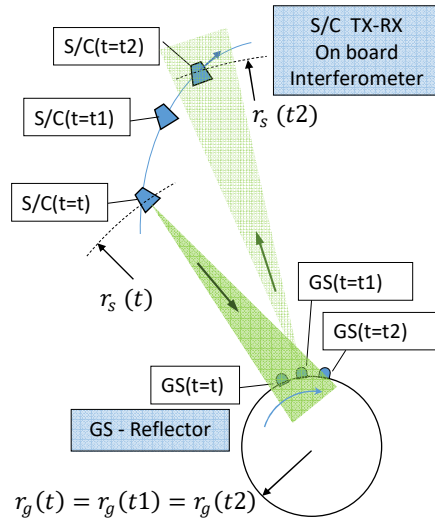


Figure 3-4 Schematics of the Twoways S/C-GS-S/C configuration

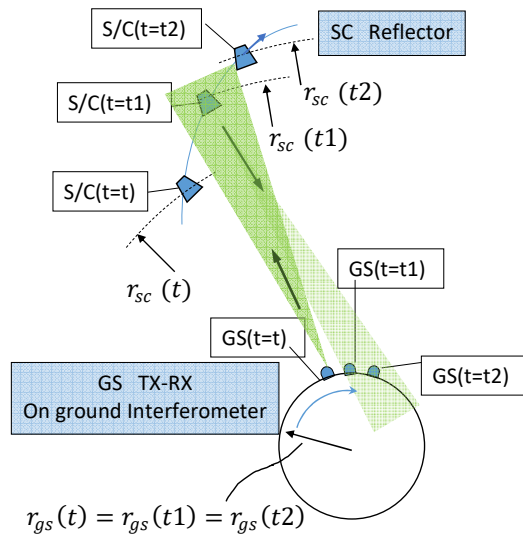


Figure 3-5 Schematics of the Twoways GS-S/C-GS configuration

3.1 Oneway configuration

The configuration schematics showing indicatively the light trajectories is given in Figure 3-6. In this schematics \vec{f} indicates the unitary 'Euclidean' vector joining the GS (at the generic time t of photon transmission) to the S/C (at the corresponding time $t1$ of photon reception) while \vec{k}_{GS} and \vec{k}_{SC} indicate the wave vector directions at the moment of transmission and the moment of reception of the 'curved' light trajectory. In this scheme a generic photon emitted by the GS at time t , reaches the S/S at time $t1$ (all this without counting the delays on the interferometer lines).

The One way configuration exploits an excellent gravitational separation between the ground and on board interferometers such that the frequency perturbation induce by the light bending (and consequently the effect on de-phasing) can be absolutely neglected w.r.t. the metric related effects (about five orders of magnitude smaller).

The schematics for light propagation is therefore assumed as shown in Figure 3-7 where 'Euclidean' trajectories are considered.

The relation between the transmitted photon frequency $\omega_{GSTX}(t)$ and the received frequency $\omega_{SCRX}(t1)$ is given by the following equation:

$$\omega_{SCRX}(t1) \cong \frac{\left[\left(1 - \frac{2GM}{c^2 r_g(t)} \right) - \beta_{\phi,g}^2(t) \right]^{\frac{1}{2}}}{\left[\left(1 - \frac{2GM}{c^2 r_s(t1)} \right) - \left(1 - \frac{2GM}{c^2 r_s(t1)} \right)^{-1} \beta_{r,s}^2(t1) - \beta_{\theta,s}^2(t1) - \beta_{\phi,s}^2(t1) \right]} * \left[\frac{1 - \frac{V_{SC//f}(t1)}{c}}{1 - \frac{V_{GS//f}(t)}{c}} \right] * \omega_{GSTX}(t) \quad (3.3)$$

where $\vec{V}_{SC} \cdot \vec{f} = V_{SC//f}(t1)$ and $\vec{V}_{GS} \cdot \vec{f} = V_{GS//f}(t)$ and the other symbols have already been defined.

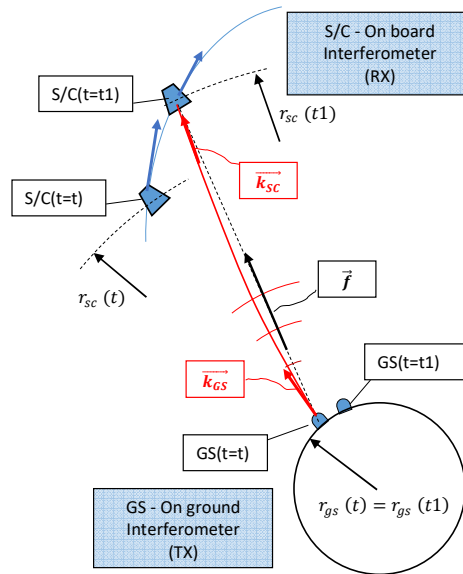


Figure 3-6 Oneway configuration with schematics of curved light beams (not to scale)

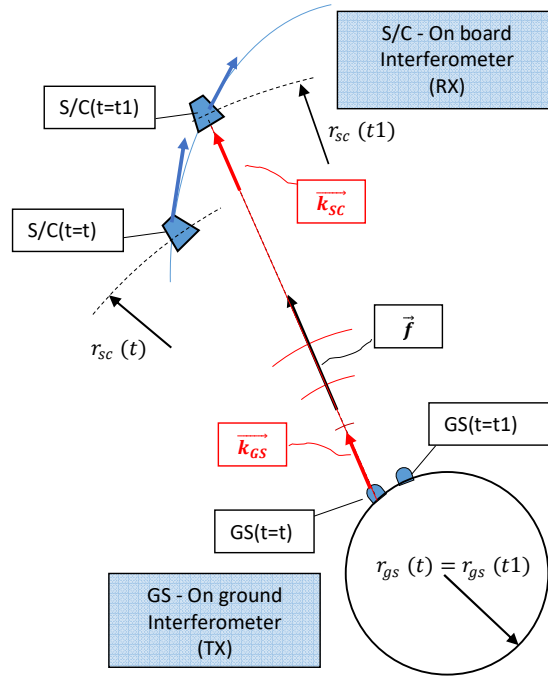


Figure 3-7 Oneway configuration with schematics of straight light beams (not to scale)

As previously pointed out the speeds $\beta_r = V_r/c$, $\beta_g = V_g/c$, $\beta_\phi = V_\phi/c$ are coordinate speeds (speeds referred to the Schwarzschild coordinates) which differ from the physical speeds as judged by a local observer. The use of physical speeds (available from local measurements) instead of coordinate speeds introduce therefore some uncertainty in the evaluation of frequency perturbation. This uncertainty depends also on the value of speed measured; an estimate for this uncertainty (see annex-B) results in the order of:

$$\left| \frac{\delta\omega}{\omega} \right| \approx 10^{-15}$$

and therefore fully negligible in this case.

3.1.1 Interferometric scheme

The general interferometric scheme for the Oneway configuration is shown in Figure 3-8 and, based on this scheme, the overall number of distinguishable spatial modes are taken to be 12 (the optical tracks which can be occupied). In this paragraph the computation of the probabilities of finding the photon at detector marked as 11 and at detector marked as 12 is explicated.

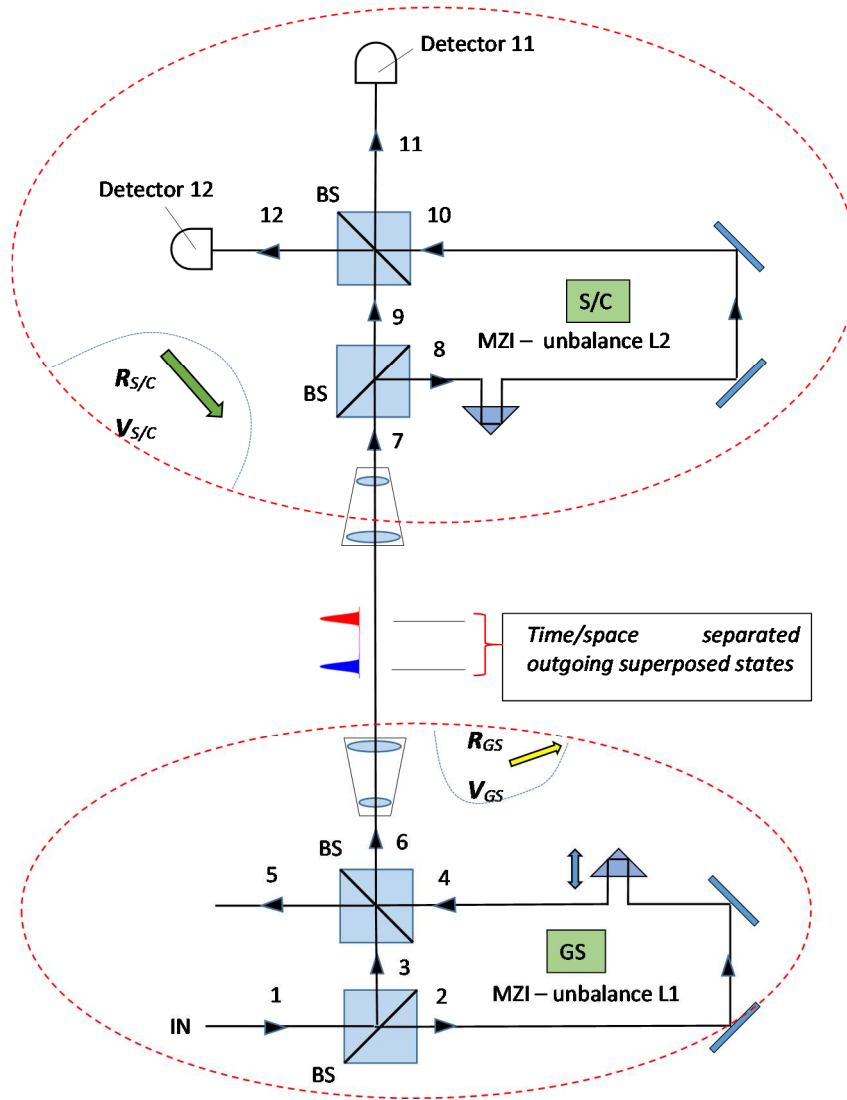


Figure 3-8 General interferometric scheme for the Oneway configuration

Some notes on used computation formalism

The computation makes use of ket symbolism and describe the photon state as superposition of up to 12 (distinguishable) spatial modes where each spatial mode can appear more times with *appropriate phase/time tagging*:

$$\begin{cases}
 |\psi\rangle = \sum_{m=1}^{m=12} \gamma_m \cdot |m\rangle & (3.4) \\
 |\psi\rangle = \text{Photon state} \\
 |i\rangle = \text{Spatial mode} \\
 \langle i|j\rangle = \delta_j^i & \text{with } (i, j = 1, \dots, 12) \\
 \gamma_m = \text{Complex coefficient} = \gamma_{m1} + \gamma_{m2} + \gamma_{m3} + \dots & \text{with } (m = 1, \dots, 12)
 \end{cases}$$

Furthermore the probability to find the photon in spatial mode $|m\rangle$ is computed depending on whether states $\gamma_{m1}|m\rangle, \gamma_{m2}|m\rangle, \gamma_{m3}|m\rangle, \dots$ are indistinguishable or distinguishable (see e.g. Ref.[14] and Ref.[15]; for example (limiting to two states):

$$P_m = |\gamma_{m1} + \gamma_{m2}|^2 \quad \text{if} \quad \gamma_{m1}|m\rangle \text{ and } \gamma_{m2}|m\rangle \text{ are indistinguishable} \quad (3.5)$$

$$P_m = |\gamma_{m1}|^2 + |\gamma_{m2}|^2 \quad \text{if} \quad \gamma_{m1}|m\rangle \text{ and } \gamma_{m2}|m\rangle \text{ are distinguishable} \quad (3.6)$$

In the above formula, distinguishability (complete) happens when the phase difference between two amplitudes γ_{m1} and γ_{m2} exceed (seen in time) the coherence time τ_c of the photon. Indistinguishability (complete) happen when such phase difference (seen in time) is much less than the photon coherence time.

The final probabilities at detectors will, at the end, depend on the total phase difference (de-phasing) between the interfering states and on a 'visibility' factor (which takes into account for a non complete indistinguishability or distinguishability). The value of the total de-phasing and the method for removal of de-phasing caused by the 'classical like Doppler effects' will be explicated in the next two paragraphs.

Ground Interferometer

A photon entering the ground interferometer along spatial mode $|1\rangle$ will undergo state superposition splitting by the Beam Splitters and will exit the interferometer along two space modes in a total of four distinguishable states:

$$|\psi_{in}\rangle \Rightarrow \frac{1}{2}(e^{i\phi} - 1)|5\rangle + i\frac{1}{2}(e^{i\phi} + 1)|6\rangle \quad (3.7)$$

$\phi = \text{Total phase accumulated in the GS interferometer by the state following the long side}$

Free space

The two distinguishable states propagating along space mode $|6\rangle$ will reach the entrance of the S/C based interferometer in spatial mode $|7\rangle$ at slightly different time separation than the initial one and with the Spacecraft in a slightly different positions relative to the GS.

Spacecraft Interferometer

The two distinguishable states entering the interferometer along space mode $|7\rangle$ will undergo further state superposition splitting by the Beam Splitters. In total, at the exit, eight states are present, four along space mode $|11\rangle$ and four along space mode $|12\rangle$.

The one photon entering the GS interferometer will therefor evolve in states according to the following equation:

$$\begin{aligned} |\psi_{in}\rangle = |1\rangle \Rightarrow & \frac{1}{2}(e^{i\phi} - 1)|5\rangle + i\frac{1}{4}e^{iR}(1 - e^{i\phi^2} + e^{i\phi^1} - e^{i\phi^1}e^{i\phi^2})|11\rangle + \\ & + \frac{1}{4}e^{iR}(-1 - e^{i\phi^2} - e^{i\phi^1} - e^{i\phi^1}e^{i\phi^2})|12\rangle \end{aligned} \quad (3.8)$$

In above equation:

ϕ_1 = Total phase *accumulated by the trailed state* from the first BS of the ground interferometer to the last BS of the interferometer on board the spacecraft

ϕ_2 = Total phase *accumulated by the leading state* from the first BS of the ground interferometer to the last BS of the interferometer on board the spacecraft

R = Common component of large phase variation (common to both states)

To summarize:

- Two distinguishable states are present in space mode |5>;
- Four states are present in space mode |11> (two of which are likely non distinguishable and can therefore interfere – see below)
- Four states are present in space mode |12> (two of which are likely non distinguishable and can therefore interfere – see below)

The overall probabilities to find the photon in space modes |5>, |11> and |12> is now computed.

➤ Overall probability to get the photon in space mode |5> (photon lost)

Two superposed states are present which are time tagged and in general separated by more the coherence time of the photon: indeed since $L_1/c = \phi/\omega_1 > \tau_c$ (photon coherence time) even for 'small' MZI unbalance, then superposed states are certainly distinguishable and the overall probabilities to get a photon exiting from channel 5 becomes:

$$P_5 = \left| \frac{1}{2} \cdot e^{i\phi} \right|^2 + \left| -\frac{1}{2} \cdot 1 \right|^2 = 1/2 \quad (3.9)$$

➤ Overall probability to get the photon in spatial mode |11> (coupled to detector 11)

Four superposed states are present which are time tagged; depending on the value of ($\phi_1 - \phi_2$) three or four distinguishable situations will be present:

$$1^{\text{st}} \text{ case } \frac{\phi_1 - \phi_2}{\omega} \ll \tau_c$$

- three distinguishable situations $1 - e^{i\phi_2} + e^{i\phi_1} - e^{i\phi_1}e^{i\phi_2}$
- $P_{11} = \left| i\frac{1}{4} \cdot e^{iR} \right|^2 + \left| i\frac{1}{4} \cdot e^{iR} (-e^{i\phi_2} + e^{i\phi_1}) \right|^2 + \left| i\frac{1}{4} \cdot e^{iR} (-e^{i\phi_1}e^{i\phi_2}) \right|^2 =$

$$P_{11} = \frac{1}{8} + \frac{1}{8} \cdot [1 - \cos(\phi_1 - \phi_2)] \quad (3.10)$$

2nd case $\frac{\phi_1 - \phi_2}{\omega} > \tau_c$

- four distinguishable situations $1 - e^{i\phi_2} + e^{i\phi_1} - e^{i\phi_1}e^{i\phi_2}$
- $P_{11} = |i\frac{1}{4} \cdot e^{iR}|^2 + |-i\frac{1}{4} \cdot e^{iR}e^{i\phi_2}|^2 + |i\frac{1}{4} \cdot e^{iR}e^{i\phi_1}|^2 + |i\frac{1}{4} \cdot e^{iR}(-e^{i\phi_1}e^{i\phi_2})|^2 = \frac{1}{4}$ (3.11)

➤ Overall probability to get the photon in spatial mode $|12\rangle$ (coupled to detector 12)

Same considerations as above applies, the overall probability results:

1st case $\frac{\phi_1 - \phi_2}{\omega} \ll \tau_c$

- $P_{12} = \frac{1}{8} + \frac{1}{8} \cdot [1 + \cos(\phi_1 - \phi_2)]$ (3.12)

2nd case $\frac{\phi_1 - \phi_2}{\omega} > \tau_c$

- $P_{12} = \frac{1}{4}$ (3.13)

Clearly, whatever the case, the overall probability to find the photon somewhere is

$$P_5 + P_{11} + P_{12} = 1 \quad (3.14)$$

The transition between the two limit cases dealt above, $\frac{\phi_1 - \phi_2}{\omega} \ll \tau_c$ and $\frac{\phi_1 - \phi_2}{\omega} > \tau_c$, is basically controlled by the amount of time/length (and therefore energy) superposition between the two interfering states which modify the probability result at the detectors. An interference 'visibility function V ' can therefore be introduced ranging from 1 (complete indistinguishability) to 0 (complete distinguishability) like qualitatively shown in Figure 3-9.

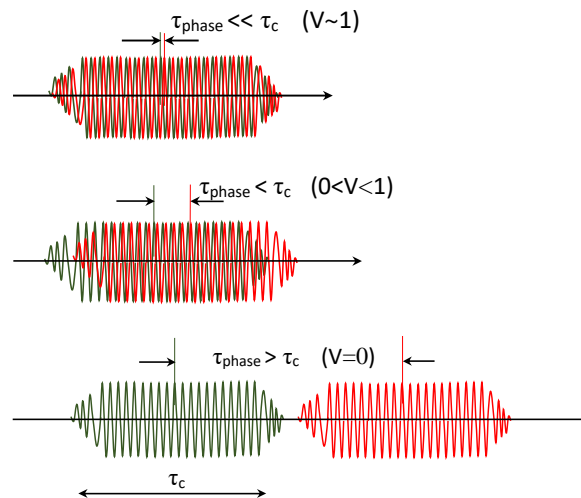


Figure 3-9 Qualitative schematics for indistinguishability, distinguishability and intermediate condition

The mathematical description of ‘V’ can be approximated in different ways; in the specific case an approach similar to the one described in Ref.[17] and Ref. [18] and dealing with matter waves is considered. The concept of interference ‘visibility’ in case of photons can therefore be introduced similarly as:

$$\begin{cases} \tau_{phase} = \frac{\phi_1 - \phi_2}{\omega} \\ \text{for } \tau_{phase} \leq \tau_c \rightarrow V = \left| \cos\left(\frac{\tau_{phase}}{\tau_c} \cdot \frac{\pi}{2}\right) \right| \\ \text{for } \tau_{phase} > \tau_c \rightarrow V = 0 \end{cases} \quad (3.15)$$

Accounting for the Visibility, the overall probabilities to find the photon in space modes $|5\rangle$, $|11\rangle$ and $|12\rangle$ can then be written:

$$\rightarrow P_5 = \frac{1}{2} \quad (3.16)$$

$$\rightarrow P_{11V} = \frac{1}{8} + \frac{1}{8} \cdot [1 - V(\phi_1, \phi_2, \tau_c, \omega) \cdot \cos(\Phi_1 - \Phi_2)] \quad (3.17)$$

$$\rightarrow P_{12V} = \frac{1}{8} + \frac{1}{8} \cdot [1 + V(\phi_1, \phi_2, \tau_c, \omega) \cdot \cos(\Phi_1 - \Phi_2)] \quad (3.18)$$

Above formulation accounts for a full range of visibility, from $V=1$ to $V=0$ over a continuous range of phase change (or time tagging). Again the overall probability to find the photon somewhere is $P_5 + P_{11V} + P_{12V} = 1$.

Each photon can arrive at the detectors according to a three or four arrival slots as schematized in Figure 3-10 depending on visibility.

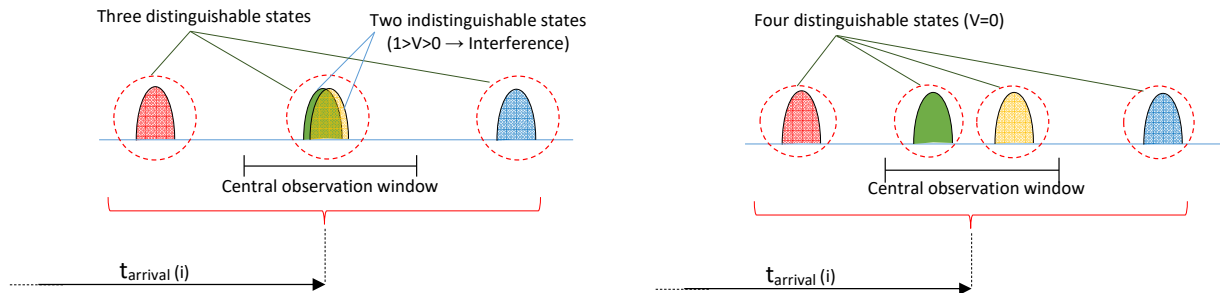


Figure 3-10 Schematics of possible arrival slots at detectors

Under ‘normal’ experimental conditions’, if no excessive macroscopic length difference between the two interferometers (as shown in the sensitivity analysis) a three slot scheme is present; in this case:

- 50% of photons will be lost in spatial mode 5 ($P_5 = 0,5$ constant);
- 25% of photons will be received by the two detectors in the ‘side slot bands’ ($P_{11sides} = P_{12sides} = 0.125$ and clearly $P_{11sides} + P_{12sides} = 0.25$ constant);
- 25% of photons will be received by the two detectors in the ‘central time band’ ($P_{11central} + P_{12central} = 0.25$ and $P_{11central}$ and $P_{12central}$ are modulated by interference)

Considering only the 25% photons reaching the central time band of the two detectors and renormalizing the $P_{11\text{central}}$ and $P_{12\text{central}}$ relative probability it will be:

$$\rightarrow P_{11CV} = \frac{1}{2} \cdot [1 - V(\phi_1, \phi_2, \tau_c, \omega) \cdot \cos(\phi_1 - \phi_2)] \quad (3.19)$$

$$\rightarrow P_{12CV} = \frac{1}{2} \cdot [1 + V(\phi_1, \phi_2, \tau_c, \omega) \cdot \cos(\phi_1 - \phi_2)] \quad (3.20)$$

It will also clearly be:

$$\rightarrow P_{11CV} + P_{12CV} = 1 \quad (3.21)$$

Let us recall that interference will be observed between the two states that run the long side of the interferometer one on the ground interferometer and one on the interferometer on board the spacecraft.

3.1.2 General considerations on classical Doppler compensation

As already pointed out the de-phasing due to the ‘classical Doppler effects’ need be eliminated in order to have a residual de-phasing due to solely (or primarily) the metric effects.

Two approaches are discussed:

- ‘double measurement scheme’ (based on Doppler effect suppression by subtracting, off-line, signals containing both such an effect);
- based on ‘interferometer length real-time control’ utilizing appropriate cancellation algorithm.

As far as the “double measurement scheme” an interesting case is reported in Ref. [8] which describe a possible experimental configuration *aiming at Equivalence Principle types verifications*. Practically two interferometric measurement schemes work in parallel: a one-way scheme and a GS-S/C-GS two ways scheme (as shown in Figure 3-11 directly taken from Ref. [8]) and both schemes (taken separately) do not implement any Doppler compensation.

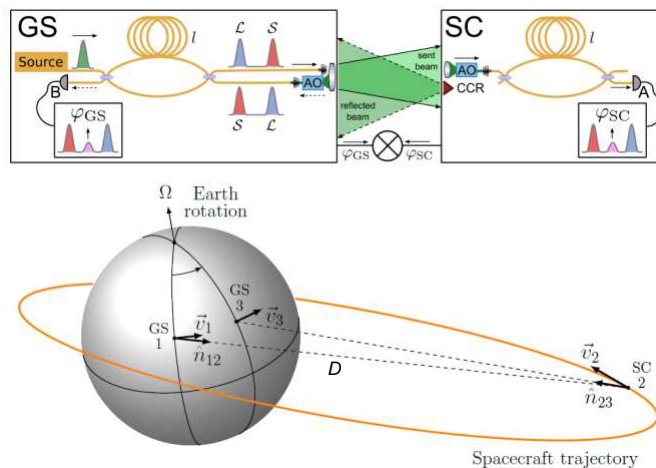


Figure 3-11 Double interferometric measurement scheme for classical Doppler management (picture from Ref. [8])

Without entering into details, upon experiment completion two recorded de-phasing files are available: $\phi_{SC}(t)$ and $\phi_{GS}(t)$ both containing classical Doppler effects.

The two signals are then appropriately post processed to remove the classical Doppler effect and the following type of expression may result (for example according to the latest version given in Ref.[19]:

$$S \equiv \varphi_{SC} - \frac{1}{2} \varphi_{GS} = \omega_0 \tau_l \left[(1 + \alpha)(U_2 - U_1) + \frac{1}{2} (\beta_2^2 - \beta_1^2) - \vec{\beta}_1 \cdot (\vec{\beta}_1 - \vec{\beta}_2) - (\Delta_2^2 - \Delta_1^2) - T \cdot (\hat{n}_{12} \cdot \vec{a}_1) \cdot \frac{1}{c} - (\vec{\beta}_2 - \vec{\beta}_1) \cdot (\vec{\beta}_2 - \vec{\beta}_1) \cdot \frac{\tau_l}{4T} + (\Delta_1 - \Delta_2)^2 \cdot \frac{\tau_l}{4T} \right] \quad (3.22)$$

where (see also Figure 3-11 for symbols):

$$\begin{aligned} U_i &= \frac{GM}{c^2 r_i} \quad (i = 1, 2) \\ \vec{\beta}_i &= \frac{\vec{v}_i}{c} \quad (\vec{v}_i = \text{speeds}) \\ \Delta_i &= \hat{n}_{12} \cdot \vec{\beta}_i \\ \vec{a}_1 &= \text{Centripetal acceleration at GS} \\ \tau_l &= \text{Interferometers line imbalance (assuming both interferometers of equal length)} \\ \omega_0 &= \text{Sent angular frequency} \\ T &= \frac{D}{c} \end{aligned}$$

Always during off line analysis, the Spaceraft speed \vec{v}_2 can be accurately reconstructed (for example with the support of high accuracy ephemeris) and also the GS speed \vec{v}_1 is known accurately. This in turn allows to determine very precisely the parameter α and a value $\alpha \neq 0$ would indicate a violation of some parts of the Equivalence Principle; above approach is certainly well suited and appropriate.

It is furthermore noted that assuming a Spacecraft placed in a perfect circular orbit, due to the presence of terms like $\vec{v}_2 \cdot \vec{v}_1$ or $\vec{v}_{1//}$ or $\vec{v}_{2//}$, S will not be constant (as per the metric part only) but will present speeds related modulation.

As far as the compensation approach based on “*interferometer length real-time control*”, it works on a different scheme and such to allow a ‘nominal constant’ de-phasing in case of Spacecraft moving along a perfect circular orbit (test of goodness of the algorithm).

This is achieved (see also schematics in Figure 3-12) by implementing real-time controlled length modulation for one of the two interferometers (e.g. the ground one) such to cancel the de-phasing effects caused by the relative motion of the interferometers. In this case very accurate speed information are necessary in real time and these can be obtained by performing laser ranging while the main experiment is running (see also paragraphs 5.1 and 5.2).

This Doppler compensation would allow for an interferometric effect at the detectors (revealed in this case by single photons counting) *directly due to the metric part only*; the approach is discussed in detail the next paragraph.

The two approaches may have different suitability conditions also depending on whether the experiment is more oriented at Quantum Interference or General Relativistic verifications. It is however noted that both approaches require retro-reflectors on board S/C and basically can differ at Ground Segment level only (Space Segment being basically the same); the experiment could be implemented from beginning to allow the transition from one technique to the other or even to allow the implementation of them both.

Should the S/C need be compatible also to the ‘double measurement scheme’, specific evaluations have to be done as far as Corner Cube Reflector(s) to kept under control the effect of return superposition (less important in the Satellite Laser Ranging based scheme).

For the studied experiment it has been considered and explored in detail the Doppler compensation algorithm based on “*interferometer length real-time control*”.

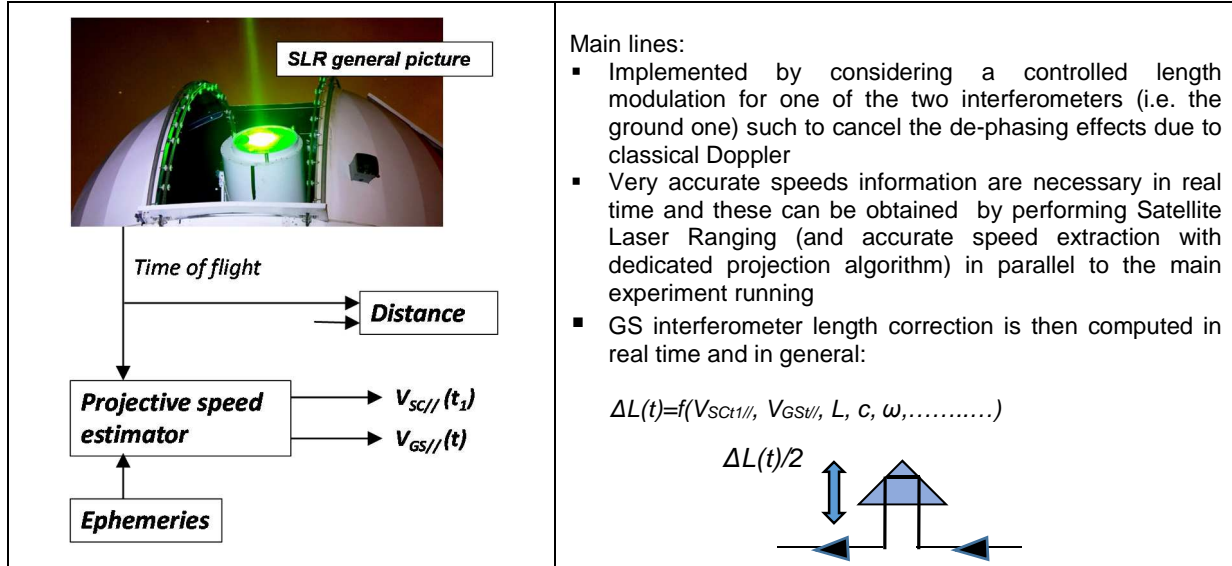


Figure 3-12 Schematics of the adopted compensation method based on “*interferometers length real-time control*”

3.1.3 Detail evaluation of the Doppler compensation approach proposed (based on interferometer length real-time control)

In this chapter two important issues will be investigated:

- The estimation of the de-phasing between the interfering superposed states ($\phi_1 - \phi_2$ or equivalently ϕ_1 and ϕ_2)
- The evaluation of the ground interferometer length correction ΔL in order to remove the part of de-phasing caused by the ‘classical Doppler effect’. The required length correction ‘intended to be applied in time (ready) and stable’ for the transit of the trailed photon state in the long arm of the ground interferometer

In general the de-phasing can be considered as a contribution of three types of effects (see also Ref. [8]):

$$\phi_1 - \phi_2 = \text{Lines effect} + \text{Space effect} + \text{Beatnote effect} \quad (3.23)$$

The *Lines effect* is indeed the one of interest and is generated by the fact that the two interferometers are placed at very well separated gravitational conditions (both in potential and speeds).

The *Space effect* is related to the fact that the trailed state reaches the spacecraft interferometer with the spacecraft in a slightly different position conditions. This slightly affect the phase accumulation of the trailed state.

The *Beatnote effect* is related to relative speed variations (acceleration) at reception of the trailed state with respect to the leading state. This frequency difference (beatnote) generate an integrated (over time) additional de-phasing.

The Space effect and Beatnote effect contributions become null as the relative speed between the GS and the S/C becomes null and non changing. As will be apparent in the next description the algorithm for classical Doppler effects compensation *compensates (in a nominal case) also the Space effect and the Beatnote effect*. It is however appropriate consider the presence of the two effects (on top of the Lines effect) since the sensitivity to 'large' variation in interferometers length introduce some small asymmetry in the compensated de-phasing curve.

This chapter is organised in three sections two of which present two alternatives in the de-phasing computation and compensation algorithm and one section reports a comparison of the two alternatives with respect to sensitivity aspects for a generic test trajectory:

- Alternative 1: Lines effects only
- Alternative 2: Lines effect plus Space effect (version 1) plus Beatnote effect
- Comparison of the two alternatives w.r.t. sensitivity issues

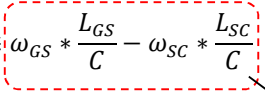
It is furthermore evidenced that during the experiment different algorithms or variants can easily be tested and verified in order to optimize the efficiency of cancellation.

3.1.3.1 Alternative 1: Lines effects only

De-phase computation scheme (approach)

The general expression for de-phasing can take the following form:

$$D\varphi \cong \omega_{GS} * \frac{L_{GS}}{C} - \omega_{SC} * \frac{L_{SC}}{C} \quad (3.24)$$



Lines main effect

In general for the ground interferometer it is:

$$L_{GS} = L + \delta L_{GS} + \Delta L \quad (3.25)$$

L = Ideal length

δL_{GS} = Length perturbations - It includes multiple of wavelength perturbations, residuals from calibrations and uncertainties (sub wavelength) - Ideally as small as possible and in general unknown

ΔL = Commanded length variation for Doppler compensation

For the space interferometer it is:

$$L_{SC} = L + \delta L_{SC} \quad (3.26)$$

L = Ideal length m

δL_{SC} = Length perturbations - It includes multiple of wavelength perturbations, residuals from calibrations and uncertainties (sub wavelength) - Ideally as small as possible and in general unknown

Doppler compensation (approach)

The objective of the 'Doppler compensation' is to eliminate the de-phasing effects induced by the presence of the two terms $V_{SC//t1}$ and $V_{GS//t}$ which are responsible for the large frequency variations with the purpose of leaving only the 'metric' induced type effects (encompassing both GR and SR dilations). In the process of algorithm derivation the quantities δL_{GS} and δL_{SC} are assumed not known (best value zero).

This is proposed to be achieved by *modulating the length of the ground interferometer* by the amount $\Delta L(t)$ which is explicated in hereafter procedure.

$$D\varphi \cong \omega_{GS} * \frac{L + \delta L_{GS} + \Delta L}{C} - \omega_{SC} * \frac{L + \delta L_{SC}}{C} \quad (3.27)$$

The compensation is searched by forcing the terms containing ΔL , $V_{SC//t1}$, $V_{GS//t}$ to zero:

$$\omega_{GS} * \frac{\Delta L}{C} - \omega_{GS} * \frac{U^{SC}}{U^{GS}} * \left(\frac{1 - V_{SC//t1}}{1 - V_{GS//t}} - 1 \right) * \frac{L}{C} \cong 0$$

$$\omega_{GS} * \frac{\Delta L}{C} \cong \omega_{GS} * \frac{U^{SC}}{U^{GS}} * \left(\frac{1 - V_{SC//t1}}{1 - V_{GS//t}} - 1 \right) * \frac{L}{C} \quad (3.28)$$

Considering that the quantities $V_{SC//t1}$, $V_{GS//t}$, U^{SC} , U^{GS} are only known in an estimated way denoted by the symbol " $\hat{}$ ", the algorithm for compensation would be:

$$\Delta L \cong \frac{\hat{U}^{SC}}{\hat{U}^{GS}} * \left(\frac{1 - \frac{\hat{V}_{SC//t1}}{\hat{C}}}{1 - \frac{\hat{V}_{GS//t}}{\hat{C}}} - 1 \right) * L \quad (3.29)$$

Summary

In summary this version of the Oneway-COW simulation program implement the following:

- De-phasing

$$D\varphi \cong \omega_{GS} * \frac{L_{GS}}{C} - \omega_{SC} * \frac{L_{SC}}{C} \quad (3.30)$$

- Compensation algorithm

$$\Delta L \cong \frac{\hat{U}^{SC}}{\hat{U}^{GS}} * \left(\frac{1 - \frac{\hat{V}_{SC//t1}}{\hat{C}}}{1 - \frac{\hat{V}_{GS//t}}{\hat{C}}} - 1 \right) * L \quad (3.31)$$

Hereafter are reported three circular test orbit for testing of the algorithm, the outcome should be, based on the implementation performed, a constant de-phasing along the whole orbit (different from orbit to orbit).

Test cases (all are circular orbits)

In the cases studied below a time base relevant to *one complete S/C orbit* is reported even if actual experiments can be carried out for elevations $> 0^\circ$ (e.g. elev. $> 20^\circ$).
(Code: cowsim292)

Test case 1

Spacecraft: $R = 7862$ km, $i = 50^\circ$ (circular)

Ground station: Lat = 40.65 N, $R = 6370$ km

Interferometers : $L = 100$ m (nominal)

Elevations $> 20^\circ$ in the time range: 2755 s, 4183 s

Theoretical expected de-phasing (only due to metric terms) ~ -0.176268166666667 rad

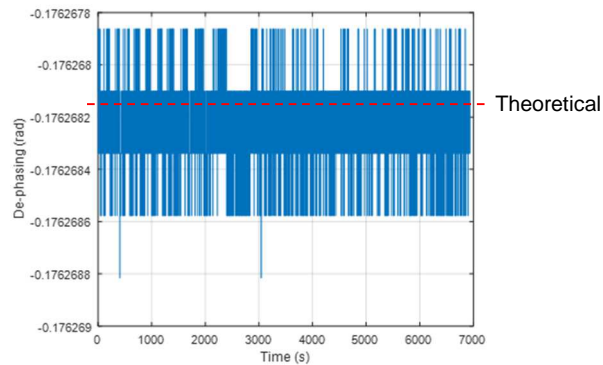


Figure 3-13 Test case 1 computed de-phasing

Method uncertainty $\sim \pm 0.0000005$ rad with 100 m class interferometers

Test case 2

Spacecraft: $R = 12000$ km, $i = 50^\circ$ (circular)

Ground station: Lat = 40.65 N, $R = 6370$ km

Interferometers : $L = 100$ m (nominal)

Elevations $> 0^\circ$ in the time range: 4178 s, 8903 s

Theoretical expected de-phasing ~ 0.167858333333333 rad

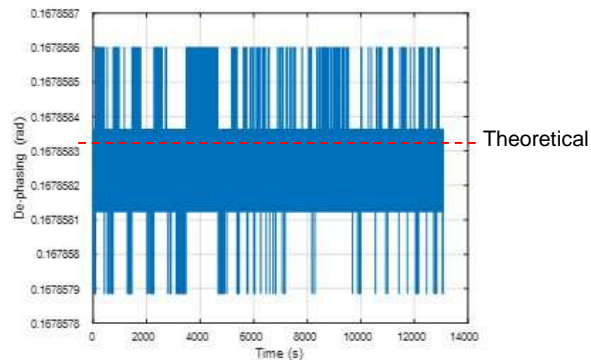


Figure 3-14 Test case 2 computed de-phasing

Method uncertainty $\sim \pm 0.0000005$ rad with 100 m class interferometers

Test case 3

Spacecraft: $R = 18000$ km, $i = 50^\circ$ (circular)

Ground station: Lat = 40.65 N, $R = 6370$ km

Interferometers : $L = 100$ m (nominal)

Elevations $> 0^\circ$ in the time range: 6178 s, 17860 s

Theoretical expected de-phasing ~ 0.385799666666667 rad

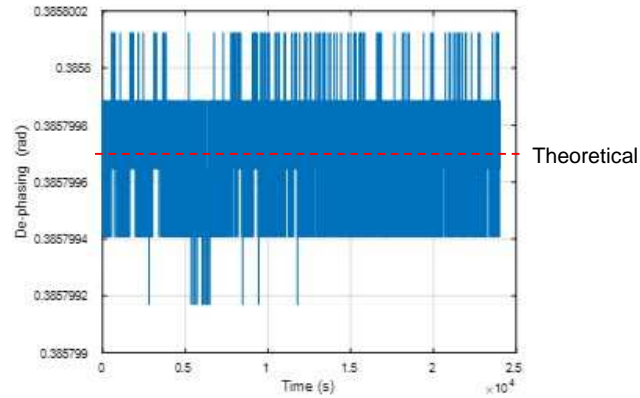


Figure 3-15 Test case 3 computed de-phasing

Method uncertainty ~ +/- 0.0000005 rad with 100 m class interferometers

3.1.3.2 Alternative 2: Lines effect plus Space effect (version 1) plus Beatnote effect

De-phase computation scheme

The general expression for de-phasing can take the following form:

$$D\varphi \cong \underbrace{\omega_{GS} * \frac{L_{GS}}{C} - \omega_{SC} * \frac{L_{SC}}{C}}_{\text{Lines main effect}} + \underbrace{\left(V_{SC//t1} * \frac{L_{GS}}{C} * \frac{\omega_{SC}}{C} - V_{GS//t} * \frac{L_{GS}}{C} * \frac{\omega_{GS}}{C} \right)}_{\text{Relative position variation effect}} + \underbrace{\int_{\xi=0}^{\xi=t1} (\delta\omega)_{BN} * d\xi + const1}_{\text{Beat note effect}} \quad (3.32)$$

In above formula the beat note $(\delta\omega)_{BN}$ is expressed as (not any more approximated):

$$\left[\begin{aligned} (\delta\omega)_{BN} &= \frac{d \left[\omega_{GS} * \frac{U_{SC}}{U_{GS}} * \left(\frac{1 - \frac{V_{SC//RX}}{C}}{1 - \frac{V_{GS//TX}}{C}} \right) \right]}{dt} * \frac{L_{GS}}{C} \rightarrow D\varphi_{BN} = \int_{\xi=0}^{\xi=t1} (\delta\omega)_{BN} * d\xi + const1 \quad (3.33) \\ &\text{Beat note - frequency difference between received (S/C) trailed state and received (S/C) leading state;} \\ &\text{depends on accelerations} \end{aligned} \right.$$

where $\frac{L_{GS}}{C}$ represents the temporal delay at emission of the second state with respect to the first one and the constant 'const1' is taken to avoid length biases over one whole trajectory.

Above equations for $D\phi$ includes the three major types of contributions mentioned.

In general for the ground interferometer it is:

$$L_{GS} = L + \delta L_{GS} + \Delta L \quad (3.34)$$

$L = \text{Ideal length}$

$\delta L_{GS} = \text{Length perturbations - It includes multiple of wavelength perturbations, residuals from calibrations and uncertainties (sub wavelength) - Ideally as small as possible and in general unknown}$

$\Delta L = \text{Commanded length variation for Doppler compensation}$

For the space interferometer it is:

$$L_{SC} = L + \delta L_{SC} \quad (3.35)$$

$L = \text{Ideal length}$

$\delta L_{SC} = \text{Length perturbations - It includes multiple of wavelength perturbations, residuals from calibrations and uncertainties (sub wavelength) - Ideally as small as possible and in general unknown}$

Doppler compensation (approach)

The objective of the ‘Doppler compensation’ is here intended to eliminate the de-phasing effects induced by the presence of the two terms V_{SC}/t_1 and V_{GS}/t which are responsible for the large frequency variations with the purpose of leaving only the ‘metric’ induced type effects (encompassing both GR and SR dilations). In the process of algorithm derivation the quantities δL_{GS} and δL_{SC} are assumed not known (best value zero).

This is proposed be achieved by *modulating the length of the ground interferometer* by the amount $\Delta L(t)$ which is explicited in hereafter procedure:

$$D\phi \cong \omega_{GS} * \frac{L+\delta L_{GS}+\Delta L}{c} - \omega_{SC} * \frac{L+\delta L_{SC}}{c} + (V_{SC}/t_1 - V_{GS}/t) * \frac{L+\delta L_{GS}+\Delta L}{c} * \frac{\omega_{GS}}{c} + \frac{\Delta\omega}{c} * V_{SC}/t_1 * \frac{L+\delta L_{GS}+\Delta L}{c} + omgi * \frac{L+\delta L_{GS}+\Delta L}{c} \quad (3.36)$$

and where:

$$\begin{aligned} \omega_{SC} &= \omega_{GS} + \Delta\omega \\ omgi &= \int_{\xi=0}^{\xi=t_1} \frac{d \left[\omega_{GS} * \frac{V_{SC}}{V_{GS}} * \left(\frac{1 - \frac{V_{SC}/RX}{c}}{1 - \frac{V_{GS}/TX}{c}} \right) \right]}{dt} * d\xi + const1 \\ const1 &= const * \frac{C}{L} \end{aligned} \quad (3.37)$$

The compensation is searched by forcing the contributions given by the sum of the terms containing ΔL , V_{SC}/t_1 , V_{GS}/t to zero:



$$\omega_{GS} * \frac{\Delta L}{C} - \omega_{GS} * \frac{U^{SC}}{U^{GS}} * \left(\frac{1 - \frac{V_{SC//t1}}{C}}{1 - \frac{V_{GS//t}}{C}} - 1 \right) * \frac{L}{C} + (V_{SC//t1} - V_{GS//t}) * \frac{L}{C} * \frac{\omega_{GS}}{C} + (V_{SC//t1} - V_{GS//t}) * \frac{\Delta L}{C} * \frac{\omega_{GS}}{C} + \frac{\Delta \omega}{C} * V_{SC//t1} * \frac{L}{C} + \frac{\Delta \omega}{C} * V_{SC//t1} * \frac{\Delta L}{C} + omgi * \frac{L}{C} + omgi * \frac{\Delta L}{C} = 0$$



$$\omega_{GS} * \frac{\Delta L}{C} * \left[1 + (V_{SC//t1} - V_{GS//t}) * \frac{1}{C} + \frac{1}{\omega_{GS}} * \frac{\Delta \omega}{C} * V_{SC//t1} + \frac{omgi}{\omega_{GS}} \right] \cong \left[\frac{U^{SC}}{U^{GS}} * \left(\frac{1 - \frac{V_{SC//RX}}{C}}{1 - \frac{V_{GS//TX}}{C}} - 1 \right) - (V_{SC//t1} - V_{GS//t}) * \frac{1}{C} - \frac{1}{\omega_{GS}} * \frac{\Delta \omega}{C} * V_{SC//t1} - \frac{omgi}{\omega_{GS}} \right] \omega_{GS} * \frac{L}{C} \quad (3.38)$$

Considering that the quantities $V_{SC//t1}$, $V_{GS//t}$, U^{SC} , U^{GS} , $\Delta \omega$ are *only known in an estimated way* denoted by the symbol “ $\hat{}$ ”, the algorithm for compensation would be:

$$\Delta L \cong \frac{1}{\left[1 + (\hat{V}_{SC//t1} - \hat{V}_{GS//t}) * \frac{1}{C} + \frac{1}{\omega_{GS}} * \frac{\hat{\Delta \omega}}{C} * \hat{V}_{SC//t1} + \frac{\widehat{omgi}}{\omega_{GS}} \right]} * \left[\frac{\hat{U}^{SC}}{\hat{U}^{GS}} * \left(\frac{1 - \frac{\hat{V}_{SC//RX}}{C}}{1 - \frac{\hat{V}_{GS//TX}}{C}} - 1 \right) - (\hat{V}_{SC//t1} - \hat{V}_{GS//t}) * \frac{1}{C} - \frac{1}{\omega_{GS}} * \frac{\hat{\Delta \omega}}{C} * \hat{V}_{SC//t1} - \frac{\widehat{omgi}}{\omega_{GS}} \right] * L \quad (3.39)$$

Summary

In summary this version of the Oneway-COW simulation program implement the following:

- De-phasing

$$D\varphi \cong \omega_{GS} * \frac{L_{GS}}{C} - \omega_{SC} * \frac{L_{SC}}{C} + \left(V_{SC//t1} * \frac{L_{GS}}{C} * \frac{\omega_{SC}}{C} - V_{GS//t} * \frac{L_{GS}}{C} * \frac{\omega_{GS}}{C} \right) + omgi * \frac{L_{GS}}{C} \quad (3.40)$$

- Compensation algorithm

$$\Delta L \cong \frac{1}{1 + (\hat{V}_{SC//t1} - \hat{V}_{GS//t}) * \frac{1}{C} + \frac{1}{\omega_{GS}} * \frac{\hat{\Delta \omega}}{C} * \hat{V}_{SC//t1} + \frac{\widehat{omgi}}{\omega_{GS}}} * \left[\frac{\hat{U}^{SC}}{\hat{U}^{GS}} * \left(\frac{1 - \frac{\hat{V}_{SC//RX}}{C}}{1 - \frac{\hat{V}_{GS//TX}}{C}} - 1 \right) - (\hat{V}_{SC//t1} - \hat{V}_{GS//t}) * \frac{1}{C} - \frac{1}{\omega_{GS}} * \frac{\hat{\Delta \omega}}{C} * \hat{V}_{SC//t1} - \frac{\widehat{omgi}}{\omega_{GS}} \right] \quad (3.41)$$

Hereafter are reported three circular test orbit will be utilized to test the algorithm, the ideal outcome should be (based on the implementation performed) a constant de-phasing along the whole orbit (different from orbit to orbit).

Test cases (all are circular orbits)

In the cases studied below a time base relevant to *one complete S/C orbit* is reported even if actual experiments can be carried out for elevations $> 0^\circ$ (e.g. elev. $> 20^\circ$).
(Code: cowsim292moddephaseB)

Test case 1

Spacecraft: $R = 7862$ km, $i = 50^\circ$ (circular)

Ground station: Lat = 40.65 N, $R = 6370$ km

Interferometers : $L = 100$ m (nominal)

Elevations $> 0^\circ$ in the time range: 2755 s, 4183 s

Theoretical expected de-phasing ~ -0.176268166666667 rad

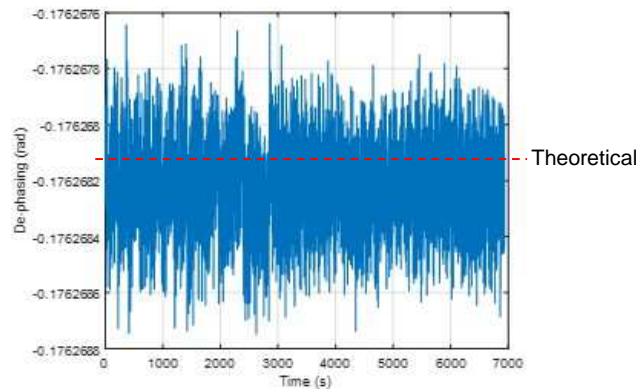


Figure 3-16 Test case 1 computed de-phasing

Method uncertainty $\sim \pm 0.0000007$ rad with 100 m class interferometers

Test case 2

Spacecraft: $R = 12000$ km, $i = 50^\circ$ (circular)

Ground station: Lat = 40.65 N, $R = 6370$ km

Interferometers : $L = 100$ m (nominal)

Elevations $> 0^\circ$ in the time range: 4178 s, 8903 s

Theoretical expected de-phasing ~ 0.167858333333333 rad

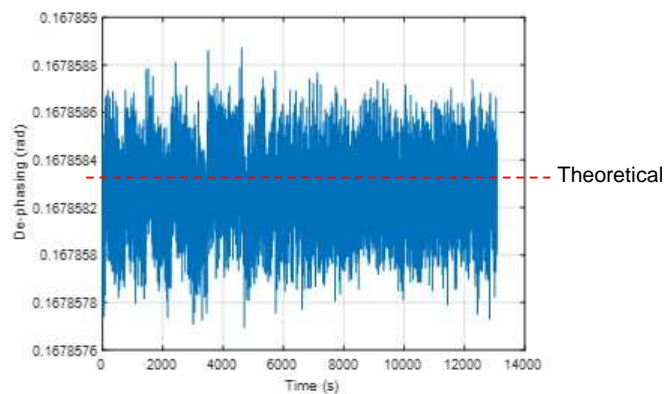


Figure 3-17 Test case 2 expected de-phasing

Method uncertainty $\sim \pm 0.0000006$ rad with 100 m class interferometers

Test case 3

Spacecraft: $R = 18000$ km, $i = 50^\circ$ (circular)

Ground station: Lat = 40.65° N, $R = 6370$ km

Interferometers : $L = 100$ m (nominal)

Elevations $> 0^\circ$ in the time range: 6178 s, 17860 s

Theoretical expected de-phasing ~ 0.385799666666667 rad

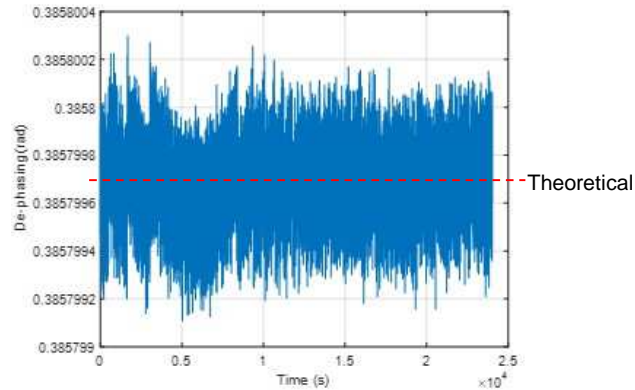


Figure 3-18 Test case 3 computed de-phasing

Method uncertainty $\sim \pm 0.0000007$ rad with 100 m class interferometers

3.1.3.3 Comparison of the three alternatives w.r.t. sensitivity issues test trajectory T1

In this chapter a comparison of the three alternatives for de-phasing computation and compensation algorithm, previously described, is given. For this comparison both nominal behaviour and sensitivity to some of the key parameters is investigated in order to get more insight on the methods. For this evaluation the following GS and S/C test trajectory (T1) are used:

S/C: in elliptic orbit, apogee passage

- Semi Minor axis: 10000 km
- Semi Major axis: 18000 km
- Inclination: 28°
- Orbital period = $1.648577657918921 \times 10^4$ s

GS: Matera SLR (Satellite Laser Ranging)

- $R = 6370$ km
- Lat. = 40.65°

For all cases two interferometers with nominal length of 600 m have been used and the compensation of 'classical Doppler effect always kept active'.

For all cases a time span equal to one complete orbital period has been shown in the figures although only a portion of this time (where the elevation of observation is e.g. $> 15^\circ$) is suitable for the experimentation.

➤ **Performance comparison in nominal conditions**

- *rbias* - Satellite POSITION measurement bias..... =0 m
- *rnoise* - Satellite POSITION measurement noise (1 sigma)..... =0 m
- *vbias* - Satellite SPEED (relative to GS) measurement bias..... =0 m/s
- *vnoise* - Satellite SPEED (relative to GS) measurement noise (1 sigma)... =0 m/s
- *pcbiasn* - Prism control bias error =0 mm
- *pcnoisen* - Prism control noise error(1 sigma)..... =0 mm
- Delta L2-L1 (e.g. calibration) = =0 μm

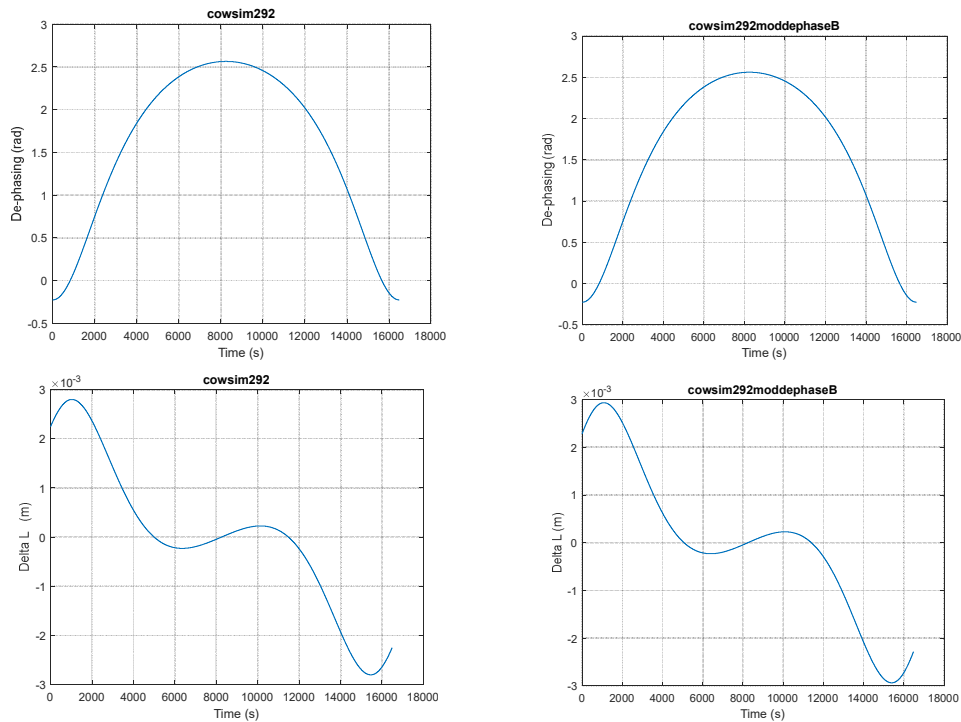


Figure 3-19 Comparison of de-phasing and length correction in nominal conditions (left: alternative 1, right: alternative 2)

➤ **Sensitivity to residual interferometers length differences**

pcbiasn - Prism control bias error =5 nm
Delta L2-L1 (e.g. calibration) = - 0.01 μm

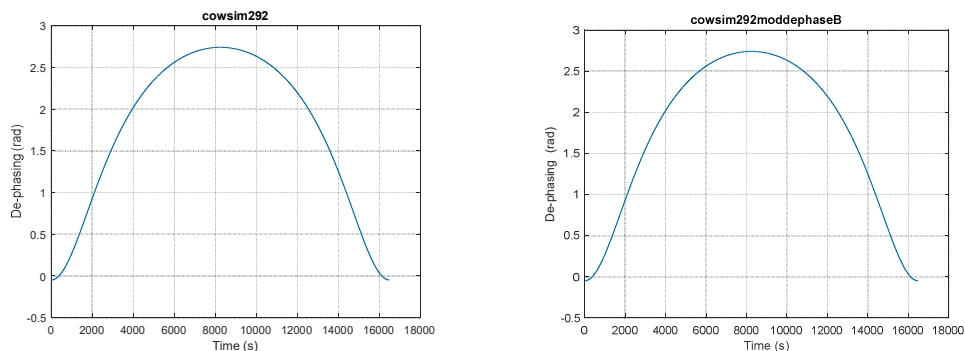


Figure 3-20 Comparison of de-phasing (left: alternative 1, right: alternative 2)

➤ **Sensitivity to GS-Satellite relative speed**

vbias - Satellite SPEED (relative to GS) measurement bias..... = 0.005 m/s

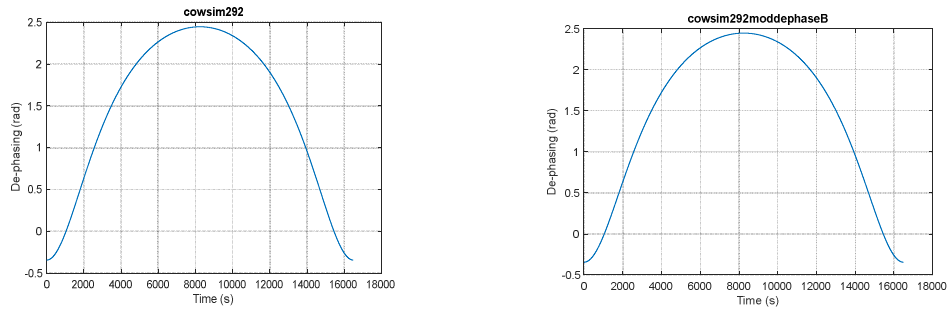


Figure 3-21 Comparison of de-phasing (left: alternative 1, right: alternative 2)

➤ **Sensitivity to 'macroscopic' interferometers length variation (multiple of λ)**

*L2ID - Ideal length of space interferometer..... = 599.99734 m (- 5000*2*pi radians w.r.t L1ID))*

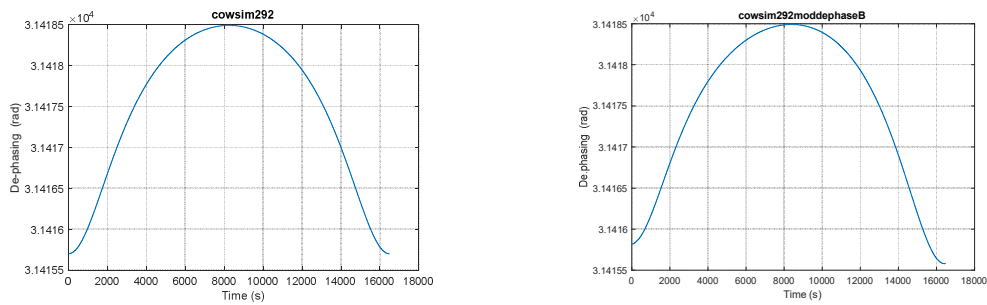


Figure 3-22 Comparison of de-phasing (left: alternative 1, right: alternative 2)

➤ **Sensitivity to 'macroscopic' interferometers length variation (multiple of λ)**

*L1ID - Ideal length of space interferometer..... = 599.99734 m (- 5000*2*pi radians w.r.t L2ID))*

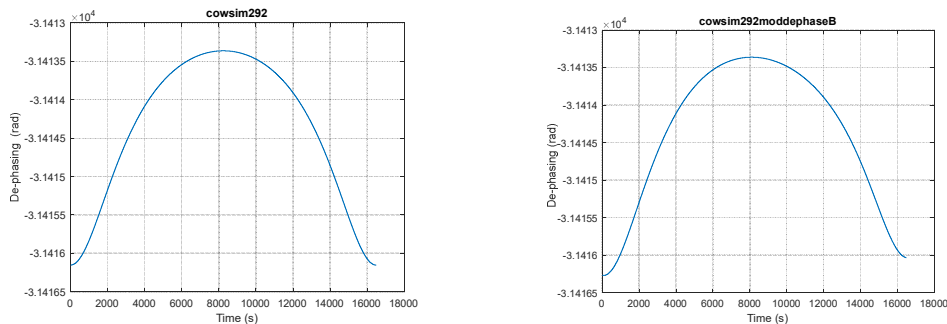


Figure 3-23 Comparison of de-phasing (left: alternative 1, right: alternative 2)

In summary for circular trajectories, the resulting de-phasing is nominally constant (a constant for each trajectory) and equal to the foreseen theoretical value. Removing the classical Doppler effects 'perfectly', the net contribution is nominally equal to the lines effect.

For a generic elliptical test trajectory if no imprecision were present, all the alternatives give the same result and coincide with the one of the sole 'line effect'. Furthermore, the sensitivity evaluations performed against variations of some of the key parameters point out a behaviour extremely similar among all of them. In case of 'large' differences in interferometer length (e.g. few millimetres) a slight skewness is present in the de-phasing curves of the more complete alternative, this can be explained.

For the next analysis the formulation considered in alternative 2 is used.

3.1.4 Nominal expected performances on a test trajectory T2

The nominal performances for the Oneway configuration is now assessed assuming the GS and S/C on a test trajectory T2.

Test trajectory T2 is set in a clear geometrical scheme with the S/C in a zero degrees inclination trajectory and the GS assumed at zero degrees latitude (to have a clear configuration for a better data interpretation). Concerning the S/C its apogee and perigee are selected to have a wide trajectory with a good height span and have been taken similar as the apogee and perigee of Galileo 201/202 spacecrafts (even if they resulted from a wrong orbital insertion for such spacecrafts). In summary for T2:

S/C: in elliptic orbit, apogee passage

- Semi Major axis (apogee) = 32582 km
- Semi Minor axis (perigee) = 23372 km
- Inclination = 0°
- Orbital period = 46571.37608455546 s

GS:

- R = 6370 km
- Latitude = 0°

The analysis (performed with cowsim292moddephaseB code) furthermore assumes the following:

- Interferometers reference length of $L_1=L_2= 6000$ m;
- Photon coherence time ~ 80 ps;
- Analysis of results are shown for observation elevations $\geq 30^\circ$.

Above test trajectory and interferometers length are *for comparison purposes only* and will be optimized for the final performance and sensitivity evaluation on the selected final experimental configuration.

The results for T2 are reported in the hereafter figures and the following comments apply:

- The test trajectory here considered the observation time (experimentation time available per orbit) is very high, about 40000 s, as shown in Figure 3-24, allowing for several sequences of experiment available during each orbit. This leave margins to possible orbital parameter optimization;
- The value of 30° elevation for initial of observation is certainly good. This can be reduced since actual observations from a Ground Station can be started for example from values of elevations e.g. $> 20^\circ$ or $> 15^\circ$ or even less depending also on atmospheric conditions;

- The de-phasing observed present a very good value excursion (almost 4π), as shown in Figure 3-25 left, and this certainly leave margin for a possible interferometer length reduction;
- The corresponding probability variations at the two detectors ranges from 0 to 1 and basically cover two complete excursions as shown in Figure 3-25 right. A reduction in interferometers length would reduce the technological difficulties still allowing good variations in probabilities (variation in photon counting);
- The quantum interference visibility is basically constant to 1 (see Figure 3-26 left) since in the nominal case the relativistic de-phasing (with the one associated to the 'classical Doppler effect' compensated) is very small w.r.t the photon coherence time;
- The ground interferometer's length correction (to be applied for the compensation of de-phasing due to the 'classical Doppler effect') requires a stroke range of about 16 mm. This stroke is quite high to be realized in practice (when combined with the required control accuracy, as later on shown); a reduction of this stroke is quite important to be implemented and to this purpose, the interferometer length and the orbit selection will play an important role.

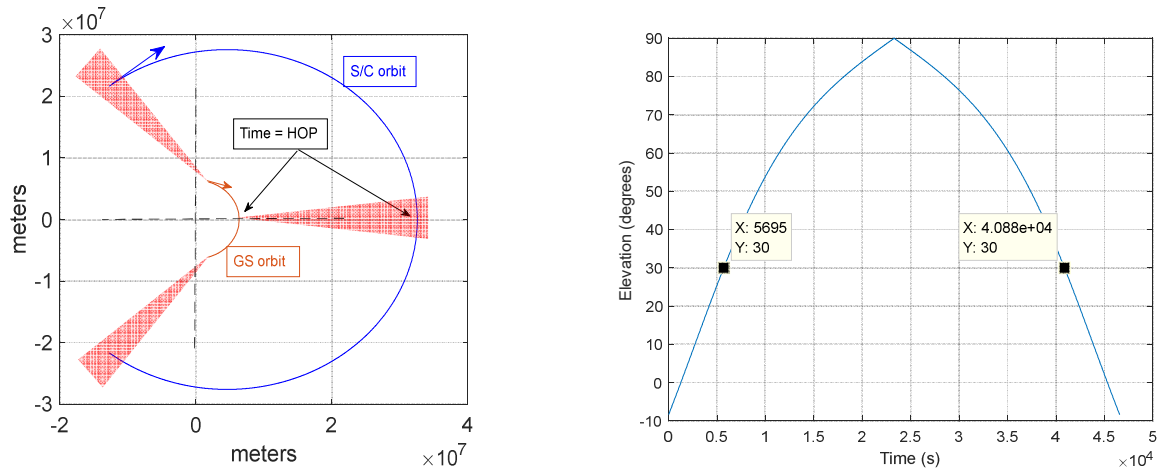


Figure 3-24 Geometry of trajectories on the equatorial plane (left), elevation of observation (right)

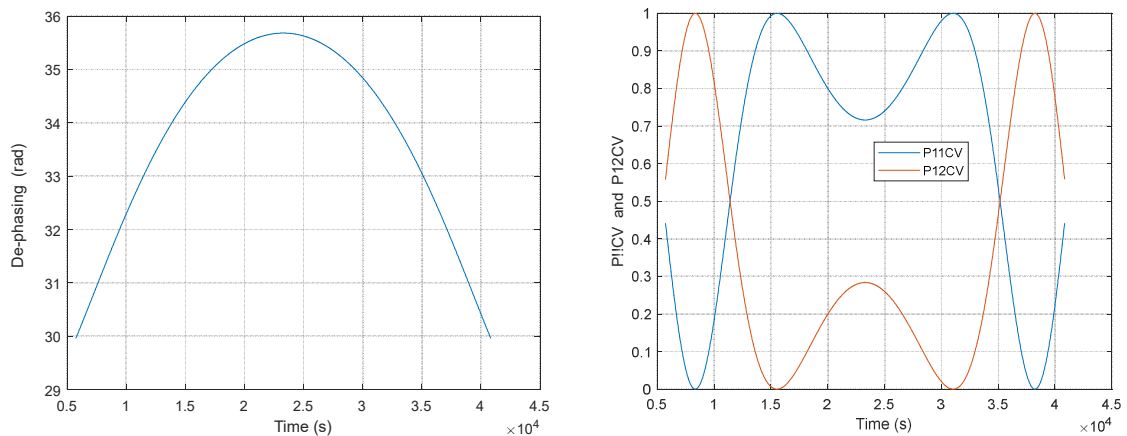


Figure 3-25 Total de-phasing (left), probabilities at the two SPADS detectors (right) (classical Doppler compensation active)

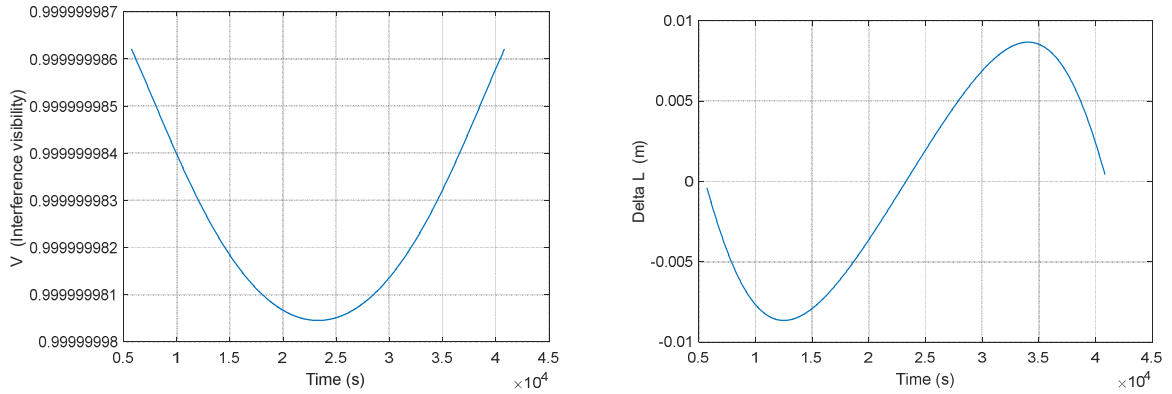


Figure 3-26 Visibility of interference (left), GS interferometer length correction (right)

3.2 Twoways configuration S/C-GS-S/C

3.2.1 General

This configuration utilize one interferometer only located on board a spacecraft while the ground station is in charge to the back reflection. The overall system schematics with light beams trajectories sketched is shown if Figure 3-27.

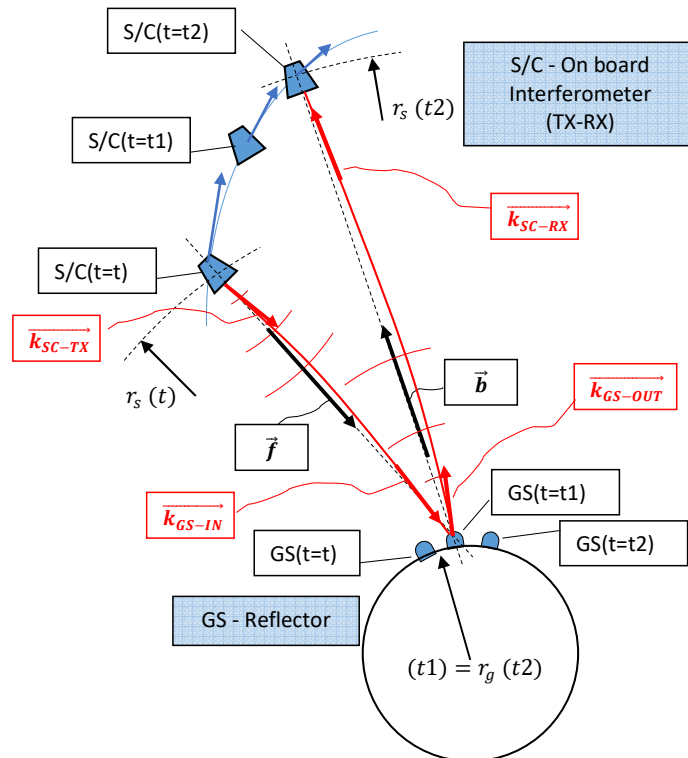
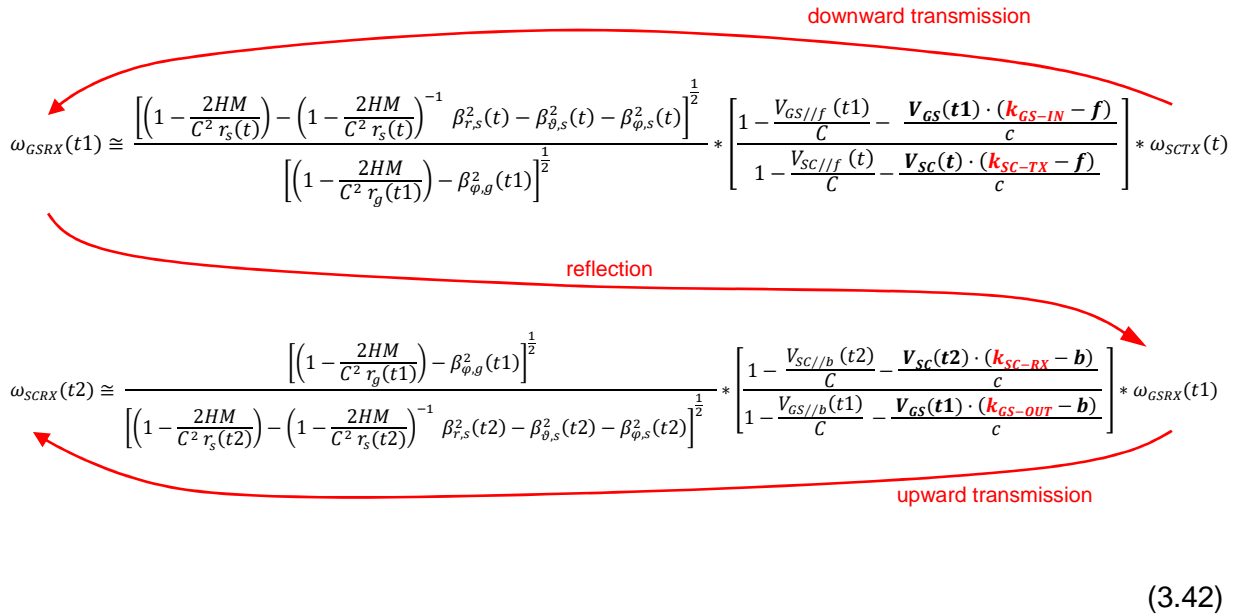


Figure 3-27 Twoways S/C-GS-S/C configuration with schematics of curved light beams (not to scale)

In this scheme a generic photon/state emitted by the S/C at time t , reaches the GS at time t_1 and, upon reflection, arrives back to the S/C at time t_2 (all this without counting the delays on the interferometry lines). The vectors in black are Euclidean while in red are schematically shown the wave vectors. The remaining symbols and convention used are similar to the oneway.

A generic photon or state is *received by the S/C that is displaced (in position and speed) only by a slight amount from the S/C at the moment of transmission*. In general the variation in altitude and speed depend on the orbit considered and the relative position between the S/C and the GS. During the round trip the S/C position can change in the range from zero to few meters (or tens of meters at most) and its speed can change at most of few centimetres per second. The useful signal (de-phasing variation and probabilities variation) are therefore expected quite small w.r.t. the Oneway scheme.

The overall geometry is more complex than the Oneway and the relation between a transmitted photon transmitted frequency and the same photon received frequency is of the following type (which can be derived from the Oneway relation and Ref. [8]):



The diagram illustrates the Twoways S/C-GS-S/C configuration. It shows a Satellite (S/C) at the top and a Ground Station (GS) at the bottom. A red curved arrow labeled "downward transmission" points from the S/C to the GS. A red curved arrow labeled "reflection" points from the GS back to the S/C. A red curved arrow labeled "upward transmission" points from the S/C to the GS. The equations for the frequencies are as follows:

$$\omega_{GSRX}(t_1) \cong \frac{\left[\left(1 - \frac{2HM}{C^2 r_s(t)} \right) - \left(1 - \frac{2HM}{C^2 r_s(t)} \right)^{-1} \beta_{r,s}^2(t) - \beta_{\vartheta,s}^2(t) - \beta_{\varphi,s}^2(t) \right]^{\frac{1}{2}}}{\left[\left(1 - \frac{2HM}{C^2 r_g(t_1)} \right) - \beta_{\varphi,g}^2(t_1) \right]^{\frac{1}{2}}} * \left[\frac{1 - \frac{V_{GS//f}(t_1)}{C} - \frac{V_{GS}(t_1) \cdot (k_{GS-IN} - f)}{c}}{1 - \frac{V_{SC//f}(t)}{C} - \frac{V_{SC}(t) \cdot (k_{SC-TX} - f)}{c}} \right] * \omega_{SCTX}(t)$$

$$\omega_{SCRX}(t_2) \cong \frac{\left[\left(1 - \frac{2HM}{C^2 r_g(t_1)} \right) - \beta_{\varphi,g}^2(t_1) \right]^{\frac{1}{2}}}{\left[\left(1 - \frac{2HM}{C^2 r_s(t_2)} \right) - \left(1 - \frac{2HM}{C^2 r_s(t_2)} \right)^{-1} \beta_{r,s}^2(t_2) - \beta_{\vartheta,s}^2(t_2) - \beta_{\varphi,s}^2(t_2) \right]^{\frac{1}{2}}} * \left[\frac{1 - \frac{V_{SC//b}(t_2)}{C} - \frac{V_{SC}(t_2) \cdot (k_{SC-RX} - b)}{c}}{1 - \frac{V_{GS//b}(t_1)}{C} - \frac{V_{GS}(t_1) \cdot (k_{GS-OUT} - b)}{c}} \right] * \omega_{GSRX}(t_1)$$

(3.42)

The general interferometric scheme for the Twoways S/C-GS-S/C configuration is shown in Figure 3-28.

By repeating state superposition propagation similar to the one shown for the Oneway scheme, the following results are obtained:

$$\rightarrow P_{10CV} = \frac{1}{2} \cdot [1 - A \cdot \cos(\phi d - \phi u)] \quad (3.43)$$

$$\rightarrow P_{9CV} = \frac{1}{2} \cdot [1 + A \cdot \cos(\phi d - \phi u)] \quad (3.44)$$

where

$$\rightarrow P_{10CV} + P_{9CV} = 1 \quad (3.45)$$

In the above formula:

- $\phi d =$ Phase accumulated by a photon following the interferometer long path while going downward and short path while going upward;
- $\phi u =$ Phase accumulated by a photon following the interferometer short path while going downward and long path while going upward.
- $\phi d - \phi u =$ Phase accumulated by a photon following the interferometer short path while going downward and long path while going upward.

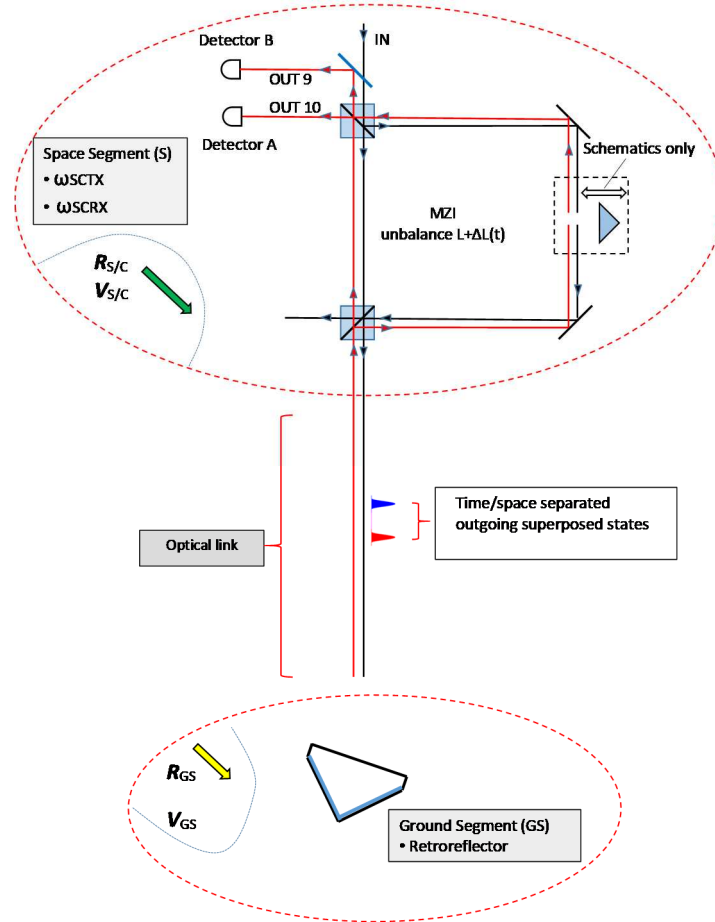


Figure 3-28 General interferometric scheme for the Twoways S/C-GS-S/C configuration

With respect to the Oneway scheme, the Twoways S/C-GS-S/C presents a much smaller useful signal and is not possible to neglect a priori the effect of light bending. The problem of de-phasing and 'classical' Doppler compensation is more complex and, in order to get a realistic order of magnitude on nominal performances, the contribution to de-phasing given by considering Euclidean trajectories (photons straight lines) and the contribution given by the light bending are separately and independently estimated. The overall superposed effect is expected, as order of magnitude, similar to (the largest) of the two independently computed. The overall effect is furthermore affected by the approximation of using physical speeds rather than coordinate speeds and this uncertainty is shown.

De-phasing and Doppler compensation assuming photons straight propagation

Assuming straight lines for photons propagation, the issues of de-phasing and Doppler compensation can be tackled (although more complex) as in the Oneway case. Also here three contributions will be present in the de-phasing: *line effect*, *space effect*, *beatnote effect*. Similarly to Oneway, the space effect and beatnote effect are relative speed dependent and will be nulled by the Doppler compensation algorithm.

To get a realistic order of magnitude on de-phasing we can therefore proceed in the derivation of both de-phasing and Doppler compensation by *considering the line effect only*.

Clearly this time only one interferometer is present and in the derivation it is assumed that during the photon round trip the interferometer length is basically constant with the exception of a *commanded variation* δL necessary for the 'classical' Doppler effects compensation.

The de-phasing is then described as:

$$D\varphi \cong \omega_{TX} * \frac{L_d}{c} - \omega_{RX} * \frac{L_u}{c} \quad (3.46)$$

$$L_u = L_d + \delta L \quad (3.47)$$

The Doppler compensation is then implemented by selection δL such to null the relative speed effects (with an approach similar to the one used for the Oneway configuration):

$$\Delta\omega * \frac{L_d}{c} + \omega_{RX} * \frac{\delta L}{c} = 0 \quad (3.48)$$

$$\Delta\omega = \omega_{RX} - \omega_{TX_{RX}} \quad (3.49)$$

After some manipulation, the compensation correction is computed as:

$$JJJ = \left[\frac{1 - \frac{V_{SC//b}(t2)}{c}}{1 - \frac{V_{GS//b}(t1)}{c}} \right] \left[\frac{1 - \frac{V_{GS//f}(t1)}{c}}{1 - \frac{V_{SC//f}(t)}{c}} \right] \quad (3.50)$$

$$U^{SC}(t2) = \frac{1}{\left[\left(1 - \frac{2GM}{c^2 r_s(t2)} \right) - \left(1 - \frac{2GM}{c^2 r_s(t2)} \right)^{-1} \beta_{r,s}^2(t2) - \beta_{\vartheta,s}^2(t2) - \beta_{\varphi,s}^2(t2) \right]^{\frac{1}{2}}} \quad (3.51)$$

$$U^{SC}(t) = \frac{1}{\left[\left(1 - \frac{2GM}{c^2 r_s(t)} \right) - \left(1 - \frac{2GM}{c^2 r_s(t)} \right)^{-1} \beta_{r,s}^2(t) - \beta_{\vartheta,s}^2(t) - \beta_{\varphi,s}^2(t) \right]^{\frac{1}{2}}} \quad (3.52)$$

$$\delta L = - \frac{\omega_{SCTX}}{\omega_{SCRX}} \cdot \frac{U^{SC}(t2)}{U^{SC}(t)} \cdot (JJJ - 1) \cdot L_d \quad (3.53)$$

However, considering that $\delta L(t)$ has to be computed on line, most of the parameters in the relevant formula are not perfectly known but are rather 'estimates'. The correct formulation for the compensation would then be:

$$\delta L = - \frac{\omega_{SCTX}}{\omega_{SCRX}} \cdot \frac{\widehat{U^{SC}(2)}}{\widehat{U^{SC}(t)}} \cdot (\widehat{JJJ} - 1) \cdot \widehat{L_d} \quad (3.54)$$

where the symbols “ ^ ” stand for best knowledge or estimates of the relevant parameters of physical entities.

The compensation, as mentioned above, has to be implemented in the time interval δL of photon roundtrip. In principle there are two approaches:

- continuously applied compensation by changing the MZI unbalance length at a speed of $\delta L / \delta t = \frac{\delta L}{(t_2 - t)}$;
- continuous compensation applied for given periods followed by a quick recovery (de-saturation) to the initial length.

In the first case the MZI unbalance length may vary a lot over a mission (e.g. 20%-50% of the interferometer initial length) while in the second case the needed length excursion is more limited and several de-saturations will be applied during the mission.

Anyway the ‘two-way’ approach case is, in this respect, more problematic than the ‘one-way’ approach where the length variations were not summing up.

Test cases (all are circular orbits)

Similarly to the Oneway case, the correctness of the compensation algorithm is tested on three Test cases, the same as previously used; being the S/C trajectories circular, no S/C altitude or (absolute) speed variations are present during a roundtrip and therefore *in the frame of the considered assumptions* no de-phase is expected.

A time base relevant to *one complete S/C orbit* is reported even if actual experiments can be carried out for elevations $> 0^\circ$ (e.g. elev. $> 20^\circ$).

(Code: twowayscow160)

Test case 1

Spacecraft: R = 7862 km, i = 50° (circular)
Ground station: Lat = 40.65 N, R = 6370 km
Interferometers: L = 100 m (nominal), Desat. = 10 m

Elevations $> 20^\circ$ in the time range: 2755 s, 4183 s

Theoretical expected de-phasing = 0 rad

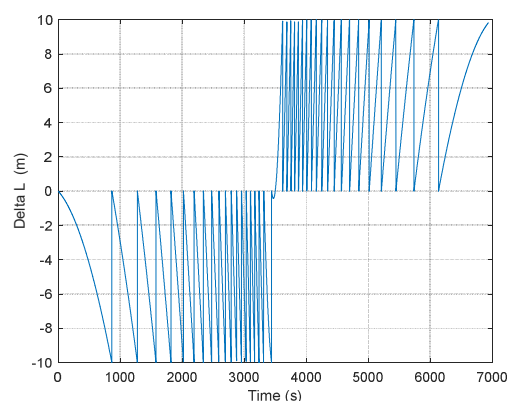
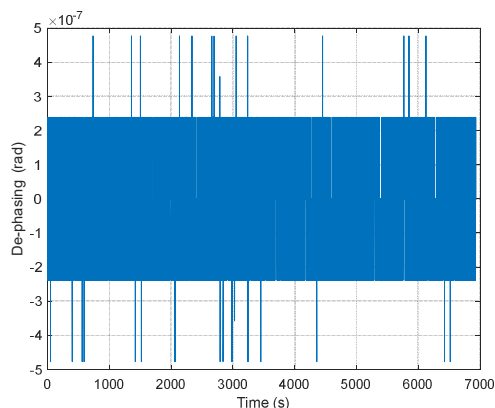


Figure 3-29 Test case 1 de-phasing (left), length correction for Doppler compensation (right)

Method uncertainty $\sim \pm 0.0000005$ rad with 100 m class interferometers

Test case 2

Spacecraft: R = 12000 km, i = 50° (circular)
 Ground station: Lat = 40.65 N, R = 6370 km
 Interferometers: L = 100 m (nominal), Desat. = 10 m

Elevations > 20° in the time range: 4178 s, 8903 s
Theoretical expected de-phasing = 0 rad

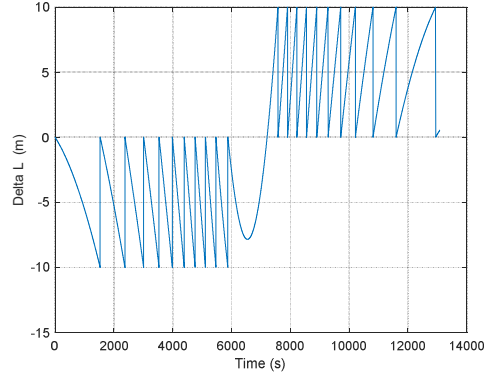
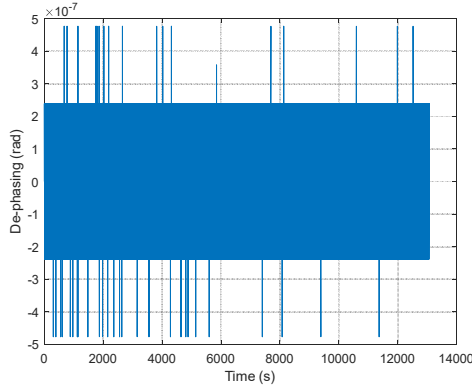


Figure 3-30 Test case 2 de-phasing (left), length correction for Doppler compensation (right)

Method uncertainty ~ +/- 0.0000005 rad with 100 m class interferometers

Test case 3

Spacecraft: R = 18000 km, i = 50° (circular)
 Ground station: Lat = 40.65 N, R = 6370 km
 Interferometers: L = 100 m (nominal), Desat. = 10 m

Elevations > 20° in the time range: 6178 s, 17860 s
Theoretical expected de-phasing = 0 rad

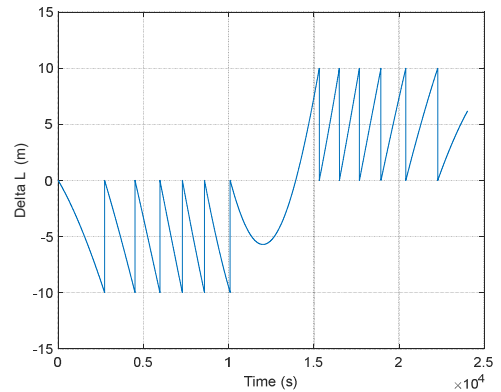
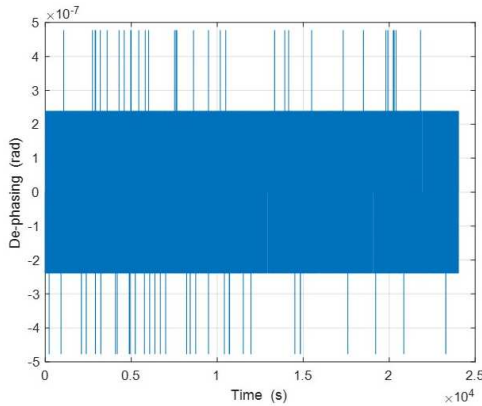


Figure 3-31 Test case 2 de-phasing (left), length correction for Doppler compensation (right)

Method accuracy capability ~ +/- 0.0000005 rad with 100 m class interferometers

De-phasing effects due to light bending

The sole effect of light bending introduces, with respect to the classical Doppler effect, a further slight de-phasing. Since this contribution is not intended to be compensated by the Doppler compensation algorithm, the contribution given by the light bending is then *considered as useful signal (albeit small)*. The frequency variation induced by the sole light bending is treated in Annex-A and the numerical results apply to a test trajectory type T2, which is utilized in the assessment of performance reported in next chapter.

3.2.2 Nominal expected performances on test trajectory T2

The characteristics of the T2 orbital configurations are hereafter recalled:

S/C: in elliptic orbit, apogee passage

- Semi Major axis (apogee) = 32582 km
- Semi Minor axis (perigee) = 23372 km
- Inclination = 0°
- Orbital period = 46571.37608455546 s

GS:

- R = 6370 km
- Latitude = 0°

The analysis (performed with : twowayscow160 code) furthermore assumes the following (as in the Oneway case at previous paragraph):

- Interferometer reference length L = 6000 m, Desat. = 10 m
- Photon coherence time 80 ps;
- Analysis of results are shown for observation elevations $\geq 30^\circ$.

De-phasing without photon trajectory bending contribution

The results for T2 are reported in the hereafter Figure 3-32 and Figure 3-33.

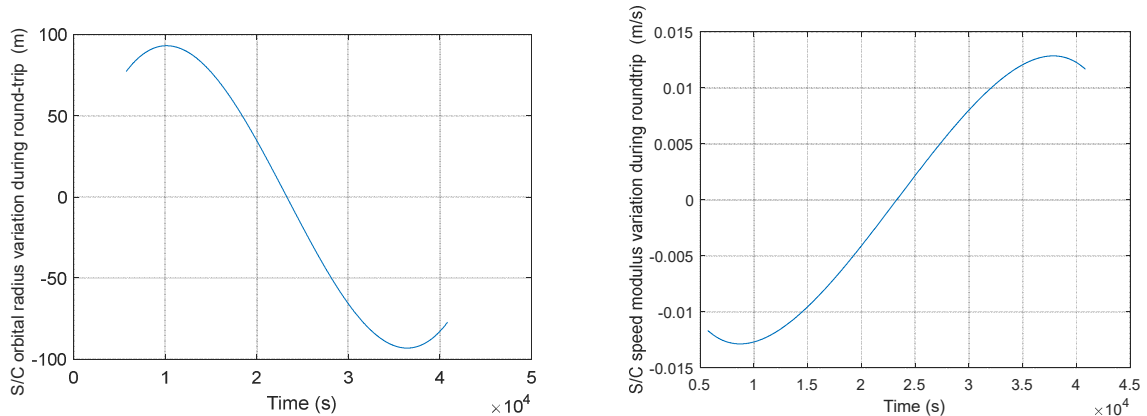


Figure 3-32 S/C radial displacement (left) and speed modulus variation (right) during a roundtrip

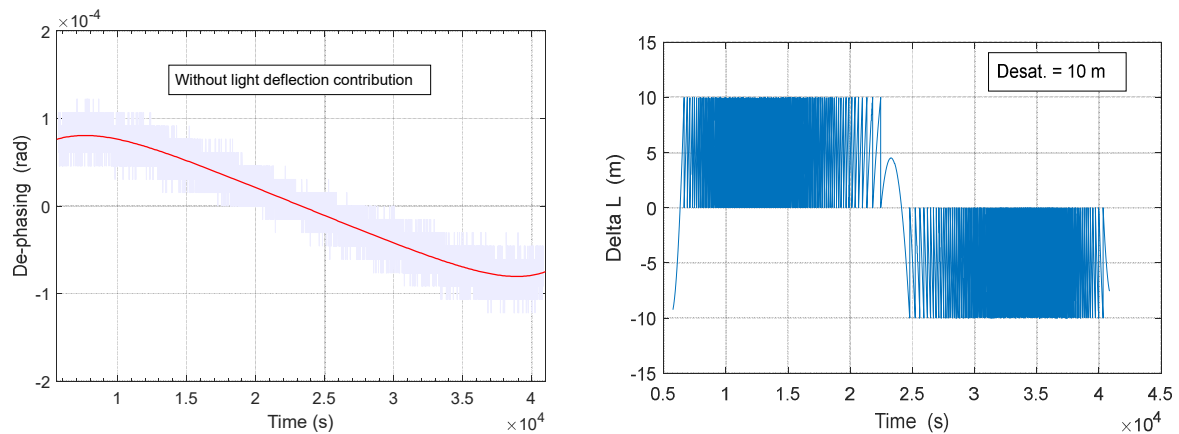


Figure 3-33 De-phasing (left), length correction for Doppler compensation (right)

The following considerations can be done:

- Variation of S/C orbital radius and absolute speed in the time-frame of photon round-trip is as expected quite small; since the Earth is at a constant potential and at a constant speed modulus, the net signal building up de-phasing would result very small;
- The de-phasing variation is consequently very small (10^5 time less than the Oneway case);
- The ground interferometer's length correction (to be applied for the compensation of de-phasing due to the 'classical Doppler effect') requires very large strokes; de-saturations are needed but even in this case the corrections required are of very large amounts.

De-phasing caused by the photon trajectory bending contribution

The presence of light bending induces a Doppler type effect that is not foreseen to be compensated by the used algorithm. This frequency variation between the downward signal and upward signal create a de-phasing on the interfering states. Considering only bending effects, with reference to T2 and to the results reported in Annex-A, the resulting de-phasing for a 6000 m interferometer is as shown in Figure 3-34.

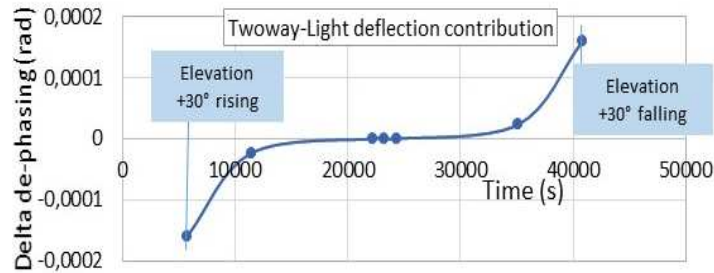


Figure 3-34 De-phasing caused by light deflection contribution

By comparing Figure 3-33 (left) and Figure 3-34 it appears that the two contribution are of the same order of magnitude even if with different temporal distributions.

Superposition between the de-phasing caused by S/C orbital parameter variations and photon trajectory bending contribution

The overall system is not linear but, for the specific case to get a trend, the contributions to frequency variations given by the S/C orbital parameters variation and given by trajectory bending can be placed in an additive form derived from the previously given relations:

$$\frac{\delta\omega}{\omega} \cong \frac{\left[\left(1 - \frac{2HM}{C^2 r_s(t)} \right) - \left(1 - \frac{2HM}{C^2 r_s(t)} \right)^{-1} \beta_{r,s}^2(t) - \beta_{\theta,s}^2(t) - \beta_{\phi,s}^2(t) \right]^{\frac{1}{2}}}{\left[\left(1 - \frac{2HM}{C^2 r_g(t1)} \right) - \beta_{\phi,g}^2(t1) \right]^{\frac{1}{2}}} + \left[- \frac{V_{GS}(t1) \cdot (k_{GS-IN} - f)}{c} + \frac{V_{SC}(t) \cdot (k_{SC-TX} - f)}{c} - \frac{V_{SC}(t2) \cdot (k_{SC-RX} - b)}{c} + \frac{V_{GS}(t1) \cdot (k_{GS-OUT} - b)}{c} \right] \quad (3.55)$$

The results for de-phasing and probabilities are shown in Figure 3-35.

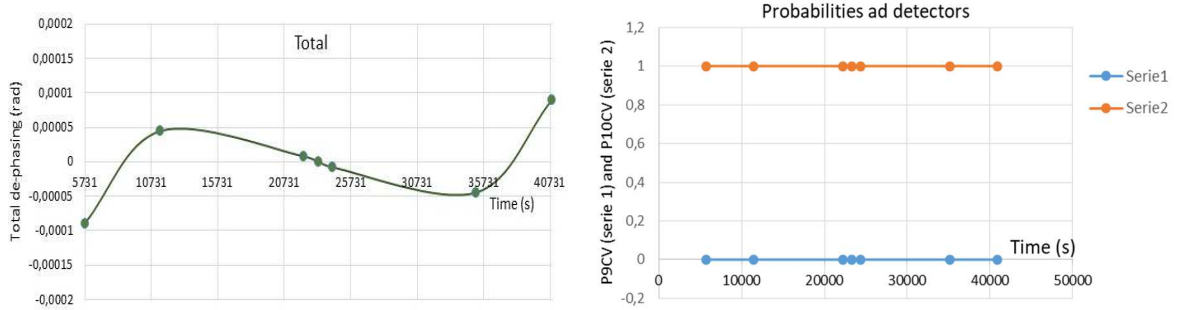


Figure 3-35 Order of magnitude for the total de-phasing

As already pointed out a further imprecision, which can also be important in this case, arises from using physical speeds rather than coordinate speed and such imprecision value changes along the trajectory (see also Annex-B).

For the specific case in Figure 3-36 are reported the value of $|V_{sc}/-V_{gs}|$ (on the left, from which the imprecision depends) and the associated imprecision on the de-phasing value (on the right).

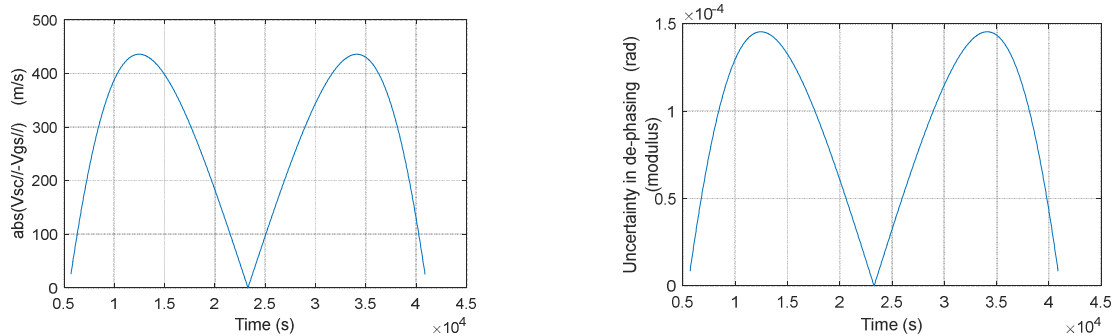


Figure 3-36 Absolute value of relative speed (left) and imprecision in de-phasing (right)

In this case the uncertainty introduced by using physical speeds instead of coordinate speeds has the same order of magnitude (even larger by a factor of two) than the useful signals.

As remark the de-phasing excursion (useful signal) available in the Oneway configuration exceeds by a factor 10^4 - 10^5 whatsoever signal available from the Twoways S/C-GS-S/C configuration.

3.3 Twoways configuration GS-S/C-GS

3.3.1 General and expected performance on test trajectory T2

This configuration utilize one interferometer only located on ground (at the GS) while the spacecraft is in charge to the back reflection. The overall system schematics with light beams trajectories sketched is shown in Figure 3-37.

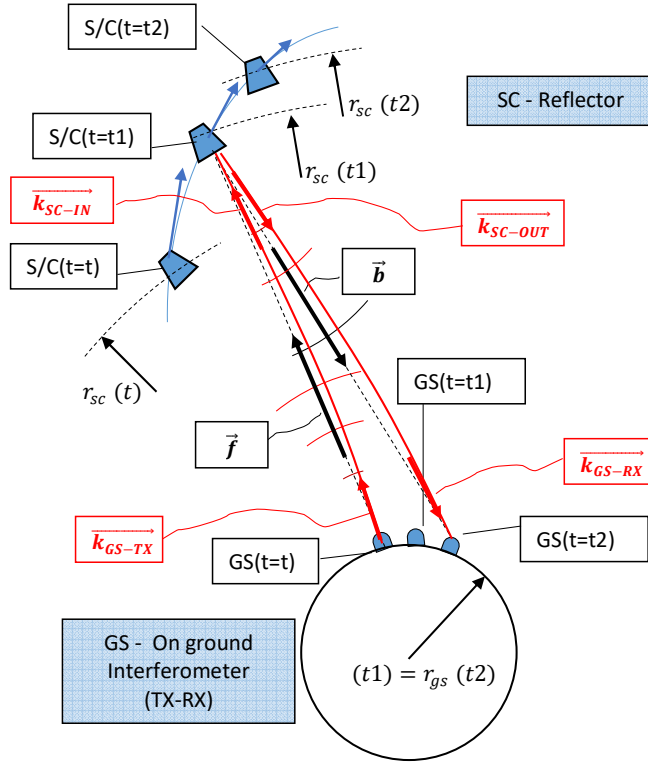


Figure 3-37 Twoways GS-S/C-GS configuration with schematics of curved light beams (not to scale)

In this scheme a generic photon/state emitted by the GS at time t , reaches the S/C at time $t1$ and, upon reflection, arrives back to the GS at time $t2$ (all this without counting the delays on the interferometry lines). The vectors in black are Euclidean while in red are schematically shown the wave vectors. The remaining symbols and convention used are similar to the ones already introduced.

A generic photon or state is *received back by the GS that is displaced (in position and speed) but always at the same potential and with the same speed modulus*.

The overall geometry is as complex as the Twoways S/C-GS-S/C and the relation between a transmitted photon transmitted frequency and the same photon received frequency is of the following type (which can be derived from the Oneway and Twoways relations and Ref. [8]):

$$\begin{aligned}
 \omega_{SCRX}(t1) &\cong \frac{\left[\left(1 - \frac{2HM}{c^2 r_g(t)} \right) - \beta_{\phi,g}^2(t) \right]^{\frac{1}{2}}}{\left[\left(1 - \frac{2HM}{c^2 r_s(t1)} \right) - \left(1 - \frac{2HM}{c^2 r_s(t1)} \right)^{-1} \beta_{r,s}^2(t1) - \beta_{\theta,s}^2(t1) - \beta_{\phi,s}^2(t1) \right]} * \left[\frac{1 - \frac{V_{SC//f}(t1)}{c} - \frac{V_{SC}(t1) \cdot (k_{SC-IN} - f)}{c}}{1 - \frac{V_{GS//f}(t)}{c} - \frac{V_{GS}(t1) \cdot (k_{GS-TX} - f)}{c}} \right] * \omega_{GSTX}(t) \\
 \omega_{GSRX}(t2) &\cong \frac{\left[\left(1 - \frac{2HM}{c^2 r_s(t1)} \right) - \left(1 - \frac{2HM}{c^2 r_s(t1)} \right)^{-1} \beta_{r,s}^2(t1) - \beta_{\theta,s}^2(t1) - \beta_{\phi,s}^2(t1) \right]}{\left[\left(1 - \frac{2HM}{c^2 r_g(t2)} \right) - \beta_{\phi,g}^2(t2) \right]^{\frac{1}{2}}} * \left[\frac{1 - \frac{V_{GS//b}(t2)}{c} - \frac{V_{GS}(t2) \cdot (k_{GS-RX} - b)}{c}}{1 - \frac{V_{SC//b}(t1)}{c} - \frac{V_{SC}(t1) \cdot (k_{SC-OUT} - b)}{c}} \right] * \omega_{SCTX}(t1)
 \end{aligned}
 \tag{3.56}$$

Taking in consideration the peculiarity above described of the Twoways GS-S/C-GS configuration the relation between the transmitted frequency and the back received frequency simplifies into:

$$\omega_{GSRX}(t_2) \cong \left[\frac{1 - \frac{v_{GS}/b(t_2)}{c} - \frac{v_{GS}(t_2) \cdot (k_{GS-RX} - b)}{c}}{1 - \frac{v_{SC}/b(t_1)}{c} - \frac{v_{SC}(t_1) \cdot (k_{SC-OUT} - b)}{c}} \right] * \left[\frac{1 - \frac{v_{SC}/f(t_1)}{c} - \frac{v_{SC}(t_1) \cdot (k_{SC-IN} - f)}{c}}{1 - \frac{v_{GS}/f(t)}{c} - \frac{v_{GS}(t_1) \cdot (k_{GS-TX} - f)}{c}} \right] * \omega_{GSTX}(t) \quad (3.57)$$

From the above it is clear that *the direct influence of the metric related parts disappear* and the relativistic effect remaining is associated to light bending (since this is not assumed compensated by the classical Doppler compensation algorithm).

The computation of de-phasing and the Doppler compensation algorithm in principle follows the same lines as already seen for the Oneway and Twoways S/C-GS-S/C schemes and the procedure is not any more repeated. In this case, as stated above, the expected de-phasing considering an Euclidean straight trajectory for the light beams is zero.

The general interferometric scheme for the Twoways GS-S/C-GS configuration is shown in Figure 3-38.

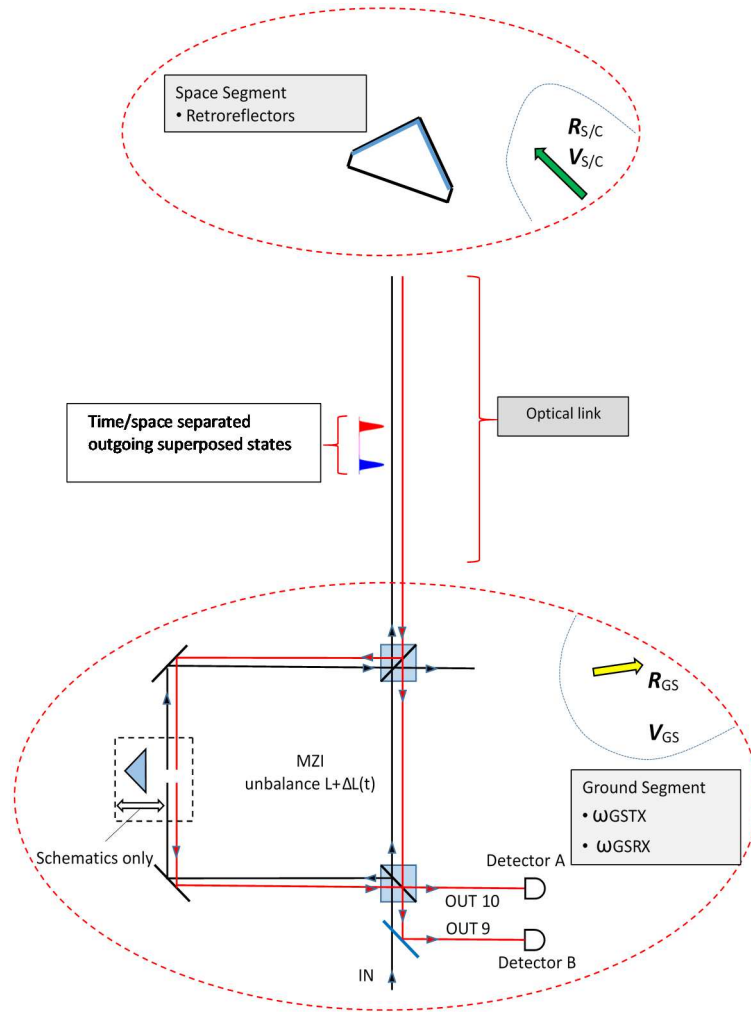


Figure 3-38 General interferometric scheme for the Twoways S/C-GS-S/C configuration

For completeness in Figure 3-39 are reported the expected de-phasing without trajectory bending contributions (left, expected in this case to be zero) and length correction for classical Doppler compensation (right). In Figure 3-40 is reported the contribution due to trajectory bending alone (given in Appendix-A and practically the same as the case Twoways S/C-GS-S/C). Test trajectory T2 has been used and is recalled to be:

S/C: in elliptic orbit, apogee passage

- Semi Major axis (apogee) = 32582 km
- Semi Minor axis (perigee) = 23372 km
- Inclination = 0°
- Orbital period = 46571.37608455546 s

GS:

- R = 6370 km
- Latitude = 0°

The analysis (performed with: twcow_gs_sc_gs_120 code) as before assumes an interferometer 6000 m unbalance.

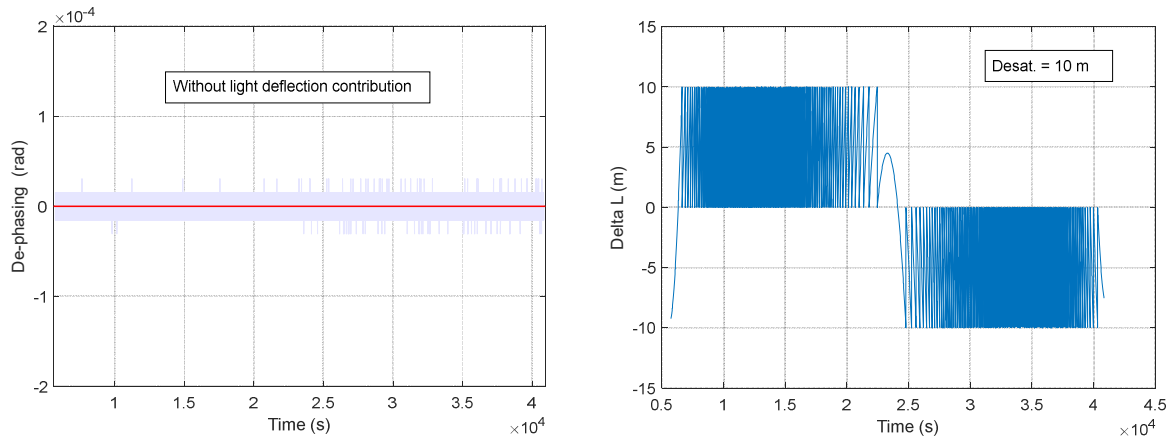


Figure 3-39 Expected de-phasing without trajectory bending contribution (left) and trajectory bending contribution (right)

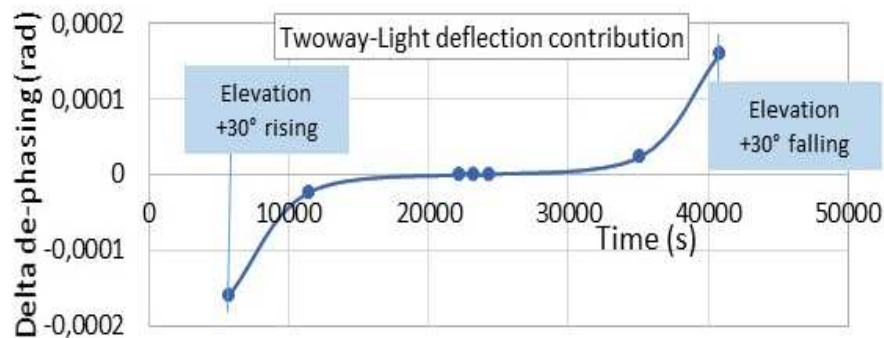


Figure 3-40 Expected de-phasing due to trajectory bending contribution

Similarly to the Twoways S/C-GS-S/C case the uncertainty introduced by using physical speeds instead of coordinate speeds has the same order of magnitude (even larger by a factor of two) than the useful signals.

Again, as remark, the de-phasing excursion (useful signal) available in the Oneway configuration exceeds by a factor 10^4 - 10^5 whatsoever signal available from the Twoways GS-S/C-GS configuration.

3.3.2 Previous utilization of Twoways GS-S/C-GS like configuration

The Twoways GS-S/C-GS configuration has already been considered and used in ‘quantum type’ research in previous studies and experiments as given for example in Ref. [20], Ref. [21], Ref. [5]. The reason being due to availability and cost issues: indeed a number of Spacecraft installing retro-reflectors *are already in orbit* and as far as Ground Stations a number of Satellite Laser Ranging facilities are present in which the *adaptations to implement the interferometric part can be made*.

In particular Ref.[5] describes an experimental activity on single photon quantum interference utilizing the Matera Laser Ranging Observatory (MLRO) facility, equipped with a dedicated interferometric part, and three satellites in Low-Earth-Orbit (LEO) (Beacon-C, Stella and Ajisai) which are equipped with efficient cube-corner retroreflectors (CCR). In the performed experiment, implemented by using a 1 m unbalanced Mach Zender Interferometer (MZI), the objective was to verify for *single photon quantum interference modulated by a de-phasing caused by the ‘classical Doppler effect’*. No Doppler compensation algorithm was present and the de-phasing caused by the Doppler effect was overwhelming with respect to the effects caused by space time curvature (by an estimated 10^5 factor).

The Ajisai tracking is hereafter simulated, also for verification, with `twcow_gs_sc_gs_120` code *excluding the Doppler compensation algorithm*. The following conditions are used:

- Spacecraft orbit (Ajisai): circular, semi axis= 7862 km, inclination= 50°
- GS: Matera MLRO (latitude= 40.65° N, R=6370 km)
- Interferometer length= 1m

An extract of simulated results in a time interval from approximately -420 s to -200 s from maximum elevation transit are shown in Figure 3-41 as far as de-phasing and probability at detector # 10.

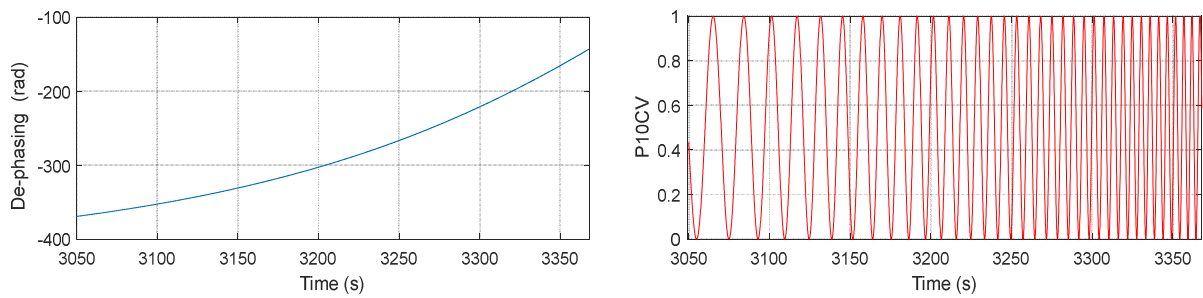


Figure 3-41 Extract of simulated results for de-phasing and probability (Doppler compensation algorithm excluded)

The obtained de-phasing is in this case very large in the simulated conditions (since dominated by Doppler effects); clearly, detecting the sole effects of space-time curvature on interference has a different degree of complexity.

3.4 Selection of configuration

The three configurations previously described present strong differences in terms of cost and time availability, technological difficulty and clearly potential scientific return. In this respect the key characteristics of the three configurations are hereafter discussed.

Oneway configuration

This configuration presents the best characteristics in terms of useful signal allowing an experiment *based on direct photon counting* at (two) detectors to provide, nominally, reconstructed de-phasing information, visibility and interference existence with good confidence/accuracy. It is by far the most complex since it makes use of two interferometers, ideally equal, which need to be guaranteed in terms of calibration and geometrical stability. Furthermore a dedicated Spacecraft need be placed on orbit (after an adequate development, qualification and flight launch phase) with cost and time impacts typical of a space program, even if the spacecraft can be in the 'small satellite' class.

Twoways S/C-GS-S/C configuration

The final useful signal (in this case the superposition of two contributions a directs metric one and a trajectory bending one) of the same order of magnitude, result *much smaller* than the Oneway case. An experiment based on direct photon counting would not be in a condition to provide an acceptable level of scientific return, even in nominal conditions. The situation would even be worse in a real case where inaccuracies on the knowledge of the system state are present and which affect the compensation algorithm of the classical Doppler compensation. With respect to the Oneway case, this configuration utilizes one interferometer only thus basically nulling the calibration and geometrical stability aspects. A newly developed spacecraft is however still be needed with an expected cost-schedule reduction quite modest with respect to the Oneway configuration.

Twoways GS-S/C-GS configuration

This configuration do not need a dedicated new spacecraft and in principle could be done by using one of the already existing in orbit spacecraft equipped with retro-reflectors (many are available). In this respect, this would provide a real drastic reduction in terms of cost and schedule. Also in this case use of one interferometer only (this time on ground) basically null the calibration/stability aspects. Unfortunately the signal available (this time only the contribution of light trajectory bending) would be extremely small, of the same order as the Twoways S/C-GS-S/C above described, jeopardizing the scientific return.

Table 3-1 synthetize the key comparative considerations: *the selected basic configuration is Oneway.*

<i>Basic configuration: Oneway GS→SC</i>	
Pros:	- Very useful and strong 'signal' available
Cons:	- Needs development and launch of dedicated satellite - Two Interferometers to 'handle/calibrate' (one on board, one on ground) - High cost
<i>Alternative configuration: Twoway S/C→GS→SC</i>	
Pros:	- One Interferometer only to 'handle' (on board)
Cons:	- Ultra small 'signal' available $\approx 10^{-5} - 10^{-4}$ of Oneway - Needs development and launch of dedicated satellite - Medium/high cost
<i>Alternative configuration: Twoway GS→S/C→GS</i>	
Pros:	- No needs development and launch of dedicated satellite - One Interferometer only to 'handle' (on ground) - Low cost
Cons:	- Ultra small 'signal' available $\approx 10^{-5} - 10^{-4}$ of Oneway

Table 3-1 Summary of comparison

(Page Intentionally Left Blank)

4 ONEWAY CONFIGURATION: ANALYSIS OF PERFORMANCE IN A REFERENCE EXPERIMENTAL SCHEME

4.1 Reference orbit (R1), reference GS and reference Interferometer length

Reference Orbit (R1) and reference GS

For the selected Oneway configuration a dedicated Spacecraft (specifically designed and placed in a suitable orbit) is needed and dedicated instrumentation need be implemented at the Ground Station.

In general an orbit with high apogee and low perigee would provide a good variation of gravitational potential and speeds (entering both the metric part) to allow for a good scientific signal. Typical launchers class Arian, Proton, Titan have no limitations at all in this respect (but launch may be quite expensive and of long handling).

However since Italy/ASI are strongly involved in VEGA launcher program ('small launcher') and also on mini satellites (e.g. PLATINO), it has been considered the possible utilization of VEGA C to place on a suitable orbit a (mini) satellite of 500 kg class. The orbit should have an inclination decently well placed to allow the possible experimentation to be carried out from the Matera Laser ranging base or low latitude bases (like Haleakala, San Fernando,).

VEGA C (an evolution of the current VEGA launch system) is not yet operative and should be tested in the inaugural flight scheduled by end 2019. According to the User Manual (see Ref. [22]) the launcher is expected have a *typical launch capability* (when referred to an almost equatorial, elliptic orbit) of the following type:

- Altitude of apogee, $h_a = 5700$ km (semi-axis = 12072 km)
- Altitude of perigee, $h_p = 250$ km (semi-axis= 6622 km)
- Inclination, $i = 6.0$ degrees
- Payload capability (up to) = 1700 kg including adapter.

This is a *capability* and the detailed achievable overall launch envelope (payload mass vs. inclination vs. apogee vs. perigee) need be verified in a specific phase with the launch organization (Arianspace).

As a preliminary estimate a verification has been performed utilizing a simulation software developed by Silverbird Astronautics (Ref.[23]) in order to get an achievable reference orbital conditions for a payload in the order of 500 kg (about 570 kg including adaptor) placed in 28° inclination orbit. Based on this evaluation *the following orbital conditions appear achievable*:

- Semi major axis = 22000 km ($h_a=11628$ km)
- Semi minor axis = 8000 km ($h_p=3628$ km)
- Inclination = 28°
- Max P/L mass (plus adapter) = 743 kg (95% confidence level 609 – 891 kg)

therefore compatible with an expected mass of 570 kg. This orbital conditions *are taken as reference*.

As far as the GS, Matera MLRO (see Ref. [24]) is considered; the following approximate coordinates hold:

- Radius = 6370 km
- Latitude 40.65° N
- Longitude= 16.70° E

Reference Interferometer length

The useful signal (variation of de-phasing during one S/C passage) is, among others, proportional to two parameters:

- the overall physical altitude excursion of the S/C in the passage;
- the interferometer length.

On the other hand, the longer the interferometers the more severe conditions exist for:

- their calibration;
- the requirements placed on the needed accuracy of S/C-GS relative speed knowledge (in order to implement an efficient Doppler compensation algorithm, see sensitivity analysis).

The orbital conditions taken as reference provides a good excursion in altitude for the S/C within the orbit and, although longer MZI unbalances have also been considered, it appears that nominal Interferometers length in the order of:

$$L_{\text{Interferometer-S/C}} = L_{\text{Interferometer-GS}} = 400 \text{ m}$$

can be considered for the purpose of this analysis. Other values can of course be selected in case.

4.2 Nominal performances under reference conditions

The nominal performances have been evaluated (performed with cowsim292moddephaseB code) under the reference conditions assumed and the results are hereafter summarized.

The following considerations apply:

- The key input data are reported in Table 4-1. In the left part are given the reference conditions while in the right part are listed the physical parameters that, afterward, will be used for the sensitivity analysis. The symbol used are somehow explicative;
- In Figure 4-1 left is shown the elevation of observation for one complete S/C orbit; clearly only when the elevation is positive and above to an assumed value (in this case selected as 20°) the observation is possible. In all remaining figures the data are shown from Time = 3130 s to Time = 15150 s and in this interval is Elev. > 20°;
- In Figure 4-1 right is shown the approximate layout of the S/C orbit (in its orbital plane) and the GS in the possible experimentation interval (note: the view is approximate since S/C and GS do not move on the same plane);
- In Figure 4-2 left is given the plot of the de-phasing: this signal (the useful signal) presents an cumulative excursion of about 2π in the experimentation window.
- In Figure 4-2 right is reported the visibility trend; basically with photons of *about 80 ps* of coherence time, no reduction of visibility is present in nominal conditions (this will not be anymore the case during sensitivity analysis)

BB - Satellite PERIGEE or APOGEE (w.r.t. e. c.)...=8000000 m AA - Satellite APOGEE o PERIGEE (w.r.t. e. c.)...=22000000 m INCLD - Orbit inclination.....=28 deg Orbital period TT= 1.828328566550028e+04 s Half orbital period= HOP = 9.141642832750142e+03 s LAMBDA GS - Latitude of GS.....=40.65 deg RGS - Ground Station altitude (w.r.t.earth centre)....=6370000 m LONGIGS0 - Initial GS longitude (@ t=0)... =-HOP*OMEGAGS rad TIN - Initial simulation time= 0 s TFIN - Final simulation time.....=18283.285 s DDTT - Satellite trajectory simulation step=0.001 s DT - Output simulation step (> DDTT - in 10 x multiples) ...=1 s λ = Wavelength= 532 nm TAUCP - Coherence time.....=80 ps	rbias - Satellite POSITION measurement bias.....=0 m noise - Satellite POSITION measurement noise (1 sigma)....=0 m vbias - Satellite SPEED measurement bias.....=0 m/s vnoise - Satellite SPEED measurement noise (1 sigma).....=0 m/s pcbiasn - Prism control bias error=0 nm pcnoisen - Prism control noise error(1 sigma).....=0 nm SCSABSERROR absolute speed scale error...(e.g. 1+/- xxx)....=1 GSSABSERROR absolute speed scale error...(e.g. 1+/- xxx)....=1 SCGSPERROR absolute rpos scale error...(e.g. 1+/- xxx).....=1 L1ID - Ideal length of ground interferometer.....=400 m L2ID - Ideal length of space interferometer.....=400 m Delta L2-L1 geometrical instability (thermomech.I)...= 0 μ m Feed Back DL1: (YES=1, NO=0)=1 Prism DISTURBANCES activation: (YES=1, NO=0)=0
---	--

Table 4-1 Simulation general input data

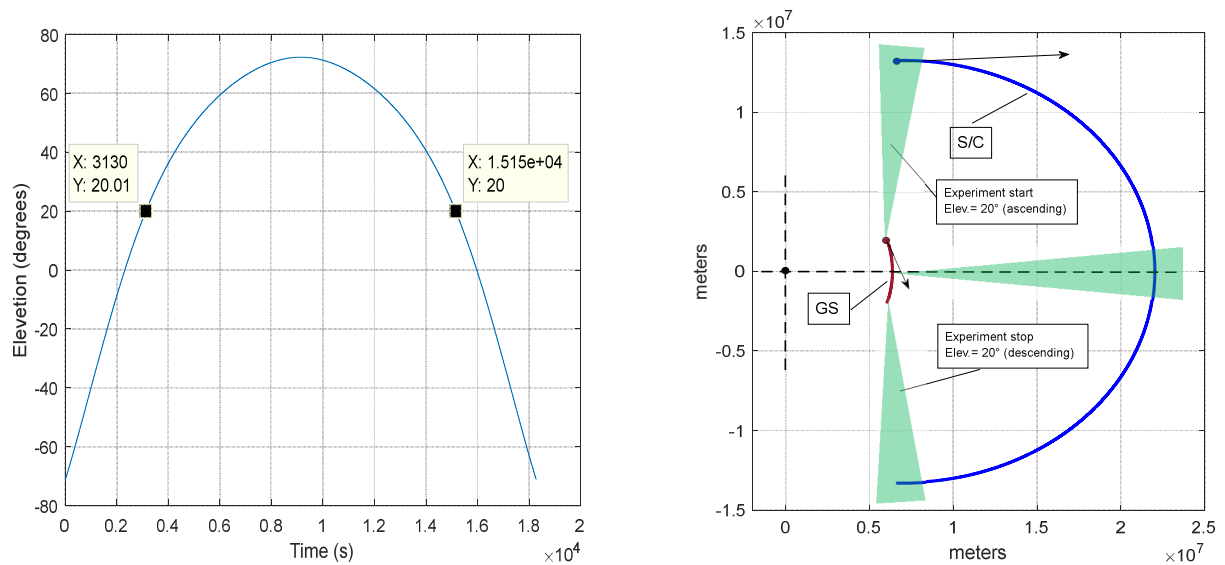


Figure 4-1 Elevation (left), approximate lay-out with S/C orbit shown in orbital plane (right)

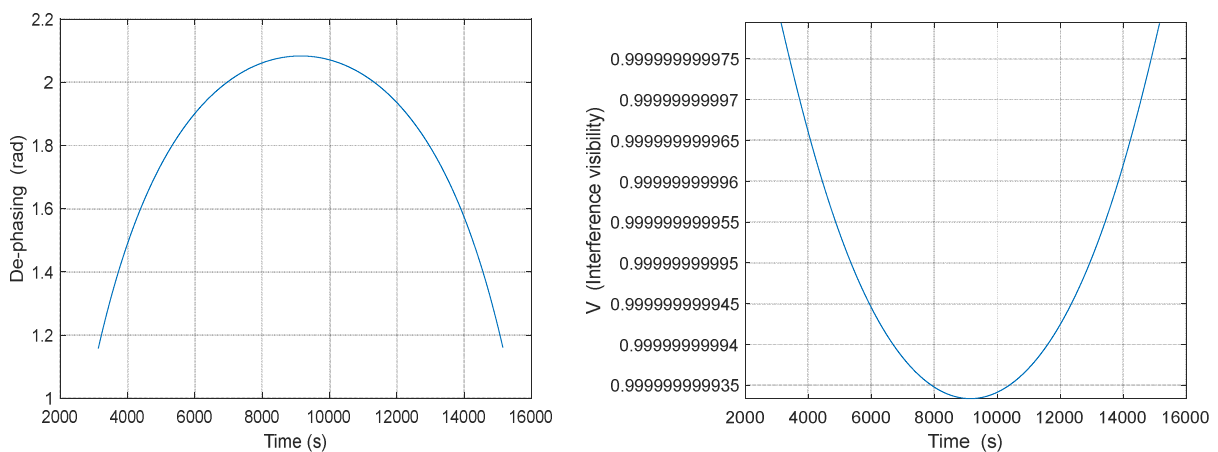


Figure 4-2 De-phasing (left), Visibility (right)

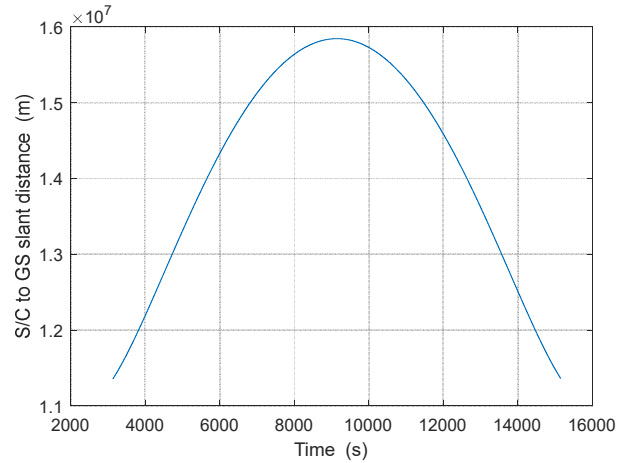
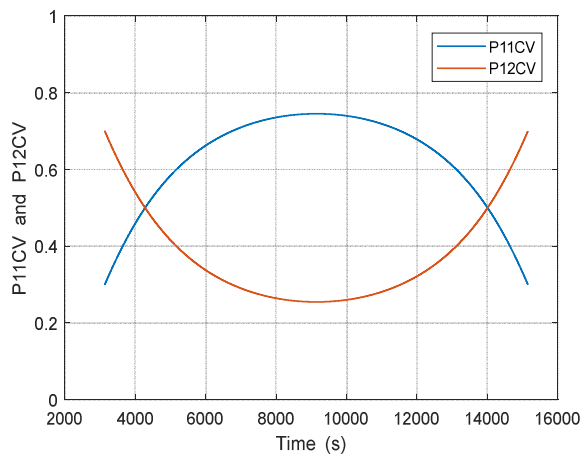


Figure 4-3 Probabilities at detectors SPAD11 and SPAD12 (left), S/C-GS slant distance (right)

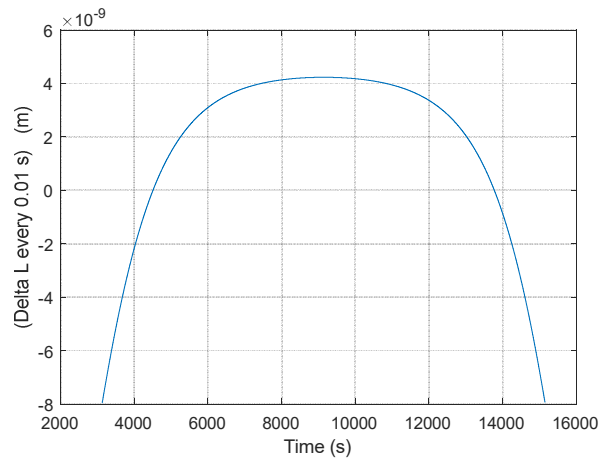
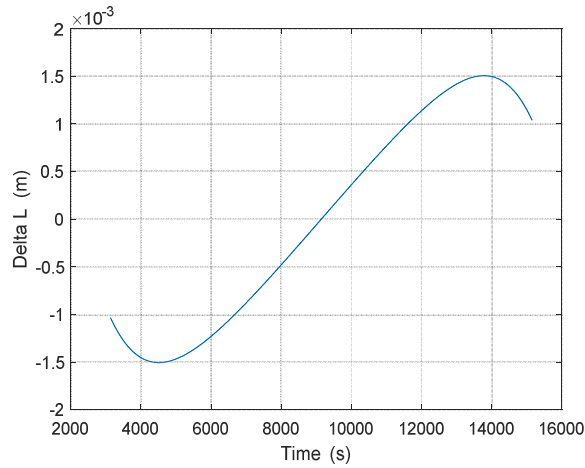


Figure 4-4 Delta L as function of time (left), needed Delta L every 0.01 (s) (right)

- In Figure 4-3 left are shown the probabilities at detectors (SPAD11 and SPAD12) and decently good variations are observed (based on the variation of de-phasing);
- In Figure 4-3 right is reported (for information) the S/C-GS slant distance during the observation period;
- In Figure 4-4 left is reported the variation of length of the ground Interferometer to apply/control in order to implement the 'classical Doppler compensation'; from the figure it appears that if the variation were applied as it appears a total stroke of about 3 (mm) would be needed but this will not be the case. The required length correction is intended to be applied, as already pointed out, 'in time (ready) and stable' for the transit of the trailed photon state in the long arm of the ground interferometer.
- In Figure 4-4 right is reported the corresponding diagram of the length corrections occurring every 0.01 s interval; this data is important in conjunction with the results of sensitivity analysis and the characteristics of the linear nano-positioners introduced in the relevant chapters.

4.3 Sensitivity analysis

The sensitivity analysis is carried out against a number of parameters that affect the effectiveness of interference directly, the 'classical Doppler' compensation algorithm, the visibility. All this clearly have direct impact on the goodness of the measured de-phasing curve and probabilities.

Specifically the following parameters are considered (Table 4-2):

Parameter
<ul style="list-style-type: none"> ▪ <i>rbias</i> - Satellite POSITION knowledge bias ▪ <i>rnoise</i> - Satellite POSITION knowledge noise (1 sigma) ▪ <i>vbias</i> - Satellite SPEED (S/C-GS radial) measurement bias ▪ <i>vnoise</i>-Satellite SPEED (S/C-GS radial) measurement noise ▪ <i>pcbiasn</i> - Prism control bias error ▪ <i>pcnoisen</i> - Prism control noise error(1 sigma) ▪ δ L1ID – Perturbation on Ideal length of ground interferometer (multiple wavelength) ▪ δ L2ID – Perturbation on Ideal length of space interferometer (multiple of wavelength) ▪ Delta L2-L1 calibration-calibration and geometrical stability included

Table 4-2 Parametes utilized for sensitivity

The perturbation given to the input parameters have been set only as *explorative* to get sensitivity and the obtained perturbed de-phasing curves have been superimposed to the nominal expected one with boundary margins set at of +/- 0.09 (radians), approximately +/- 5°. (Code: cowsim292moddephaseB)

4.3.1 Sensitivity to each of the parameters

➤ Sensitivity to Satellite position knowledge

The set of exploring accuracies are.

- *rbias* - Satellite POSITION knowledge bias..... = 5 m
- *rnoise* - Satellite POSITION knowledge noise (1 sigma)....= 1.5 m

The results obtained are reported in Figure 4-5.

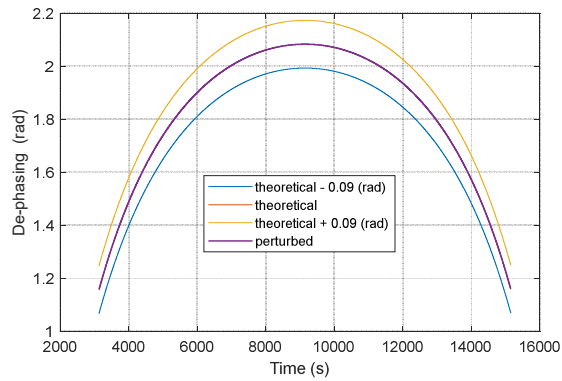


Figure 4-5 Sensitivity against Satellite position knowledge

As observation, the perturbed curve is practically superimposed to the theoretical curve.

➤ Sensitivity to Satellite speed (S/C-GS radial)

The set of exploring accuracies are:

- v_{bias} - Satellite SPEED (S/C-GS radial) measurement bias..... = 0.002 m/s
- v_{noise} -Satellite SPEED (S/C-GS radial) measurement noise (1 sigma).. = 0.0002 m/s

The results obtained are reported in Figure 4-6.

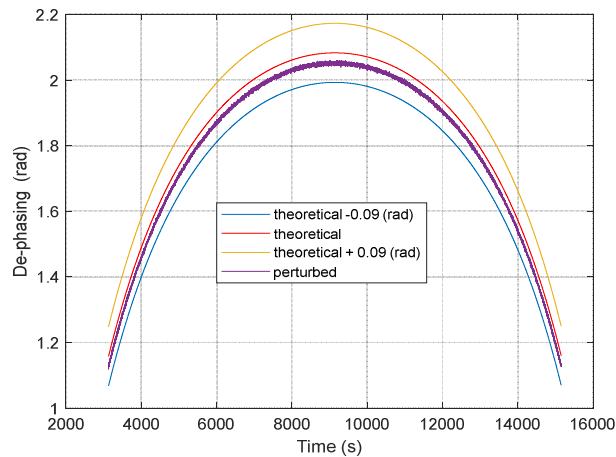


Figure 4-6 Sensitivity against S/C-GS relative speed knowlwdgw

As appears from the figure, the sensitivity appears to be ~ -150 rad/(m/s).

➤ Sensitivity to Prism control error

The set of exploring accuracies are:

- pc_{biasn} - Prism control bias error = 4 nm
- pc_{noisen} - Prism control noise error(1 sigma)..... = 0.4 nm

The results obtained are reported in Figure 4-7.

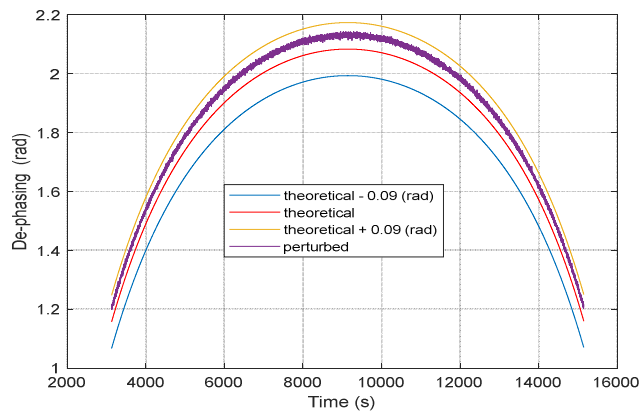


Figure 4-7 Sensitivity against Prism control errors

As appears from the figure, the sensitivity appears to be ~ 0.01 rad/(nm).

➤ Sensitivity to perturbation on length of ground interferometer (multiple wavelength)

The set exploring accuracies are:

- $\delta L1ID$ -Perturbation (multiple wavelength) on Ideal length of ground interferometer.....
 $= 400.000532 (+1000 \lambda) \text{ m}$

The results for the perturbed de-phasing curve are obtained are reported in Figure 4-8 (left) while in Figure 4-8 (right) is shown the comparison (with the perturbed curve scaled down by a constant $1000 \cdot 2 \cdot \pi$ rad).

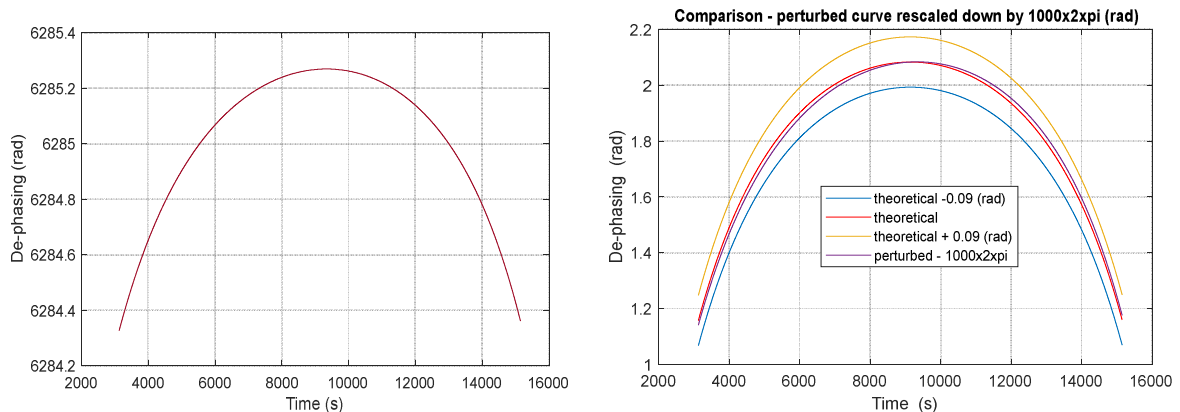


Figure 4-8 Sensitivity against perturbation (multiple wavelength) of ground interferometer

As appears from the figure, some skewness and asymmetry appears in the order of 0.01 rad.

➤ Sensitivity to perturbation on Ideal length of S/C interferometer (multiple wavelength)

The set of exploring accuracies are:

- $\delta L2ID$ -Perturbation (multiple wavelength) on Ideal length of S/C interferometer.....
 $= 400.000532 (+1000 \lambda) \text{ m}$

The results for the perturbed de-phasing curve obtained are reported in Figure 4-9 (left) while in Figure 4-9 (right) is shown the comparison (with the perturbed curve scaled up by a constant $1000 \cdot 2 \cdot \pi$ rad).

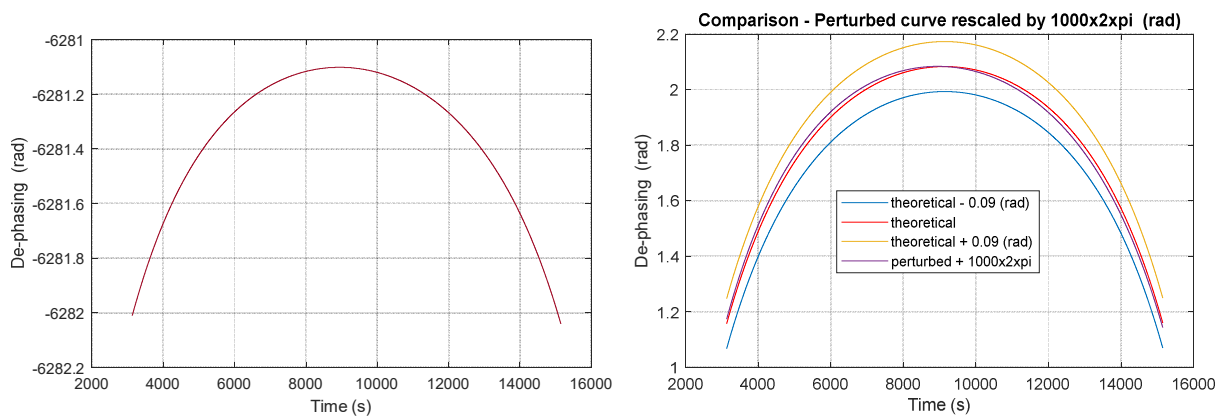


Figure 4-9 Sensitivity against perturbation (multiple wavelength) of ground interferometer

As appears from the figure, some skewness appears in the order of 0.01 rad. This skewness and asymmetry is opposite to the one of the Ground interferometer since the two perturbations have been kept of the same sign.

➤ Sensitivity to delta L2-L1 calibration-calibration and geometrical stability included

This perturbation includes the residual of calibration and the geometrical stability from calibration to calibration. The set of exploring accuracies are:

- *Delta L2-L1 calibration-calibration and geometrical stability included = 0.008 μm*

As appears from Figure 4-10, the sensitivity appears to be $\sim -0.01 \text{ rad}/(\text{nm})$ clearly the same (in modulus) as the sensitivity to prism control.

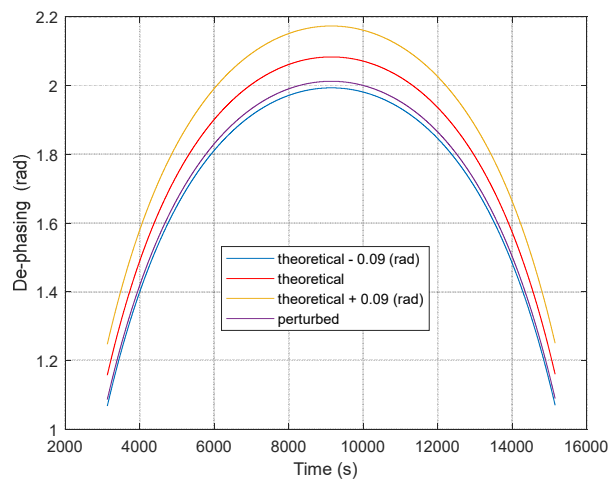


Figure 4-10 Sensitivity to Delta L2-L1 parameter

4.3.2 Sensitivity to all parameters superimposed and tentative requirements

All parameters uncertainty evaluated in the previous paragraph are now superimposed with the sign taken such to add-up all perturbations so to create a worst case combination:

- *rbias – Satellite POSITION knowledge bias..... = 5 m*
- *rnoise – Satellite POSITION knowledge noise (1 sigma).... = 1.5 m*
- *vbias – Satellite SPEED (S/C-GS radial) measurement bias..... = - 0.002 m/s*

- *vnoise-Satellite SPEED (S/C-GS radial) measurement noise (1 sigma)..= 0.0002 m/s*
- *pcbiasn – Prism control bias error = 4 nm*
- *pcnoisen – Prism control noise error(1 sigma)..... = 0.4 nm*
- *δ L1ID-Perturbation (multiple wavelength) on Ideal length of ground interferometer..... = 400.000532 (+ 1000 λ) m*
- *δ L2ID-Perturbation (multiple wavelength) on Ideal length of ground interferometer..... = 399.999468 (- 1000 λ) m*
- *Delta L2-L1 calibration-calibration and geometrical stability included = - 0.008 μ m*

The obtained results for de-phasing and probabilities are shown in Figure 4-12, Figure 4-13 and Figure 4-13. Considering also the previous results on sensitivity, the following points are noted:

- With the values of perturbation used (considered only as explorative values), the de-phasing error amounts to about 0.2 – 0.22 rad, approximately 11 – 12 deg;
- The sign values taken are a worst case condition since the six basic contributions (S/C position, S/C speed, Prism control, 'multiple wavelength' length perturbation of S/C and GS interferometers and calibration/geometrical stability, have all been chosen to be additive;
- The most large contribution comes from the '*calibration-calibration and geometrical stability*' which perturbation of 8 nm should be tried to be reduced. As tentative requirement a reference value of 4 nm could be considered;
- Also the prism control error gives a significant contribution. A reduction on the assumed input perturbation of 4 nm might be possible but likely requires a specific dedicated development activity. As a tentative requirement a value of 3 nm could be considered;
- The relative S/C-GS speed measurement accuracy should also tried to be reduced (it will be evaluated in a dedicated chapter). As a tentative requirement a value of 1 mm/s could be considered;
- As far as the 'multiple wavelength' type contribution, it is related primarily to thermal stability. Also based on the type of fibre optic, the multiple wavelength par of deformation can change and, to partly reduce its effect, a tentative reference value of 500 λ could be considered.

Based on above considerations, a tentative set of key requirements are given in Table 4-3 **Errore. L'origine riferimento non è stata trovata.** and the resulting de-phasing is shown in Figure 4-14 while probabilities are shown in Figure 4-15.

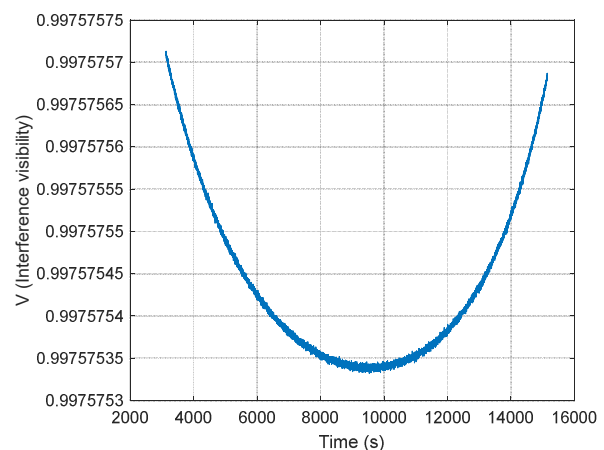
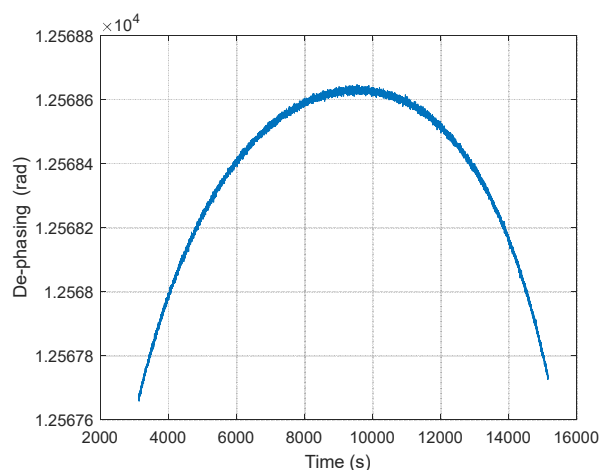


Figure 4-11 All effects superimposed: de-phasing (left), Visibility (right)

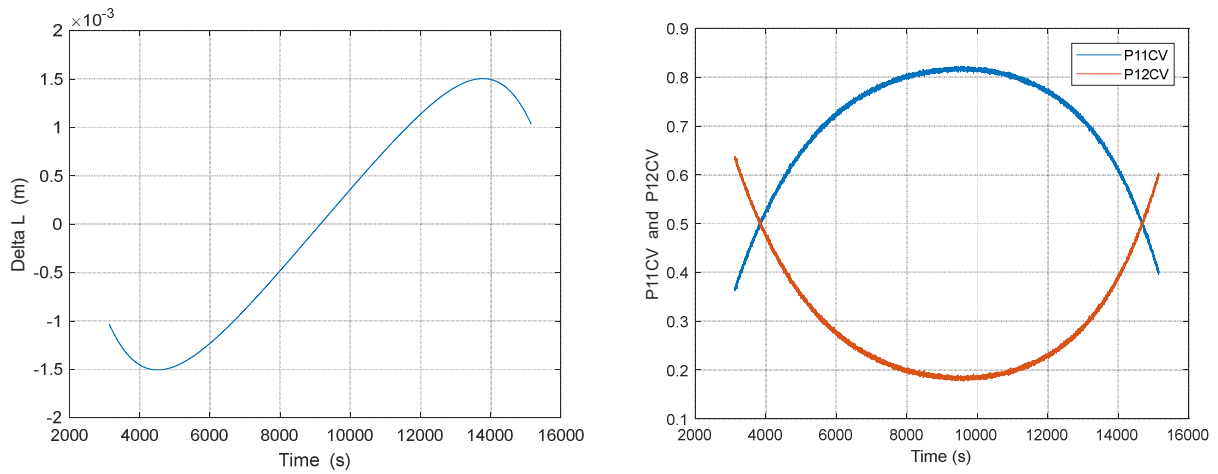


Figure 4-12 All effects superimposed: Delta L (left), Probabilities at detectors (right)

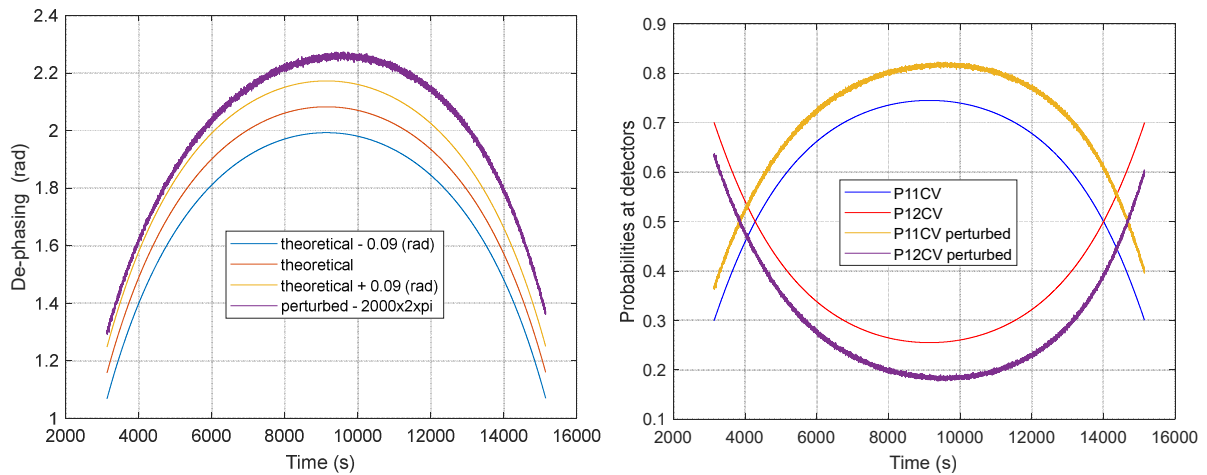


Figure 4-13 All effects superimposed: comparison of unperturbed and perturbed de-phasing (left), comparison of unperturbed and perturbed probabilities (right)

- r_{bias} – Satellite POSITION knowledge bias..... = 5 m
- r_{noise} – Satellite POSITION knowledge noise (1 sigma).... = 1.5 m
- v_{bias} – Satellite SPEED (S/C-GS radial) measurement bias... = - 0.001 m/s
- v_{noise} – Satellite SPEED (S/C-GS radial) measurement noise (1 sigma).. = 0.0002 m/s
- p_{cbiasn} – Prism control bias error = 3 nm
- $p_{cnoisen}$ – Prism control noise error(1 sigma)..... = 0.4 nm
- $\delta L1ID$ – Perturbation (multiple w. l.) on Ideal length of GS interferometer.. = + 500 λ
(= 400.000266 m)
- $\delta L2ID$ – Perturbation (multiple w. l.) on Ideal length of S/C interferometer.. = - 500 λ
(= 399.999734 m)
- Delta L2-L1 calibration-calibration and geometrical stability included = - 0.004 μm

Table 4-3 Tentative set of key requirements

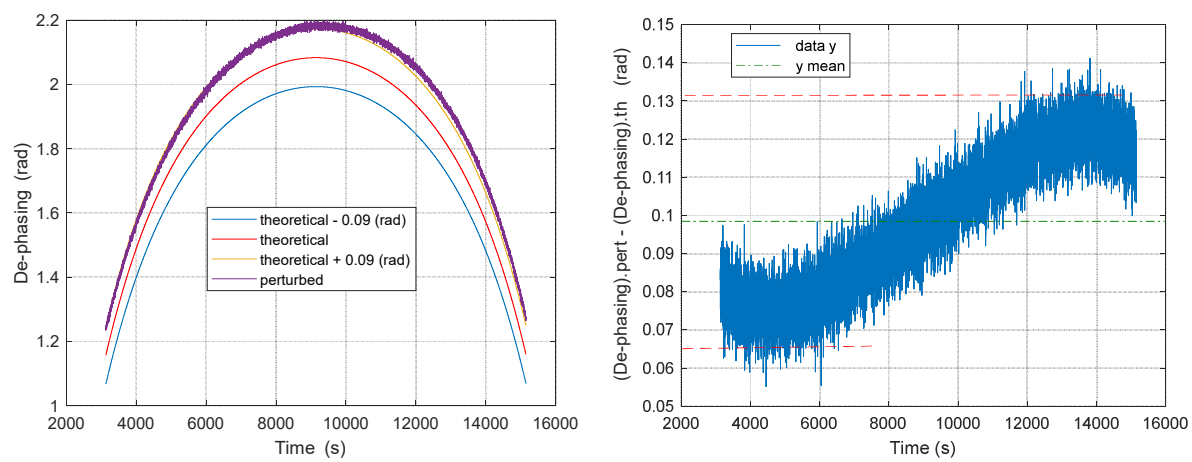


Figure 4-14 De-phasing (left) and de-phasing error (right) for input perturbations according to tentative requirements

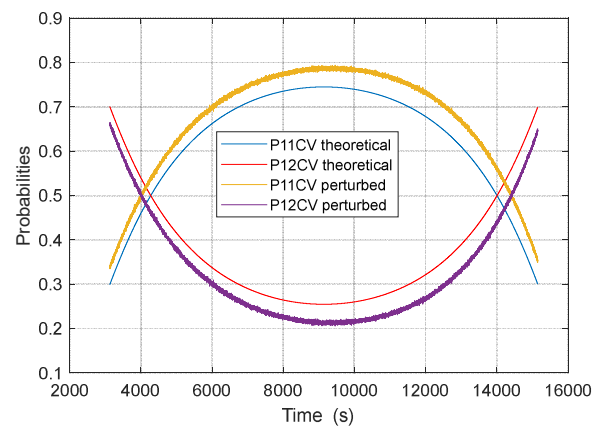


Figure 4-15 Probability at detectors for input perturbations according to tentative requirements

(Page Intentionally Left Blank)

5 TECHNOLOGY AND IMPLEMENTATION ISSUES

Should a One-way type Interferometric experiment be pursued it is certainly necessary to perform a very detailed feasibility/development activity, involving both universities and industry. Of the many critical technological areas, three are extremely important in order to be able to implement the experiment and certainly deserve special attention:

- Spacecraft accurate real-time speed prediction (needed for compensation of the 'classical' Doppler effect when utilizing the 'interferometer length modulation' approach);
- Accurate real-time Ground Interferometer length control (needed for compensation of the 'classical' Doppler effect when utilizing the 'interferometer length modulation' approach);
- Accurate Interferometers calibration.

Three further technological areas will be introduced: some issues on fibre optic technology (specifically for the aspects of thermal stability and attenuation), Single Photon Detectors, special requirements on retro-reflector(s) on board the S/C (should the design be also compatible to the compensation of the 'classical' Doppler effect based on the 'double measurement scheme').

5.1 Spacecraft speed predictor

Quantity to be estimated

Let us consider the Oneway experiment scheme as shown in Figure 5-1 .

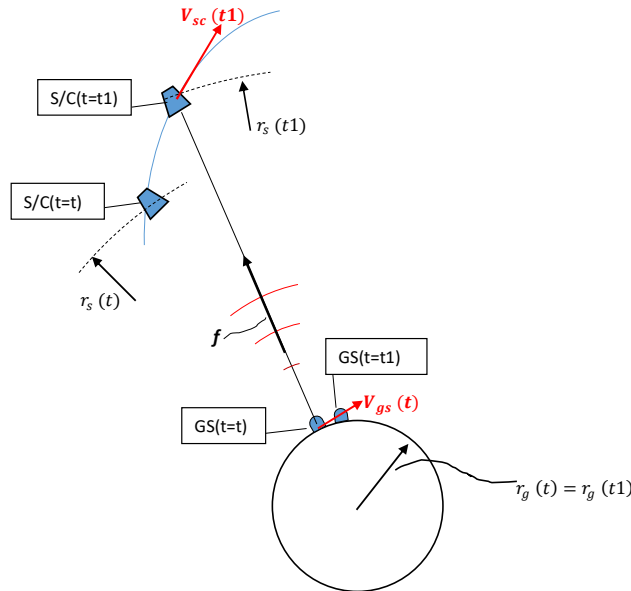


Figure 5-1 Oneway experiment scheme

In order to implement the Doppler compensation the knowledge of the quantities $V_{SC//f}(t1)$ and $V_{GS//f}(t)$ is necessary at time t^- (where t is the time the photon is launched from the GS and t^- means that the data is available in time for being used at time t). In some all seen Doppler compensation scheme is also present the term:

$$\frac{1 - \frac{V_{SC//f}(t1)}{c}}{1 - \frac{V_{GS//f}(t)}{c}} - 1 \quad (5.1)$$

which is certainly known if both $V_{SC//f}(t1)$ and $V_{GS//f}(t)$ are known. In practice however the term can be expanded into:

$$\frac{1 - \frac{V_{SC//f}(t1)}{c}}{1 - \frac{V_{GS//f}(t)}{c}} - 1 = -\frac{V_{SC//f}(t1) - V_{GS//f}(t)}{c} - \frac{V_{SC//f}(t1) * V_{GS//f}(t)}{c^2} - \frac{[V_{GS//f}(t)]^2}{c^2} + o(c^{-3}) + \dots \quad (5.2)$$

and the knowledge of the term in consideration in practice is equivalent to the knowledge of $\left[\frac{V_{SC//f}(t1)}{c} - \frac{V_{GS//f}(t)}{c}\right]$ as can result from the evaluation of the different order of magnitudes. In fact for trajectories potentially appropriate for some hundreds meters class interferometers, the following rough orders of magnitude's are expected for the first, second and third terms of above expression (the right hand side):

$$\text{o.o.m.} \left(\frac{V_{SC//f}(t1) * V_{GS//f}(t)}{c^2} - \frac{c}{V_{SC//f}(t1) - V_{GS//f}(t)} \right) \sim 10^{-10} - 10^{-9}$$

$$\text{o.o.m. (max)} \left(\frac{V_{SC//f}(t1) - V_{GS//f}(t)}{c} \right) \sim 10^{-6} - 10^{-5}$$

$$\text{o.o.m. (max)} \left(\frac{V_{SC//f}(t1) * V_{GS//f}(t)}{c^2} \right) \sim 10^{-15} - 10^{-14}$$

The speed estimator considered and here described is based on Satellite Laser Ranging (*laser ranging action seen superimposed to the quantum experiment - so there are two things, the quantum experiment and the SLR*) and is conceived to provide an estimate of the following quantity:

$$Vdc.estimated = [V_{SC//f}(t) - V_{GS//f}(t)] \quad (5.3)$$

Once $Vdc.estimated$ is computed then it is compared (in difference) with respect to the theoretical desired exact value:

$$Vdc.theoretical = [V_{SC//f}(t) - V_{GS//f}(t)] \quad (5.4)$$

Structure of the estimator

The estimator implemented is also a predictor and has to be able to provide the necessary speed information $Vdc.estimated(t^-)$ in time to implement the length correction of the ground interferometer ready for 'the photon' to be emitted at time t . The speed estimation prediction can clearly be *computed utilizing only the time-round-trip (of the SLR) available at time t^-* and therefore the ones of the SLR pulses emitted

The estimator/predictor is hereafter synthetically described with reference to SLR schematics reported in Figure 5-2 and data organization reported in Table 5-1.



The diagram illustrates the data flow and timing for the PONP algorithm. A grid shows a horizontal blue line representing a threshold $T_r (< t_e(k))$. A dashed box highlights data points used for best fit and projection. A callout states "These data are not known at time $t_e(k)$ ". The diagram is divided into two sections: PONP (top) and NDELAYT (bottom), separated by a dashed line.

65

To prepare and test the predictor the following steps/points are noted:

- A sequence of 'real' ($d_{\text{uplink}} + d_{\text{downlink}}$) is computed by the orbit simulator and passed as input to the speed estimator;
- The round trip times TRT are generated by the input sequence of ($d_{\text{uplink}} + d_{\text{downlink}}$) and corrupted by selectable *bias*, *random white noise*, *random walk* (times) disturbances (this RTR is basically what available from Laser Ranging);
- The round trip times (TRT) data are progressively filling the shown data table and at a generic instant $t(k)$ only data significantly 'old' are available;
- At a generic time $t^-(k)$ the columns of the table are updated filling the line of the table relevant to the emission time of the last received (or useful) round trip returned SLR pulse. So at a generic time $t^-(k)$ part of the tale is empty but it is NOT used;
- The estimator consists of two parts:
 - the polynomial fitter
 - the projector
- The polynomial fitter makes solely use of available data (e.g. the last 60 seconds of the available table's data (e.g. of the last column of speeds data) and best fit according to a polynomial typically of second order (we are dealing with speeds and second order suffices);
- The returned polynomial coefficients are used to construct the polynomial best fit and to *project the results slightly outside* of the available dataset used. Typical ahead projection is in the order of 0.1 s or 0.11 s larger than the maximum round delay of the considered trajectory.
- The orbit simulator compute and passes to the speed estimator the 'real' parameters $V_{SC//f}(t_1)$ and $V_{GS//f}(t)$ in order to compute the reference *Vdc.theoretical*;
- The projected results (*Vdc.estimated*), which are estimates, are then compared with the theoretical ones (*Vdc.theoretical*).

As already mentioned, only data available from SLR are used and complex modelling is purposely avoided. Two transformations are present in the scheme (see also the figure of the table):

- A transformation T1 for *estimation/extraction of the 'uplink' distance from the round trip time* (which relates to the sum of the uplink plus downlink distance);
- A transformation T2 which *relates the time variation of the uplink length estimate to the speeds projections* of interest.

For the transformations T1 and T2 only a quite approximate estimate of the GS speed projection $V_{GS//}$ is needed.

For the purpose of the simulation this $\hat{V}_{GS//}$ speed estimate has been computed by taking the nominal theoretical one and corrupting it by a large quantity (5% linearity plus a constant error of 3 m/s) resulting in simulated speed errors raising up to 3-20 m/s certainly huge with respect to what can be estimated real time.

Some implementation details are shown in Table 5-2.

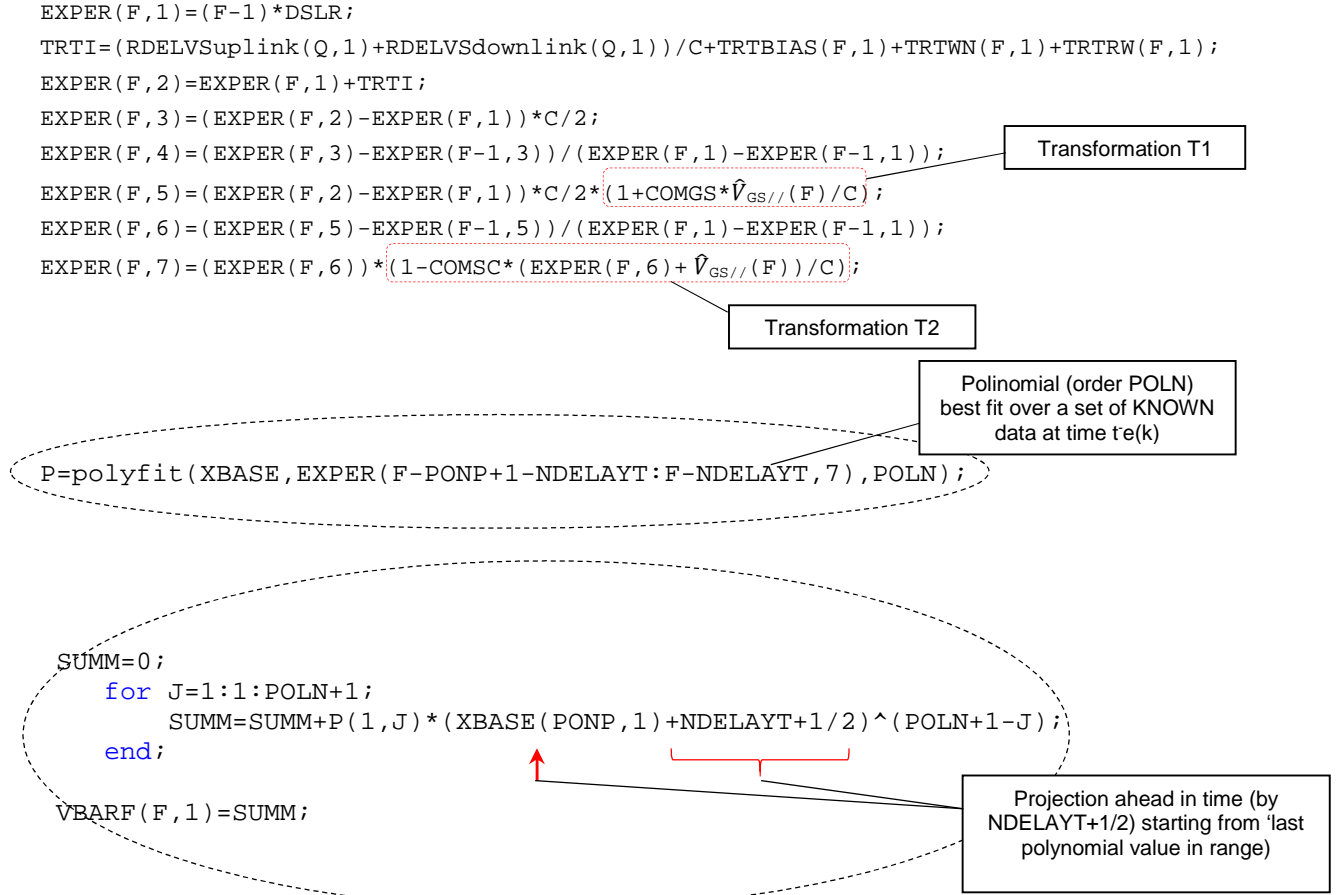


Table 5-2 Some implementation details of the predictor

Simulation results

Some reference cases have been evaluated (code: speedestimator18), with parameters as summarized in the following Table 5-3, and the results reported in the next Figure 5-3 (data cover the tracking conditions Elev. > 20°); for all cases the coordinates of the GS are the one of Matera MLRO.

As far as the 'Polynomial Order' in all cases shown is taken to be 2 (since the physical quantity dealt with is speed, up to the derivative of the acceleration are taken into account). The other two basic parameters of 'Polynomial Fitting Time' and 'Ranging frequency' can be adapted to the type of S/C orbit and measurement noise in order to have low errors (*slowly varying error and noise*).

As example:

- Trajectories above 8000/10000 km
 - Polynomial fitting time = 30 s
 - SLR frequency = 10 Hz
- Trajectories below 8000/10000 km
 - Polynomial fitting time = 3 s
 - SLR frequency = 50 Hz (e.g. > 20 Hz)

For the reference trajectory considered, the following performances (or better, depending on optimization) can be adopted:

- |Slowly varying error| < 0.2 mm/s
- Noise < 0.15 mm/s ($\sim 1\sigma$)

Case	Orbit data	Passage type	Assumed disturbances on TRT ps	Estimator data	Speeds estimation error (Vdc.estimated-Vdc.theoretical) mm/s
1 (Ajisai)	P=7862 km A=7862 km i=50°		Bias=2 White noise=2 Random walk=0.2	Projection time=0.05 s Time best fit= 3 s Poly order= 2 SLR freq. = 50 Hz	Slowly varying error < 0.3 Noise < 3 ($\sim 3\sigma$)
2	P=10000 km A=18000 km i=28°	A	Bias=2 White noise=2 Random walk=0.2	Projection time=0.10 s Time best fit= 30 s Poly order= 2 SLR freq. = 10 Hz	Slowly varying error < 0.2 Noise < 0.3 ($\sim 3\sigma$)
3 (Reference)	P=8000 km A=22000 km i=28°	A	Bias=2 White noise=2 Random walk=0.2	Projection time=0.12 s Time best fit= 30 s Poly order= 2 SLR freq. = 10 Hz	Slowly varying error < 0.2 Noise < 0.4 ($\sim 3\sigma$)
4	P=8000 km A=36000 km i=28°	A	Bias=2 White noise=2 Random walk=0.2	Projection time=0.2 s Time best fit= 30 s Poly order= 2 SLR freq. = 10 Hz	Slowly varying error < 0.3 Noise < 0.4 ($\sim 3\sigma$)

Table 5-3 Test cases for the speed estimator

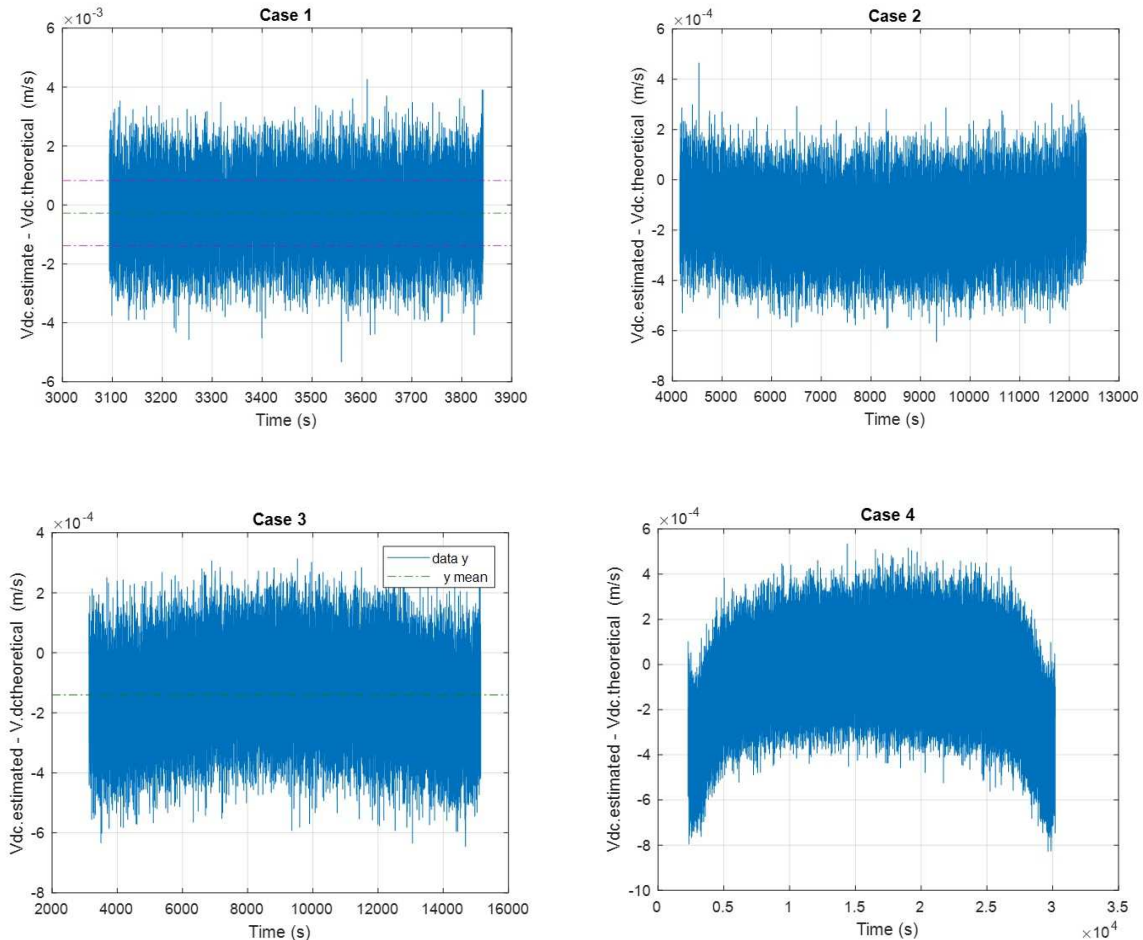


Figure 5-3 Examples of speed estimator performances

Indeed only the first one of the Doppler compensation algorithm makes use of the quantity ($V_{dc.estimated}-V_{dc.theoretical}$). The second one needs also the knowledge of $V_{SC//}$. The third one needs the full vector speeds knowledge even if the needed accuracy is only in the relative radial components (the transversal ones can be as wrong as 1%, a huge number). So also an accurate estimate of $V_{GS//}$ alone is necessary.

In this respect the Spacecraft in charge of the experiment is equipped by retro-reflectors and on board Global Positioning System (GPS) and these two elements allow, after some initial assessment by Satellite Tracking or Inter Satellite Links, the updated dissemination of satellite Ephemeris. These Ephemeris allow a generic user to extrapolate by 'simple algorithm' the real-time position of the S/C w.r.t the GS in an ECEF frame (Earth Centered Earth Fixed frame). In this respect (see for example Ref. [25]) even a simple Ephemeris scheme like the GLONASS 9 d.o.f. state:

X_0, Y_0, Z_0	Position in Cartesian ECEF coordinates
$\dot{X}_0, \dot{Y}_0, \dot{Z}_0$	Velocity in Cartesian ECEF coordinates
$\ddot{X}_{Res}, \ddot{Y}_{Res}, \ddot{Z}_{Res}$	Residual acceleration over the fit interval, mainly due to luni-solar attraction, in Cartesian ECEF coordinates
t_0	Reference time of Ephemeris

would allow real time position projection (with initial conditions specified by the 9 states referenced at the 'reference time Ephemeris') with accuracies below 1 m and for projection times up to e.g. 30 minutes ahead of the 'reference time Ephemeris'. More complex Ephemeris (e.g. GLONASS 12 or 15 d.o.f.) would allow even better real time performances.

To be in a total safe side let consider a worst case accuracy knowledge of 3 m.

This relative position knowledge allows to project the Ground Station speed vector along the parallel direction and, for trajectories similar to the reference one, the expected error would be definitely less than:

$$\delta(V_{GS//}) \sim |\vec{V}_{GS} \cdot \cos(Elevation)| \cdot \frac{\delta x}{x} < |\vec{V}_{GS}| \cdot \frac{\delta x}{x} \approx 0.0001 \quad m/s \quad (5.5)$$

Therefore, for a general MEO trajectory, the accuracies achievable in the estimate of both ($V_{SC//}$ - $V_{GS//}$) or $V_{SC//}$ can preliminary be set to:

- |Slowly varying error| < 0.4 mm/s
- Noise < 0.2 mm/s ($\sim 1\sigma$)

As mentioned above, some accuracy improvements are possible for the reference trajectory.

5.1.1 Development needs

Should the One-way experiment be pursued it is advisable to perform in advance verification tests to confirm that the accuracies considered can actually be achieved by using a predictor scheme as considered. No major hardware developments is needed for the testing and the verification would consists in comparing (a posteriori) the real-time estimated speed against the

most accurate speed reconstruction achievable with a verification off-line by using accurate ephemeris.

5.2 Prism positioner for Doppler effects compensation

In this paragraph the specific issues of prism/mirror positioning associated to the Doppler effect compensation function are discussed in order to investigate its criticality and feasibility trying to identify the needed improvement areas.

5.2.1 General considerations

As previously discussed for the reference trajectory (paragraph 4.2), compensation length of about 3 - 4 mm with positioning accuracies in the order some nanometres (e.g. 3 nm or better) are necessary for the Doppler compensation approach based on (ground) interferometer length control. The mass to displace is quite modest, in the order of 30 g or less (mass of reflecting mirror/prism).

Several miniaturized linear stages products (with strokes in the millimetres range) exist on the market many of them realized by making use of piezo driving technology (of different variants). However, in spite their real outstanding performances, the two requirements of several millimetre stroke and positioning accuracy are *quite difficult to be achieved in a combined way*.

Some examples of excellent millimetre(s) stroke class products are shown in Table 5-4 (taken from Ref. [26] and Ref. [27]).

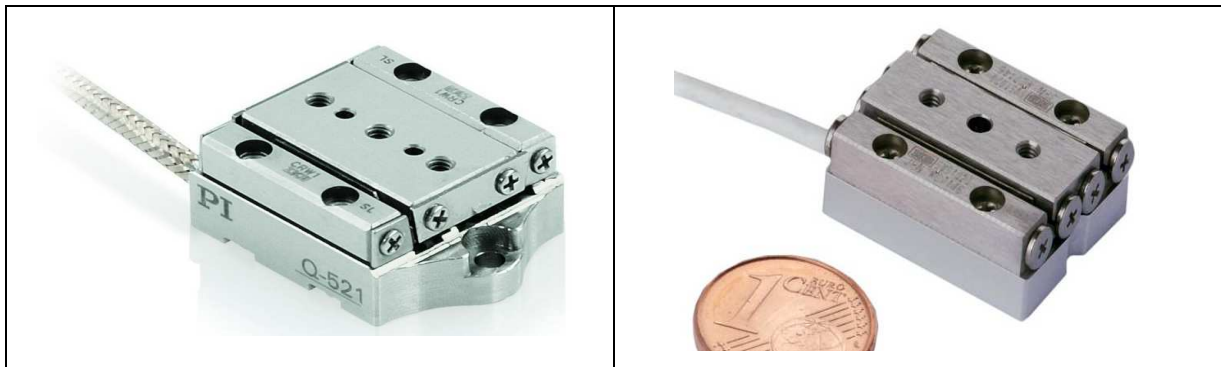


Table 5-4 Two examples of linear positioners: PI Q-521 Q-Motion® Miniature Linear Stage (left), SMARACT SLC-1720 (right)

The two shown stages are capable of 12 mm total stroke and nanometric type motion resolution. However considering all the possible error contributions (including repeatability), positioning inaccuracies in the order of several nanometers (10-20) may arise during the implemented travel. Another point of concern is the angular inaccuracies, building up during the travel.

To overcome this issue the 'Modulus $N \cdot \lambda$ ' compensation is introduced (with N integer). This exploits the fact that de-phasing variations multiple of $N \cdot 2\pi$ (or length correction variations multiple of $N \cdot \lambda$) do not cause significant variation of interference probability (but for a tolerable reduction in the Visibility of the interference process). This strongly reduces the overall necessary physical stroke allowing the utilization of nanopositioners with stroke capability in the order of ten or some tens of micrometers, much less than the one needed in case of full

compensation. In this case the displacement profiles will be a sequence of accurately controlled short profiles followed by fast position recovery.

5.2.2 The 'Modulus $N \cdot \lambda$ ' compensation

As previously evidenced the length correction reported in Figure 4-4 left, although a small one, is unfortunately huge from the point of view of its implementation in conjunction to the required accuracy: the longer is the needed stroke of the nano-positioner, the lower is its performance. Therefore, the compensation algorithm is modified by implementing a 'Modulus $N \cdot \lambda$ ' compensation with the objective to be able to achieve the exact Doppler compensation with nan-opositioners of small stroke (for example 50 μm or less instead of 3 mm) and still be able to extract the correct de-phasing curve.

The modified algorithm has the following features:

- The length correction ΔL is first computed as the algorithm(s) discussed at paragraph 3.1.3 (*if applied* would lead to a de-phasing plot exactly the same as foreseen by metric part);
- A new correction $\Delta L_{N\lambda}$ is computed (in line) as follows:

$$\Delta L_{N\lambda} = \Delta L - \left[\text{fix} \left(\frac{\Delta L}{N \cdot \lambda} \right) \right] \cdot N \cdot \lambda \quad (5.6)$$

- When this new correction is applied two consequences are present:
 - The stroke needed by the nano-positioner is necessarily limited to $N \cdot \lambda$ (e.g. if $N=40$ and $\lambda= 532 \text{ nm}$ then *the total stroke needed would be $< 50 \mu\text{m}$ or $\pm 25 \mu\text{m}$*);
 - The resulting de-phasing profile, when plot, would be different than the theoretical one but *will be shifted, over discrete time intervals, by very large multiples of $N \cdot 2\pi$* . Since these multiples may change from interval to interval, the gross appearance of the new curve may look externally quite different from the initial one
- This means that the probabilities at the detectors, when computed with the new de-phasing curve, will be *identical to the original theoretical ones*.

As an example, in Figure 5-4 are reported the results for the reference trajectory with a new simulation code (code: cowsim292moddephaseBN) implementing the 'Modulus $N \cdot \lambda$ ' compensation and selecting $N=40$. The blue encased part represent the flow associated to the complete compensation while the red encased part represent the flow associated to the 'Modulus $N \cdot \lambda$ ' compensation. The resulting probabilities are basically identical.

Since in the real experiment the logical flow would be:

Counting of photons \rightarrow Extraction of probabilities \rightarrow Extraction of de-phasing curve

then it follows that the original theoretical de-phasing curve can be, at least ideally, well extracted.

In the final experiment simulation (implemented by photon counting) this can be assessed and quantified.

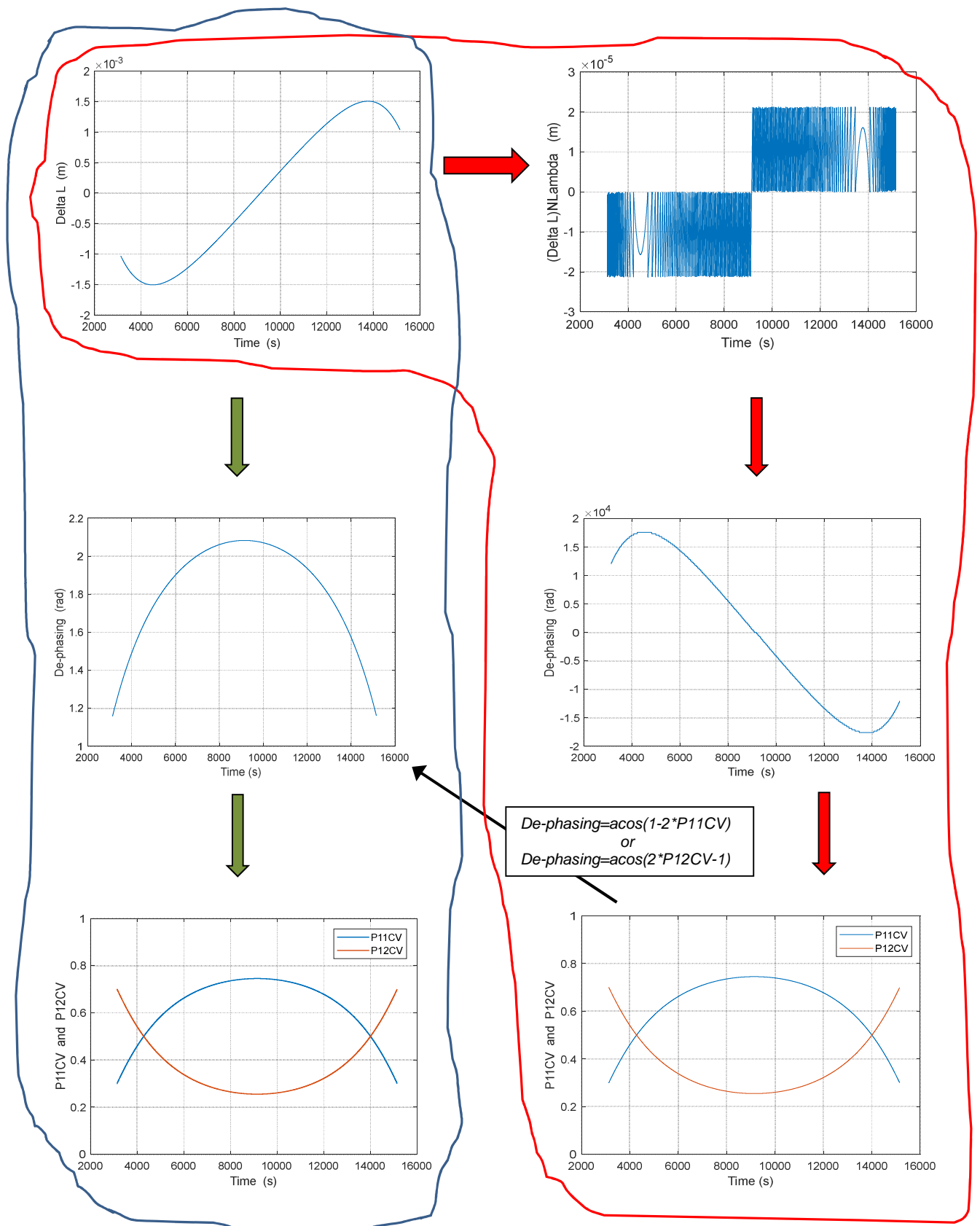


Figure 5-4 Logic sequence for the complete compensation (blue encased) and utilization of 'Modulus N-λ' compensation with N=40 (red encased)

The use of the Modulus $N \cdot \lambda$ compensation in place of the complete one generate a slight degradation of the Visibility, as shown in Figure 5-5. The degradation is anyway quite modest and fully acceptable.

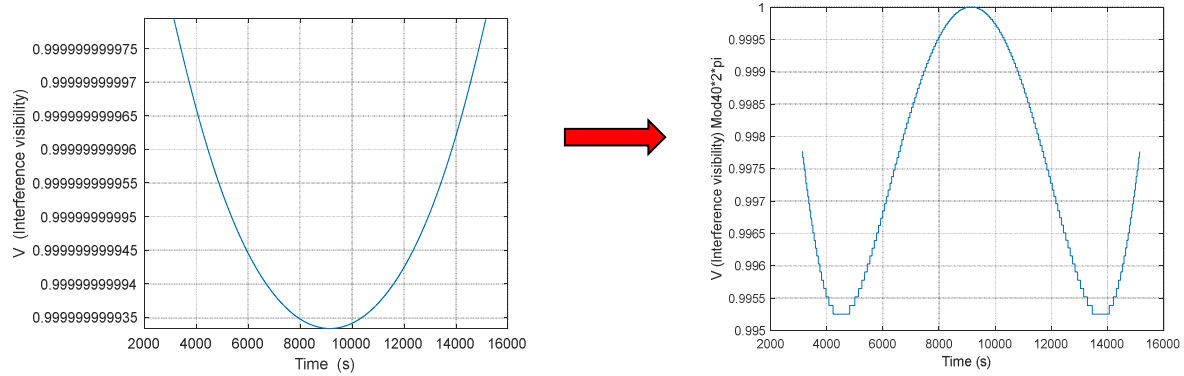


Figure 5-5 Some loss of Visibility ($< 0.5\%$)

As far as the length correction implementation, in Figure 5-6 (left) is shown an expansion from time=8720 s to time=8820 s of the complete diagram where are clearly visible the nano-positioner stroke recovery that happen, in the interval considered, about every 50 seconds. Due to the specific choice of $N=40$ and $\lambda = 532$ Nm, the stroke recovery is about $21\mu\text{m}$.

In Figure 5-6 (right) is instead shown (for information) the *amount of length correction occurring every 0.01 s*.

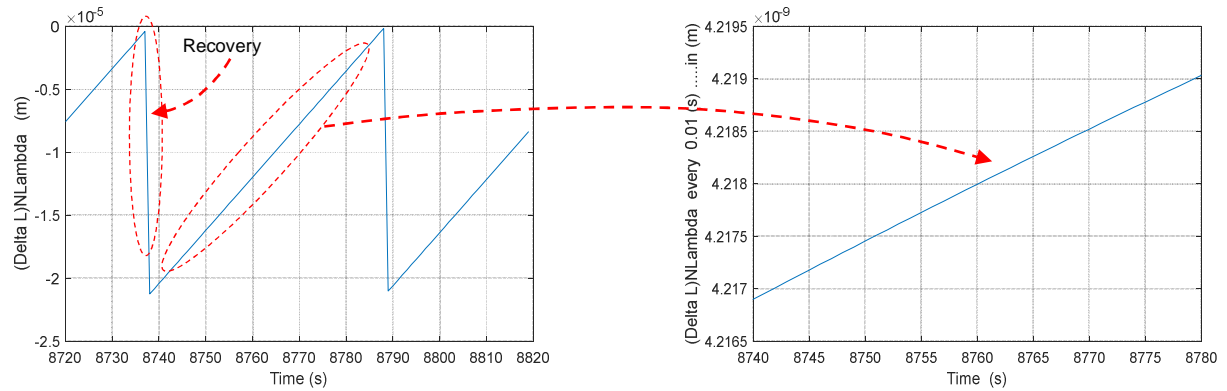


Figure 5-6 Some details on the required length correction

5.2.3 Candidate nano-positioner

The requirement to achieve positioning accuracies as good as 3 nm or better over strokes of micrometers is certainly an easier requirement to pursue than in the case of millimetres stroke, especially in dynamic conditions.

The positioning technology considered is based on single axis piezo nanopositioning stages with direct drive actuation and frictionless flexture guidance. They are, as reference, selected

to operate over a total strokes of less than 10 μm in order to keep reduced the errors associated to non linearities.

The dynamic Delta L compensation expected for the reference trajectory can be computed by simulating an $N \cdot \lambda$ compensation with $N = 9$ (to certainly guarantee a total required stroke < 10 μm). The results of the simulation are reported in Figure 5-7. Similarly as before, the compensation results as sequences of controlled trajectories and controlled fast recoveries. The controlled trajectories are not linear but are however very smooth with compensation speeds, which depend on time, in the rough order of magnitudes of 500 (nm)/s or less. The interval between recoveries result to be about 10 s or more, again depending on time.

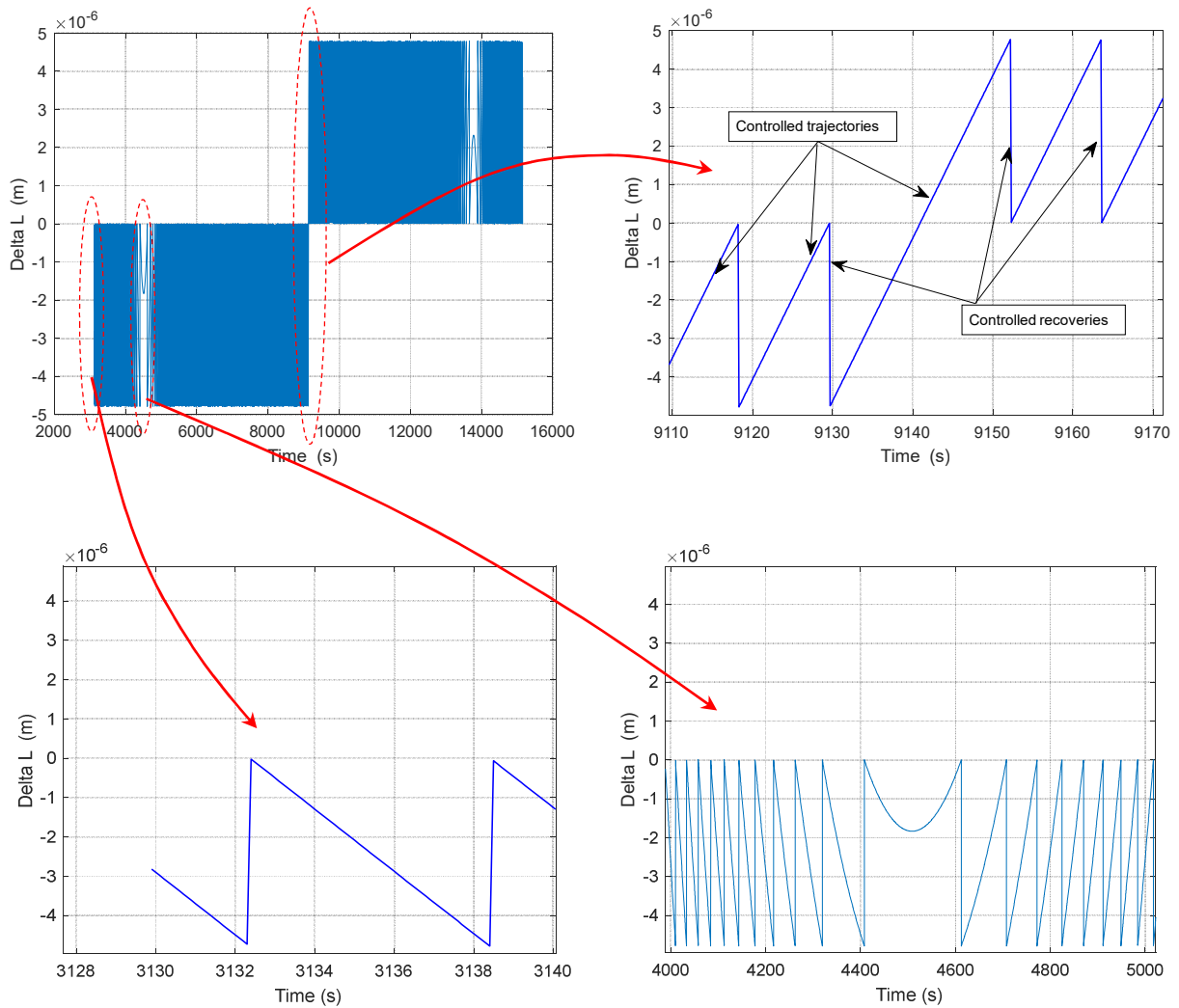


Figure 5-7 Simulation of the required Delta L compensation for $N=9$ (and $\lambda=532 \text{ nm}$)

Indeed if the compensation Delta L is implemented by displacing a reflective prism/mirror, the following occur:

- the total stroke needed by the prism halves with respect to the required correction;
- the speed of the prism halves with respect to the time derivative of the required correction;
- the time between recoveries do not change.

In practice, with *reference to the above simulated case*, the total prism stroke utilized during compensation will be $< 5 \mu\text{m}$, or within the range $\pm 2.5 \mu\text{m}$.

In Table 5-5, Table 5-6, Table 5-7 are reported the main characteristics of three nano-positioning stages (present in the market and from different manufacturers) that present interesting performances and which could constitute a good starting point for a possible future customization activity. The data presented are a synthetic summary of the most important features given in the relevant data sheets (Ref. [28] for PI, Ref. [29] for Mad City Lab and Ref.[30] for Aerotech).


	<ul style="list-style-type: none"> Travel range (in closed loop) = $15 \mu\text{m}$ Integrated sensor = Capacitive Resolution in closed loop = 0.1 nm..... typ. Linearity error in closed loop = 0.03%typ. Repeatability = $\pm 1 \text{ nm}$..... typ. Pitch/Yow = $\pm 5 \mu\text{rad}$ typ. Stiffness in motion direction = $45 \text{ N}/\mu\text{rad}$ $\pm 20 \%$ Resonant frequency (no load) = 5.6 kHz $\pm 20 \%$ Resonant frequency (100 g load) = 2.5 kHz $\pm 20 \%$ Material = Steel Controller: PI-E754
---	--

Table 5-5 Main features of PI-LISA P 753.1CD stage (data extracted from Ref. [28])


	<ul style="list-style-type: none"> Travel range (in closed loop) = $10 \mu\text{m}$ Integrated sensor = Yes: PicoQ® proprietary Resolution = 0.01 nm Sensor linearity error $< 0.01 \%$ Resonant frequency (no load) = 4.6 kHz Material = Aluminum Controller: Nano-Drive®
---	--

Table 5-6 Main features of MCL Nano-MET 10 (data extracted from Ref. [29])


	<ul style="list-style-type: none"> Travel range (in closed loop) = $10 \mu\text{m}$ Integrated sensor = Capacitive Resolution in closed loop = 0.05 nm Linearity error in closed loop = 0.02% Bi-directional repeatability = 1 nm Pitch/Yow = $\pm 5 \mu\text{rad}$ Stiffness in motion direction = $60 \text{ N}/\mu\text{rad}$ $\pm 20 \%$ Resonant frequency (no load) = 7 kHz $\pm 20 \%$ Resonant frequency (200 g load) = 2.5 kHz . $\pm 20 \%$ Material = Stainless steel Controller: Ensemble QLAB
---	--

Table 5-7 Main features of QNP_{HD}30L 10 (data extracted from Ref. [30])

The piezo actuators are ‘continuous’ machines with theoretically infinite resolution but when used in open loop they are subject to the presence of hysteresis, repeatability and linearity errors. When utilized in close loop, the resulting inaccuracies (normally quantified under the terms resolution, repeatability, linearity) are mostly related to the sensor, electronics and control loop. Just for example assuming a nano-positioner in closed loop (with mated electronics) with the following key characteristics (basically already allowed by commercial products):

Resolution in closed loop = 0.1 nm
 Linearity error in closed loop = 0.01 %
 Bi-directional repeatability = 1 nm

the following error on the interferometer length compensation (ΔL) are likely present:

$$\delta(\Delta L) = 2 \cdot (0.0001 \cdot 2500 + 1) = 2.5 \text{ nm ('slow' varying error)}$$

$$\delta(\Delta L) = 2 \cdot 0.1 = 0.2 \text{ nm (noise error)}$$

Clearly all also depend on how the declared data are defined and measured.

Another important point is related to the difference in accuracies between 'static' and 'on the fly', reachable while executing the trajectory. To improve the performances stiff platforms are preferred and sufficiently large bandwidth control loops (with feed forward action) are important; input commands need be at sufficiently high frequency and duly micro-interpolated. The presence of external ultra-precise sensors can furthermore complement the internal one; it may also allow to define a 'zero' position in robust way w.r.t. local thermal deformations (see for example schematics in Figure 5-8).

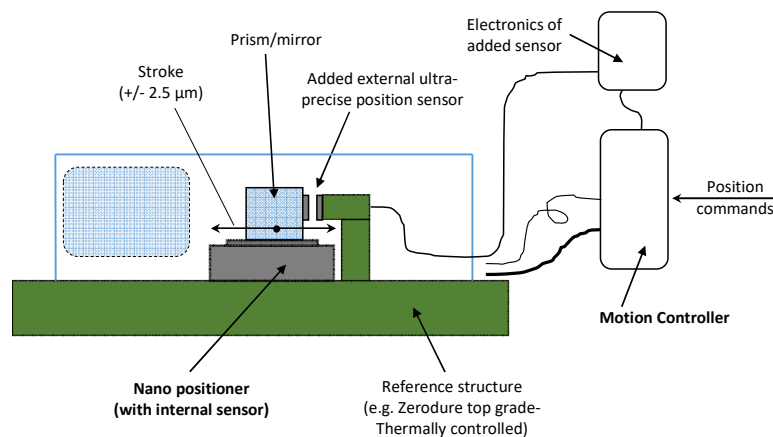


Figure 5-8 General schematics

Therefore considering commercial products (as available on the market or with minor customizations), the following performances could be already reachable:

- $\delta(\Delta L) = 3 \text{ nm}$ ('slow' varying error)
- $\delta(\Delta L) = 0.3 \text{ nm}$ (noise error)

Assuming an appropriate development activity (involving the component manufactures), the following tentative **performances (goal)** can be considered:

- $\delta(\Delta L) = 1 \text{ nm}$ ('slow' varying error)
- $\delta(\Delta L) = 0.1 \text{ nm}$ (noise error)

5.2.4 Development needs

Based on the general characteristics of the products in order to confirm (3 nm class) and likely improve (1 nm goal) the assumed performances under dynamic conditions, appropriate *specific customization and development activities are necessary*, involving areas such as:

- Screening of components to select top performing;
- Implementation of compensation tables, repeatability improvements and sensor(s);
- Optimization of control strategy and control loop ('on the fly' vs. 'command and stabilize', feed forward, gains, nesting scheme, input set points frequency and resolution);
- Customization of materials (steel, invar,...);
- Evaluation testing and extended characterization.

Some of above activities need be carried out by the manufacturer, some by the user.

5.3 Interferometers calibration

5.3.1 General considerations

One of the criticalities in the Oneway scheme, taken as reference, is related to the presence of two interferometers considered as 'equal', separated by thousands of kilometres and operating in very diverse environments.

Indeed the two assumed MZI interferometers (with arm unbalance of e.g. 400 m) *do not need be exactly the same* and their unbalance can differ by an amount in the range of the millimetre that can be seen having two types of contributions:

- a multiple wavelength part (amounting for example to 0.532 – 1.064 mm corresponding to a number of wavelength of e.g. 500 or 1000, for the case of $\lambda = 0.532 \mu\text{m}$);
- a small residual that was indicated in the order of e.g. 2-3 nm (or smaller).

The large 'multiple wavelength' difference is responsible to a slight modification of interference visibility (anyway fully acceptable) while the small unknown residual (together with other contributions) affects the real performance. The key points is therefore associated to availability of a calibration scheme/procedure which allows to maintain the residual as small as possible, anyway less than a max allowed value.

In principle two types of calibrations could be considered: *continuous* or made by *sequences of calibration steps and free run periods* (e.g. a calibration step every 10 – 60 seconds). Clearly in case of *calibration-free run* sequence approach, the length drift during the free run period need be appropriately small.

Key to a good calibration procedure is the availability of an ultra-stable beam (in terms of line-width and drift) allowing to tune the interferometers length to the required accuracy. This *apply to both interferometers on board and on ground and the ultra-stable beam shall be available both on board and on ground*.

The approach of generating an ultra-stable reference at one location only, for example on ground, and transmitting it to the on-board system presents serious criticalities. Indeed the received beam is shifted in frequency due to both the large relative speed between Ground Station and Spacecraft ('classical' Doppler effect) and by the Relativistic metric effects (which are expected be the basic causes of the single photon quantum interference modifications, the objective of the experiment).

Therefore a calibration method independent from the basic phenomena involved in the experiment objectives is considered and the main lines of this approach are sketched in Figure 5-9; with reference to this figure, the following key remarks/considerations applies:

- two 'identical' ultra-stable sources are prepared (same approach, same design, same lot components, same manufacturing process);
- the sources shall be of rugged type (capable to support launch conditions) and thermally stabilizable to a given operative point;
- the two units will be subject to a relative tuning operation on ground aiming at locking them on the same central frequency (identifying the cavity mode);
- extensive verifications/tuning to have the two units working 'in the same way' in a robust manner;
- one of the units remain at the Ground Station and serves for the *calibration of the ground interferometer* and possibly for the *derivation of the frequency for the mode-locked beam to generate the pulses* (carrying the photons for the experiment);
- the second unit is integrated in the spacecraft and serves for the *calibration of the on-board interferometer*.

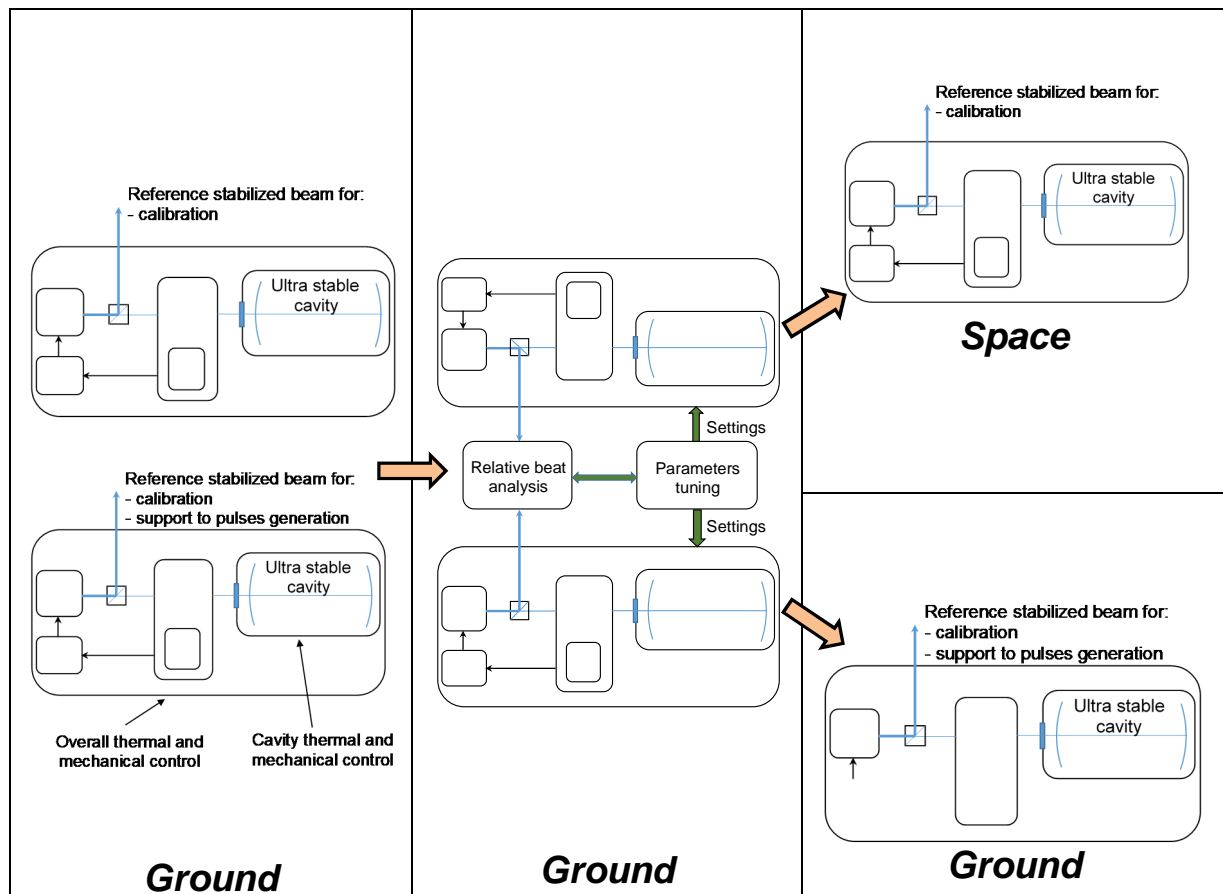


Figure 5-9 Possible approach for ultra-stable sources tuning and finalization

5.3.2 Requirements on frequencies overall accuracy

The on ground and on board frequency sources need be very matched one to the other throughout the time of the experimentation; for example taking as reference the trajectory defined at paragraph 4.1, orbital periods of about six hours are considered of which only four are used for the actual measurements.

Concerning the frequency deviations, three major effects contribute:

- Initial frequency matching;
- Cavity frequency drift;
- Line-width and centre frequency lock.

The 'initial frequency matching' is here intended to be the initial matching in the centre frequency at power on (or for example after two hours from power on, basically after an initial stabilization). The 'cavity frequency drift' is primarily related to the reference ultra-stable cavity stability especially with respect to thermal environment. The line-width and centre frequency lock are related to the performances of the frequency stabilization method used.

In terms of (relative) frequency, the situation could be as shown in Figure 5-10.

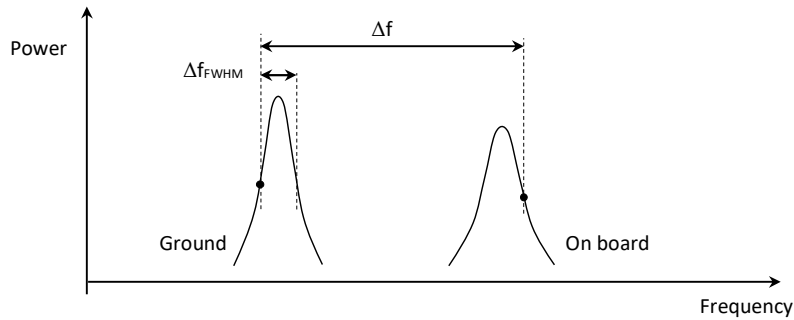


Figure 5-10 Schematics of relative frequency operations for the Ground and On board reference lasers (at generic time)

An overall relative frequency accuracy requirement (Δf_{REQ}) can therefore be defined as shown in Figure 5-10 as the maximum allowed frequency separation occurring during the experimentation time; this frequency separation can be referred to Full Width Half Maximum (FWHM) conditions.

The requirement on frequency for calibration purposes depend also on the interferometers length and on the nominal frequency utilized for the calibration itself; the basic relation linking the required interferometers geometrical length difference to the required frequency difference is given by:

$$\Delta f_{REQ} = \frac{c}{\lambda_{CAL}} \cdot \frac{\Delta L_{REQ}}{L_{NOM}} \quad (5.7)$$

where:

λ_{CAL} = Calibration wavelength used

ΔL_{REQ} = Required accuracy in interferometers length difference

L_{NOM} = Nominal interferometers length

Considering an interferometer mismatch of 4 nm (as preliminary indicated in Table 4-3 and *here taken for discussion only*), the required relative frequency matching (Δf_{REQ}) as a function of the wavelength used results as in Table 5-8 (for interferometers of nominal 400 m length).

	$L_{NOM} = 400\text{ m}$		
	$\Delta L_{REQ} = 4\text{ nm}$		
	$\lambda_{CAL} = 256\text{ nm}$	$\lambda_{CAL} = 532\text{ nm}$	$\lambda_{CAL} = 1064\text{ nm}$
$\Delta f_{REQ}\text{ kHz}$	11.28	5.64	2.82

Table 5-8 Calibration sources relative frequency matching requirements (tentative) assuming an allowed mismatch of 4 nm (here taken for discussion only)

Clearly is possible to work in terms of relative frequency matching requirements because the 'experimental photon' frequency is derived (on ground) from the calibration source.

The overall frequency matching requirement can furthermore be split into three contributions of:

- Initial Matching (IM at start of experiment session);
- Cavity Frequency Drift (CFD through the e.g. 4 hours of experiment session);
- Linewidth and Centre frequency Lock (LCL through the e.g. 4 hours of experiment session);

With reference to the case of a calibration wavelength of 532 nm, and assuming (for exercise purposes) 4 nm length mismatch, a tentative frequency error apportionment can be assumed (which can be fully additive in worst conditions) splitting the shown 5.6 kHz into:

$$\Delta f_{REQ-IM} \cong 0.5\text{ kHz} - \text{Relative} -$$

$$\Delta f_{REQ-CFD} \cong 4.6\text{ kHz} - \text{Each unit } 2.3\text{ kHz allowed}-$$

$$\Delta f_{REQ-LCL} \cong 0.5\text{ kHz} - \text{Each unit } 0.25\text{ kHz allowed}-$$

Above frequency matching conditions are certainly within the range of laser instrumentation available for scientific advanced laboratory applications and some good examples are provided in Figure 5-11 (see Ref. [31] and Ref. [32]).

It is however noted that in the specific case considered the environmental and operative conditions are quite far from laboratory ones (especially for the on board equipment where also strong constraints in terms of mass and consumables exist).

Therefore the specific issues affecting such frequency variations are hereafter revisited also in relation to the specific application considered.

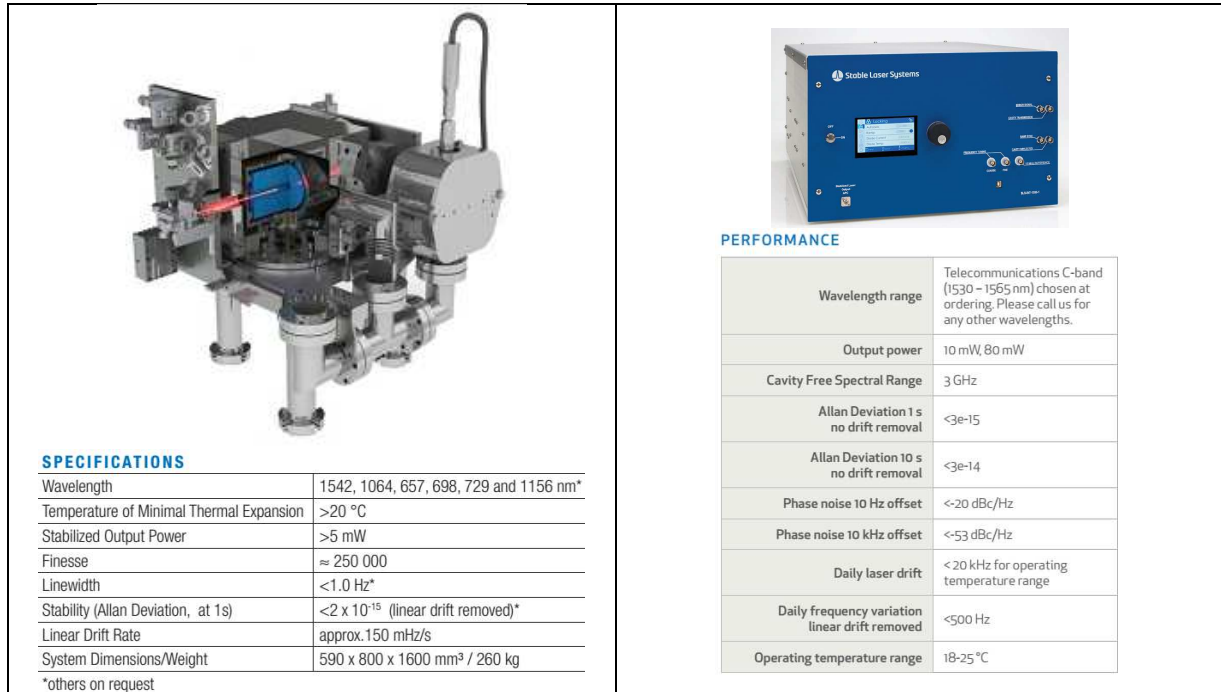


Figure 5-11 ORS Ultra stable laser from Menlo System (left), Hz-Level Rack Mounted Laser System from Stable Laser System SLS-INT-1550-200-1

5.3.3 Frequency Initial Matching

When the two cavities are manufactured they cannot be of perfectly the same length and, as built, a resonance frequency mismatch is therefore present. Assuming a nominal cavity length of L with a residual mismatch of ΔL , the difference in frequency (on the same mode m) can be quantified as:

$$\frac{\Delta f}{f} = -\frac{\Delta L}{L} \quad (5.8)$$

As an example, for nominal cavities of $L=50$ mm and assuming a difference of $\Delta L= -0.01\mu\text{m}$, the following is obtained:

$$\begin{aligned} \text{FSR} &= 3 \cdot 10^9 \text{ Hz} && \text{Cavity Free Spectral Range} \\ m &= 187970 \\ f &= 5.63910 \cdot 10^{14} \text{ Hz} \\ \Delta f &= 1.127824 \cdot 10^8 \text{ Hz} \end{aligned}$$

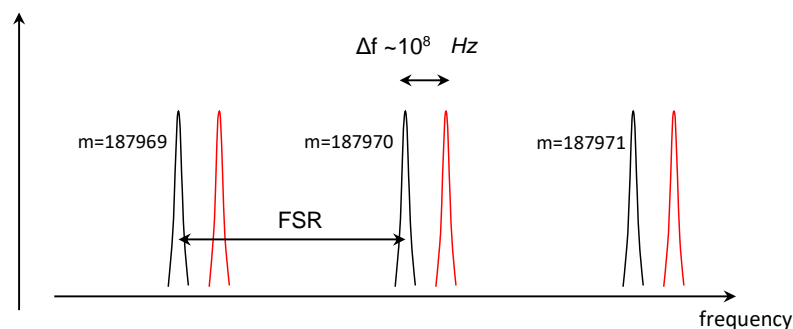


Figure 5-12 Spectra shift due to initial (uncompensated) length mismatch (schematics only)

The mismatch in resonance can be evaluated via beat note analysis between the two cavities with extreme accuracy (see for example Ref. [33]). The two cavities can then be relatively further tuned by controlling the length of one of the two by forcing a short length reduction in the one with lower resonance frequency as schematically shown in Figure 5-13.

In the specific example considered, clearly, the longer one need be reduced in length by about $0.01\ \mu\text{m}$ and during the process of length control their relative frequency is continuously monitored until a required matching is achieved.

During the process of matching the temperatures of the cavities need be *controlled and kept at given values* (as also described in the paragraph relevant to cavity stability).

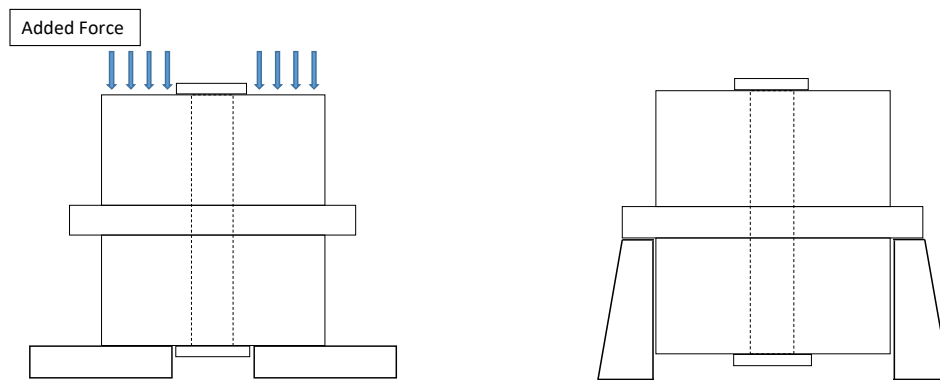


Figure 5-13 Schematics of the two cavities during matching (left the initially longer one, right the shorter one)-Thermal control items not shown

Based on the characteristics of the Ultra Low Expansion material (ULE) used for the cavity spacing (Ref.[34]), in order to obtain the $0.01\ \mu\text{m}$ displacement of the example, an overall force of about 30 N need be uniformly applied. This can be achieved by using disk piezo actuators but also, for the cavity remaining on ground, by loading the cavity with a given mass; in this last case, the loaded cavity will remain positioned for the ground interferometer while the other cavity (duly suspended) will be destined for flight. The mass to add would take into account the additional effects of mounting/positioning interfaces (for example the own weight acting with a net compression effect).

The tuning need be done with the two cavities integrated in the relevant thermo-mechanical 'environment' in order not to induce unwanted variations during disassembly-assembly. The passive matching has the advantage of not needing a continuous control and has no power/thermal dissipation and do not preclude the installation/presence of a piezo actuator.

The preliminary value *some hundreds of Hz of initial relative matching should be achievable* in a reliable and robust way and a goal of 100 Hz can certainly be considered.

5.3.4 Cavity Frequency Drift: ultra-stable optical cavities and temperature stability

In Figure 5-14, Figure 5-15 and Figure 5-16 are reported some characteristics relevant to ultra-stable cavities developed by different organizations; the list is not intended to be exhaustive and other suppliers/developers exist. In general these cavities are highly performing and their development methodology follows specific requirements and customization activities and performance assessment tests.

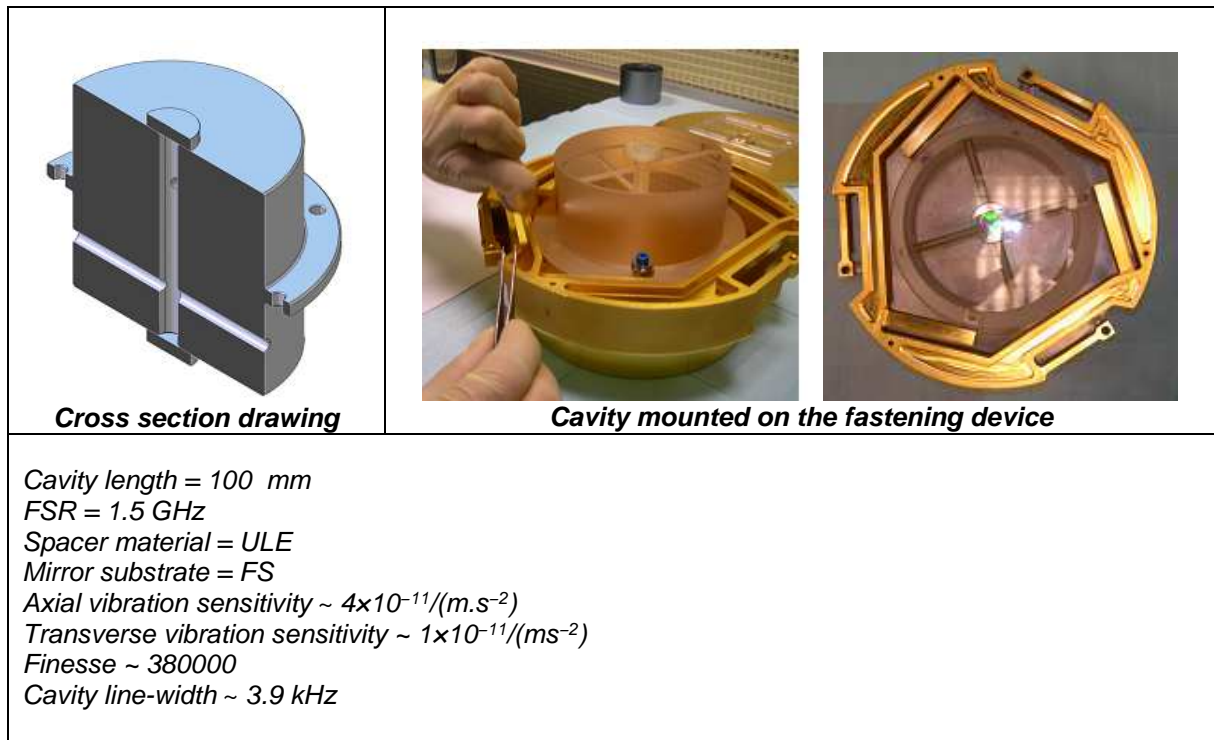


Figure 5-14 Example of ultra-stable cavity studied, realized and assembled by SODERN space company under CNES (French Space Agency) procurement (Ref. [35])

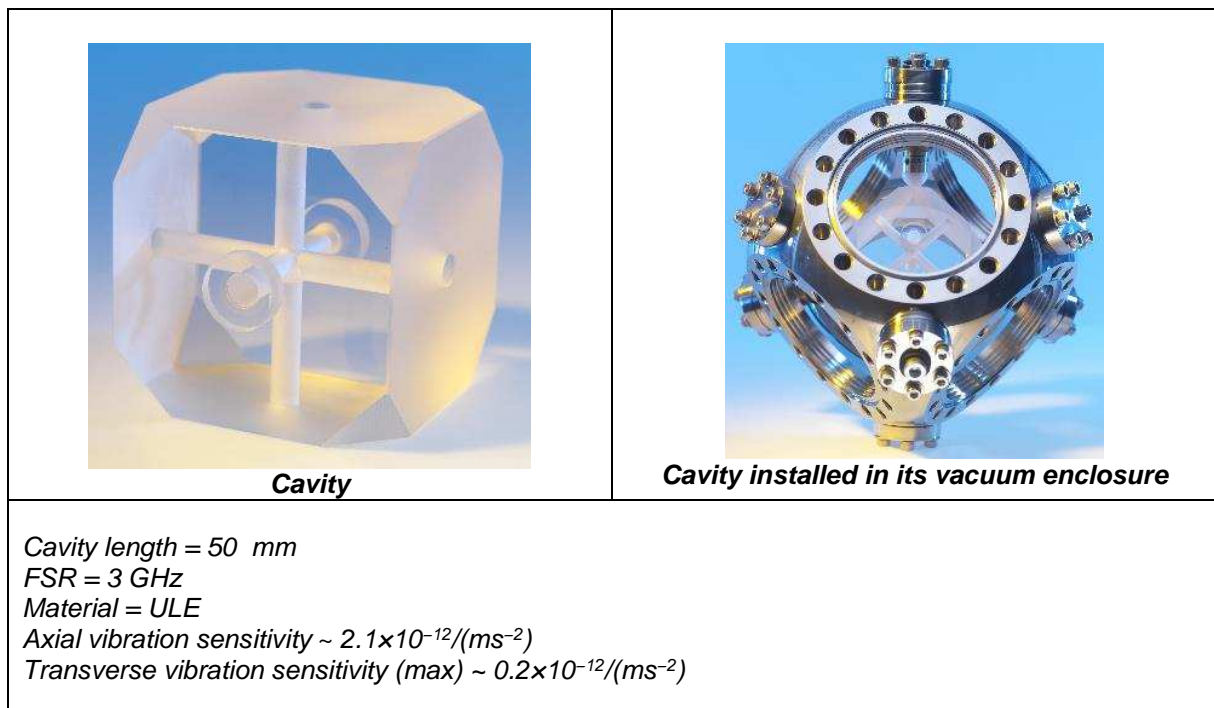

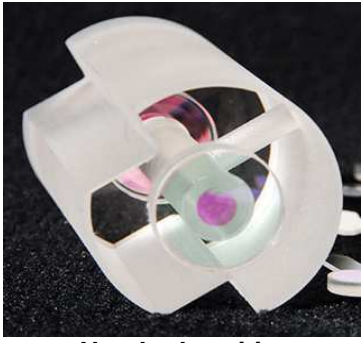


Figure 5-15 Example of a cubic Optical Reference Cavity for Space developed by NPL (National Physics Laboratory – UK) (Ref. [36] and Ref. [37]))

 <p style="text-align: center;">Cavity</p>	<p style="text-align: center;"><i>Some general features (summary)</i></p> <ul style="list-style-type: none"> ▪ Cylindrical cavities offers locked laser line-widths at the 40 Hz level ▪ 100 mm long ▪ 1.5 GHz FSR ▪ 50 mm diameter ▪ Standard mirror configuration is plano-50 cm ROC
 <p style="text-align: center;">Notched cavities</p>	<p style="text-align: center;"><i>Some general features (summary)</i></p> <ul style="list-style-type: none"> ▪ Notched cavities offer reduced acceleration sensitivity as compared to a cylindrical design ▪ Long spacer lengths, such as 100 – 300 mm, it is easier to achieve the lowest thermal noise floor and narrowest laser line-widths ▪ 1.5 GHz FSR (for 100 mm length) ▪ Acceleration sensitivity $< 5 \times 10^{-12} / (\text{ms}^{-2})$ ▪ Notched cavity geometry recommend a when locked <i>Hz-level line-widths and low frequency drift are paramount</i>
<p>Spacer material (in general) = ULE Mirror substrate (in general) = FS SLS offer wide customization support, e.g.:</p> <ul style="list-style-type: none"> – Mirror coatings capable of finesse values ranging from 20 to 500,000 – Multi-band mirror coatings using IBS dielectrics; crystalline mirrors – Spacers that are long, Z-shape, or which have multi-beam access for atomic physics & sensing – Unique options: build-up cavity, ULE ring cavity, confocal cavity – Folded cavities up to 300 mm in length for spectroscopy 	

**Figure 5-16 Examples of ultra-stable cavities developed by SLS (Stable Laser System, USA)
(Ref. [38] and Ref. [39])**

From a manufacturing point of view the cavities are in general constituted by the following elements/parts:

- a spacer, normally of top grade ULE;
- the two mirrors substrate (examples exists with substrates in Fused Silica as well as ULE);
- high quality mirror coating (e.g. some tens of layers of different dielectrics like SiO_2 and Ta_2O_5).

Normally the body of the spacer implements also the mechanical interfaces to the surrounding structures and as seen from the previous examples several possibilities are experimented. As far as the mirrors one of the two can be flat and the other with some concavity in order to present a well separated TEM_{00} mode and allow for a narrow linewidth.

The two most important features of Free Spectral Range and Finesse depend from the nominal cavity length, the mirrors characteristics and geometrical 'perfection' of realization (e.g. alignments, mirror flatness and curvature,).

Two of the key external environmental conditions which affect the performances are instead related to:

- sensitivity to mechanical loads/vibrations;
- sensitivity to thermal variations.

These two aspects are hereafter investigated.

Sensitivity to mechanical loads environment

The environments in which the integrated cavities operate are in general characterized by static and dynamic vibration loads which can perturb the geometry (and hence the frequency performances) of the cavity themselves; the parameter which indicates the goodness against loads/vibrations is normally called *acceleration or vibration sensitivity* with units $\#/(m/s^2)$.

In the considered case two cavities are present one for the ground interferometer and one for the interferometer on board the spacecraft; both cavities are considered matched when already integrated in their final structural and thermal containment housing.

As far as the *ground cavity* this is tuned at the ground station site while on anti-vibration suspensions. After matching no major frequency shifts are expected due to the mechanical environment since no major variation of loads/vibrations are present after tuning (tuned on site and used on site).

As far as the *on board destined cavity*, after matching (also tuned at the ground station site while on anti vibration suspension) will be integrated on the Spacecraft and later on placed on orbit; two environments will therefore be sequentially encountered:

- Handling, integration on the spacecraft and launch;
- Operative on orbit.

In the final operative environment no deformation due to gravity and no vibration will affect the performances of the cavity on board. However, since it has been tuned in *one g* conditions ($1g \sim 9.81 \text{ m/s}^2$), a certain amount of frequency shift is expected. This shift (for the on board cavity) can be estimated to be in the order of:

$$\begin{aligned} \text{sensitivity} &= 3 \cdot 10^{-12} \text{ } \#/(m/s^2) && (\text{assumed based on previous best cavity examples}) \\ \Delta f \sim f \cdot \text{sensitivity} \cdot 9.81 &\sim 17 \text{ kHz} && (\text{assuming } f = 5.63910 \cdot 10^{14} \text{ Hz}) \end{aligned}$$

This frequency shift is too large and need be compensated. This compensation can be already implemented on ground for example during cavities tuning by:

- determining the sign of the sensitivity (by e.g. turning the 'flight' integrated cavity upside down by 180°);
- matching with a residual off-set equal and opposite to the frequency shift expected when on orbit.

Assuming a 5% accuracy in this procedure a residual of 0.9 kHz shift can be considered.

As far as the environment encountered by the flight destined cavity during 'handling, integration on the Spacecraft and launch', the major concern is associated to the presence of possible

residual deformations caused by the experienced loads. This is difficult to estimate and can be assessed and verified during specific development (and final qualification) activity. The results obtained during development tests provide inputs to the cavity final design especially as far as its interfaces with the supporting structures and mechanical robustness.

Sensitivity to thermal variations

The cavities are basically all manufactured in top grade ULE (apart the mirror dielectric coatings) and therefore using a topmost thermal ultra-stable material. Nevertheless, residual inaccuracies in thermal stabilization temperatures can affect frequency stability in an important way. An example of thermal expansion curve is shown in Figure 5-17 Ref. [34]) and present a flat behaviour around 5-15°C.

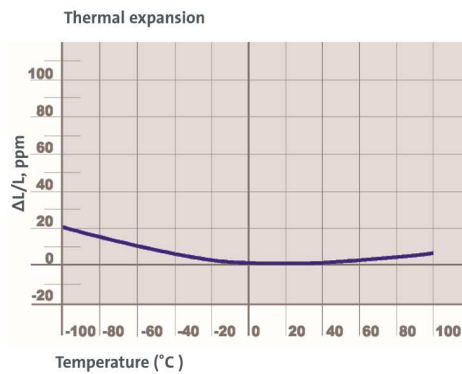


Figure 5-17 ULE example of coefficient of temperature expansion trend (Ref. [34])

Also based on Ref. [33], the trend for the CTE curve can be approximated (around the 'zero expansion temperature') by a quadratic law of the following type:

$$CTE = E \cdot (T - T_c)^2 \quad (5.9)$$

$$E \sim \text{Coefficient } \# / K^2$$

$$T_c = \text{Zero expansion temperature}$$

The coefficients E and T_c have a certain variability, depending on the specific lot/part of material, which can be determined by test.

The coefficient E could fall in the range 0 ± 10^{-9} and due screening would then allow to select a sample with minimum E (the more near zero); for the purposes of this discussion values of $E = 5 \cdot 10^{-10}$ and $T_c = 10^\circ\text{C}$ can be considered.

Following the exercise so far performed, and using a remaining apportionment of about $4.6 - 0.9 = 3.7 \text{ kHz}$ (as contribution of the combined space plus ground thermal related effects), a net remaining requirement of $3.7/2 = 1.85 \text{ kHz}$ would be present for each of the interferometers.

Taking into account the overall relation between frequency stability and temperature variation given by:

$$\Delta f = f \cdot E \cdot (T - T_c)^2 < 1850 \text{ Hz} \quad (5.10)$$

the following requirement can be derived for the temperature stability (using both the frequency stability of 1850 Hz and four times less):

$$\Delta f \leq 1850 \text{ Hz} \rightarrow (T - T_c) \leq 0.081 \text{ }^{\circ}\text{C}$$

$$\Delta f \leq 450 \text{ Hz} \rightarrow (T - T_c) \leq 0.04 \text{ }^{\circ}\text{C}$$

Thermal control stability requirement of $(T - T_c) < \pm 0.04 \text{ }^{\circ}\text{C}$ could be considered since in principle compatible with overall geometrical stabilities in the 1 nm range (rather than 4 considered for the exercise).

5.3.5 Frequency stabilization and first and second order PDH compensation

The laser frequency stabilization can be implemented by applying the Pound-Drever-Hall (PDH) technique to a tuneable laser source by making use of the ultra-stable optical cavity. PDH technique is very effective and is used in many advanced applications/developments (see for example Ref. [40], Ref. [41]); the general reference scheme is shown in Figure 5-18.

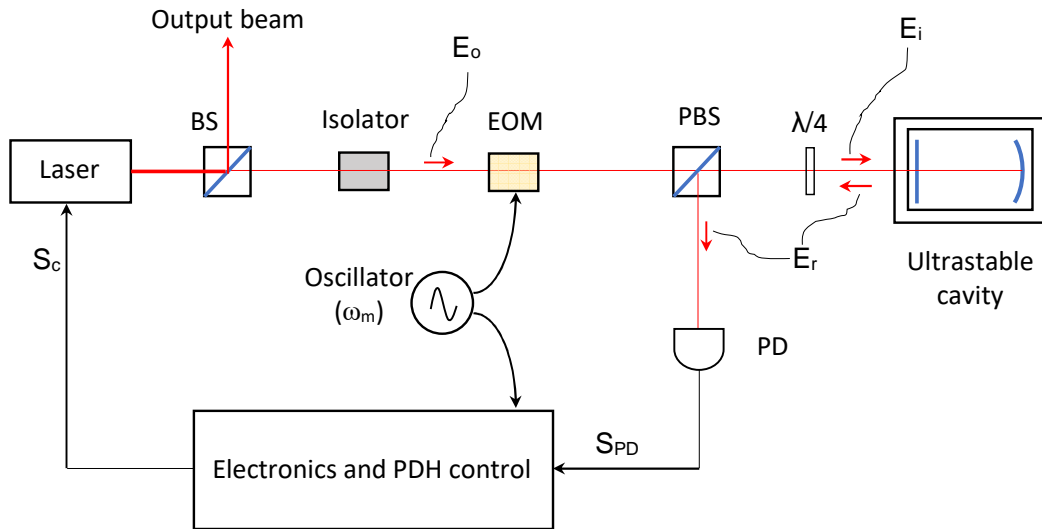


Figure 5-18 General schematics for the implementation of the PDH technique

With reference to Figure 5-18 and the symbols contained, and without entering excessive details, the main characteristics of the technique are hereafter noted (see e.g. Ref. [42]):

- initial (electric) amplitude

$$E_0 = E \cdot e^{i\omega t} \quad (5.11)$$

- electric amplitude after the EOM

$$E_i \approx E \cdot e^{i\omega t} \left(1 + \frac{\beta}{2} e^{i\omega_m t} - \frac{\beta}{2} e^{-i\omega_m t} \right) \quad (5.12)$$

where:

ω_m = EOM modulation frequency

β = EOM modulation depth (assumed $\ll 1$)

- ratio between cavity electric field reflected amplitude to cavity electric field incident amplitude

$$\frac{E_r}{E_i} = \frac{-r_1 + (r_1^2 + t_1^2)r_2 e^{i2\alpha}}{1 - r_1 r_2 e^{i2\alpha}} = R(\omega) \quad (5.13)$$

where:

E_i, E_r = Cavity reflected and incident (electric) amplitudes

r_1, t_1 = Reflection and transmission coefficients of cavity 'first' mirror

r_2 = Reflection and transmission coefficients of cavity 'second' mirror

$$\alpha = \frac{\omega L}{c}$$

- electric signal available after the Photo Diode (PD)

$$\begin{aligned} S_{PD} \propto |E|^2 |R(\omega)|^2 + |E|^2 \frac{\beta^2}{4} \{ & |R(\omega + \omega_m)|^2 + |R(\omega - \omega_m)|^2 \} + \\ & + |E|^2 \beta \{ R_e[\chi(\omega)] \cos(\omega_m t) + I_m[\chi(\omega)] \sin(\omega_m t) \} \\ & + |E|^2 K \{ R_e[\xi(\omega)] \cos(2\omega_m t) + I_m[\xi(\omega)] \sin(2\omega_m t) \} \end{aligned} \quad (5.14)$$

As can be seen the electric signal S_{PD} is made of three parts:

- a time constant part;
- a part varying at frequency ω_m modulated in amplitude by $\chi(\omega)$;
- a part varying at frequency $2\omega_m$ modulated in amplitude by $\xi(\omega)$.

The most important information, for frequency stabilization, associated to S_{PD} is constituted by $\chi(\omega)$ and (to a lesser extent) by $\xi(\omega)$.

Parameter $\chi(\omega)$

This can be extracted from the signal S_{PD} by *amplitude demodulation of the carrier ' ω_m '* and results to be *anti-symmetric* with respect to $(\omega - \omega_{res})$ where ω_{res} is the cavity resonant frequency on which the locking is performed. The structure of $\chi(\omega)$ results to be the following (see e.g. Ref. [42]):

$$\chi(\omega) = R(\omega)R^*(\omega + \omega_m) - R(\omega)R^*(\omega - \omega_m) \quad (5.15)$$

The parameter $\chi(\omega)$ thus provide a good and useful error signal (with sign) on how much the actual frequency ω is out from the desired frequency ω_{res} :

$$\epsilon_1 \propto \chi(\omega)$$

Once ϵ_1 is extracted it can be directly utilized to construct the signal S_c for commanding the laser tuning mechanism.

An example of error signal anti-symmetric profile is sketched in Figure 5-19 (taken from Ref. [42]); the part useful for control is the 'linear' part crossing the origin.

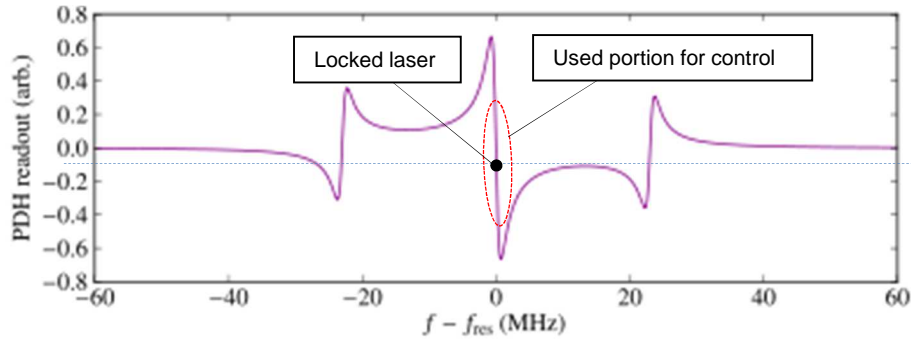


Figure 5-19 Example of PDH error signal anti-symmetric around f_{res} (qualitative only)

Parameter $\xi(\omega)$

This can be extracted from the signal S_{PD} by *amplitude demodulation of the carrier* $2\omega_m$ and results to be a *symmetric* with respect to $(\omega - \omega_{\text{res}})$ where ω_{res} is the cavity resonant frequency on which the locking is performed. In this case the parameter $\xi(\omega)$, a second order function, is not the primary source for construct an error signal; however it can provide useful information to be used as complement to the key anti-symmetric type error. As per Ref. [43] the structure of the symmetric error signal ϵ_2 , that can be built on $\xi(\omega)$, appears to be (around the resonance conditions):

$$\epsilon_2 = A \cdot (\omega - \omega_m)^2 + B \propto \xi(\omega) \quad (5.16)$$

In Ref. [43] the use of this symmetric correction has been to overcome dead zones in the measurement of the error signal of anti-symmetric type; in figure Figure 5-20 (taken from Ref. [43]) is shown the qualitative shape of the symmetric error with indication of the locked condition.

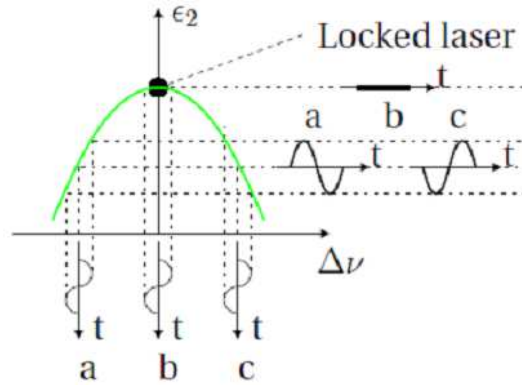


Figure 5-20 Symmetric type error that can be extracted from the 2ω (example only – Picture from Ref. [43])

The necessity/advantage to using the symmetric error (as support to the anti-symmetric one) has anyway to be evaluated on a specific bases.

Overall schematics of PDC control

The extraction of error signal in PDH type control can be as per the logical schematics shown in Figure 5-21 (see also Ref. [43]).

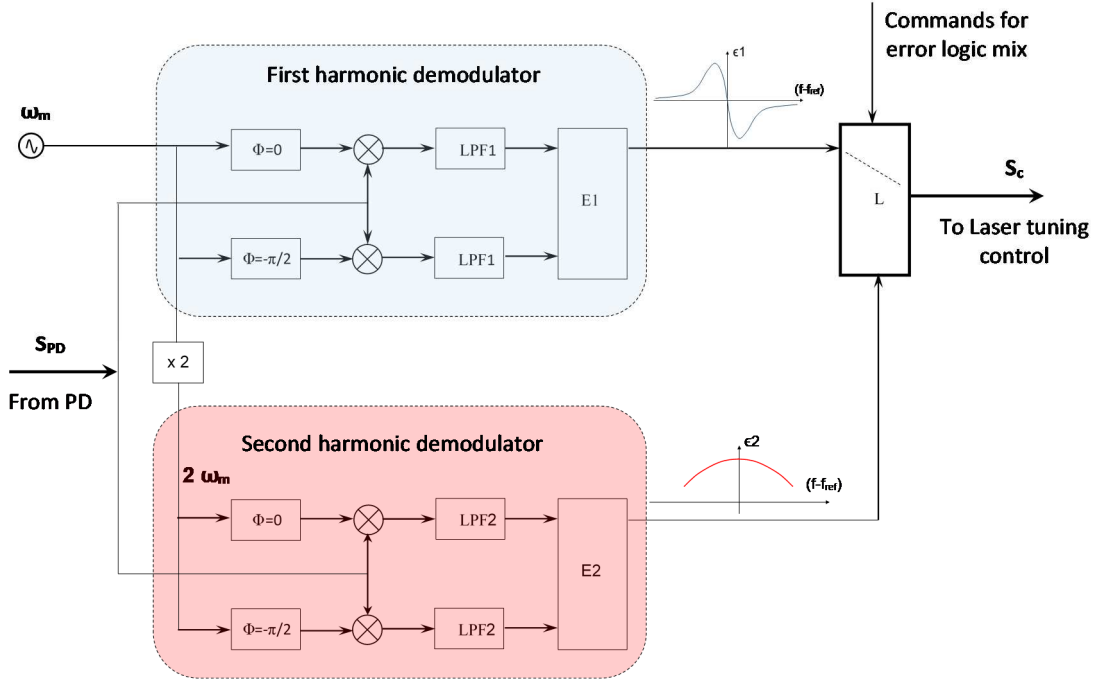


Figure 5-21 Logical schematics for error signal extraction in PDH type control

With reference to above scheme, the following observations can be done:

- The input data are the signal S_{PD} (from the PD), the reference frequency ω_m and commands for the logic on error type mix/selection;
- In the complete version, two amplitude demodulators are implemented: on the first harmonic carrier ω_m and on the second harmonic carrier $2\omega_m$;
- A logic circuit, based on external commands, select/merge the two types of signals error available: the anti-symmetric (the primary one) and the symmetric (which can be also excluded);
- The output data is the signal S_c to be sent to the laser for frequency tuning;
- The scheme shown is functional and not implementative (e.g. converters and circuitry not shown).

Consideration on frequency stabilization performances

The preliminary considered value of $\Delta f_{REQ-LCL} \cong 0.25 \text{ kHz}$ on each unit is indeed a mix between a slight centre frequency offset ($f-f_{ref}$) combined with a finite line width control.

Advanced laboratory applications often refer to achievable frequency stabilization which can in the Hz range and sometimes even of sub-Hz (as far as line-width).

Although the studied application is *not a laboratory one* (one of the unit is assumed on board a satellite) it can for now be assumed that a performance in the order of tens of Hz could be preliminary achievable (to be confirmed by future verifications tests).

5.3.6 Development needs

The issue of interferometers calibration based on frequency ultra-stable sources is definitely an important and critical matter. In principle, performances as assumed (on Δf_{REQ-IM} , $\Delta f_{REQ-CFD}$,

$\Delta f_{REQ-LCL}$) are achievable for advanced laboratory applications but the problems associated to a One-way experiment scenario are different:

- one of the two interferometers is installed and operative on-board a spacecraft in a very harsh environment especially from a thermal point of view and for the heavy mechanical loads and vibrations arising during launch conditions;
- after system deployment is not any more possible to intervene (physically) on the space based interferometers to correct or overcome possible (un-expected) arising problems.

It is therefore *necessary*, should the experimentation be really pursued, to perform a prototyping/development activity with the main objective to verify the design, the achievable calibration performances (for example overall 4 nm or 1 nm as goal) and reliability after units qualification testing for flight. In particular the following steps ought to be preliminary considered:

- Detailed study, manufacturing and development of two representative Units (prototypes) of interferometers (one aimed at Ground Station, one aimed at Space) and associated electronics and instruments;
- Effectiveness and repeatability of the procedure for initial interferometers matching;
- Overall prototypes performance characterization and comparison (frequency behaviour, thermal control effectiveness and stability, frequency lock,);
- Execution of the typical space qualification tests (normally foreseen for the Units intended to fly). In particular: *thermal-vacuum and launch conditions/loads*. These tests can potentially be 'destructive' and could create residual geometrical and structural modification on the items tested. Clearly of major concern are potential distortion on the ultra-stable cavity;
- Repetition of all performance characterization tests to check potential degradations *after* the high level space qualification loads.

These activities are expected to be demanding in terms of both schedule and costs.

5.4 Fibre optic thermal stability and attenuation

The long arm of the Mach-Zender interferometers, both on ground and on board the spacecraft, are realized through fibre optic of single mode type.

Although several products of excellent performance exist on the market for commercial applications, two points deserve specific considerations: thermal stability and attenuation.

Thermal stability

The actual length of the fibre optic depends on the initial reference length (for example the nominal 400 m), the coefficient of temperature expansion (primarily core/cladding, assuming a soft jacket), the temperature variation around a reference and the temperature distribution uniformity. As the simulation pointed out a certain length variation multiple of wavelength is tolerable, assuming 'frequent calibrations (wavelength zero passage)'.

The multiple wavelength residual *should not however be excessive* since it can induce loss of (interference) visibility and distortion in the phase response curve (see also paragraph 4.3.1). A possible approach in order to keep limited this 'multiple wavelength length variation' is the following:

- utilize fibres with low CTE, like Fused Silica (silica glass) presenting CTE $\sim 0.5 \cdot 10^{-6}$;

- keep the temperature of the spool controlled to a good (but achievable) accuracy, for example $\Delta T_c = \pm 5^\circ\text{C}$ around some reference value;
- measure the temperature of the spool to a good accuracy, for example $\Delta T_m = \pm 0.5^\circ\text{C}$;
- perform a *fibre length compensation in open loop by means of a piezo controlled prism/mirrors* utilizing the temperature information.

The residual fibre length error, after open loop compensation, is therefore in the order of:

$$\Delta L = L \cdot \text{CTE} \cdot (\Delta T)_m \quad (5.17)$$

As an indication, under these assumptions, a 400 m fibre in Fused Silica would present a residual error in length of about 0.1 mm (approximately 188 wavelengths at 532 nm, after zero phase calibration). This length variation with respect to the nominal length is acceptable for the application.

The possibility to achieve such compensation would however depend on the uniformity of the spool temperature distribution and measurement point.

Attenuation

The useful signal in the proposed experiment is the de-phasing and such signal increases as the utilized wavelength decreases; in Figure 5-22 is reported a comparison, under same conditions, of the expected de-phasing in case a wavelength of 1064 nm were used as compared to 532 nm used so far in the simulations. From this point of view low wavelength are preferred.

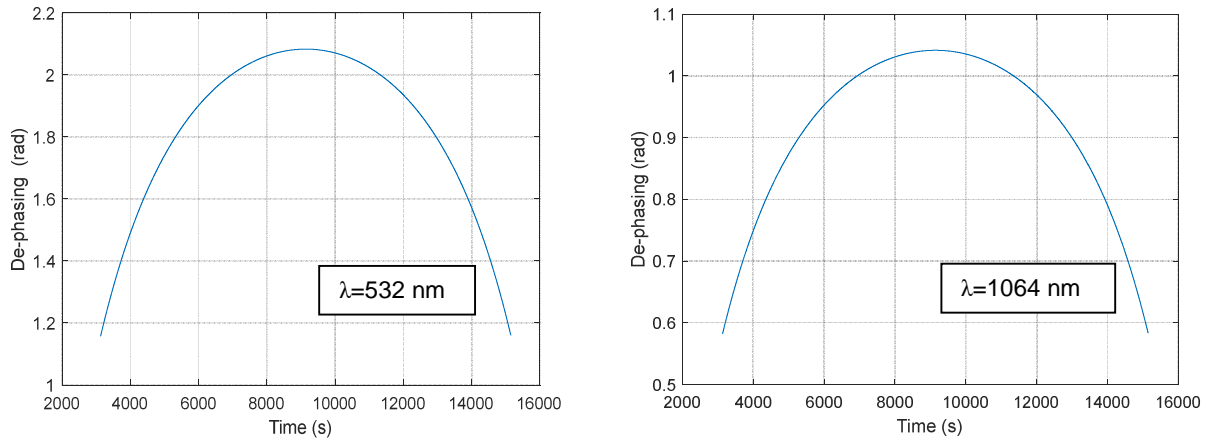


Figure 5-22 De-phasing signal comparison between 532 nm (left-for 532 nm same picture as reported in Figure 4-2 has been used) and 1064 nm (right)

As far as fibre optic, their overall attenuation depends on wavelength as reported in Figure 5-23 (taken from Ref. [44]). The attenuation presents minimum toward the 1.5 μm range typical for telecommunication applications.

For lower wavelength, for example moving toward 532 nm, the attenuation increases and becomes dominated by the Rayleigh scattering and an estimate can be done using the following relation (taken from Ref. [44]):

$$\alpha(\lambda) = \alpha_0 \left(\frac{\lambda_0}{\lambda} \right)^4 \quad (5.18)$$

where:

$$\alpha_0 = 1.7 \text{ dB/km} \quad \text{at } \lambda_0 = 0.85 \mu\text{m}$$

For $\lambda=532$ nm this lead to an attenuation of ~ -12 dB/km which is in line with the curve in Figure 5-23 by slightly extending its horizontal scale to the left.

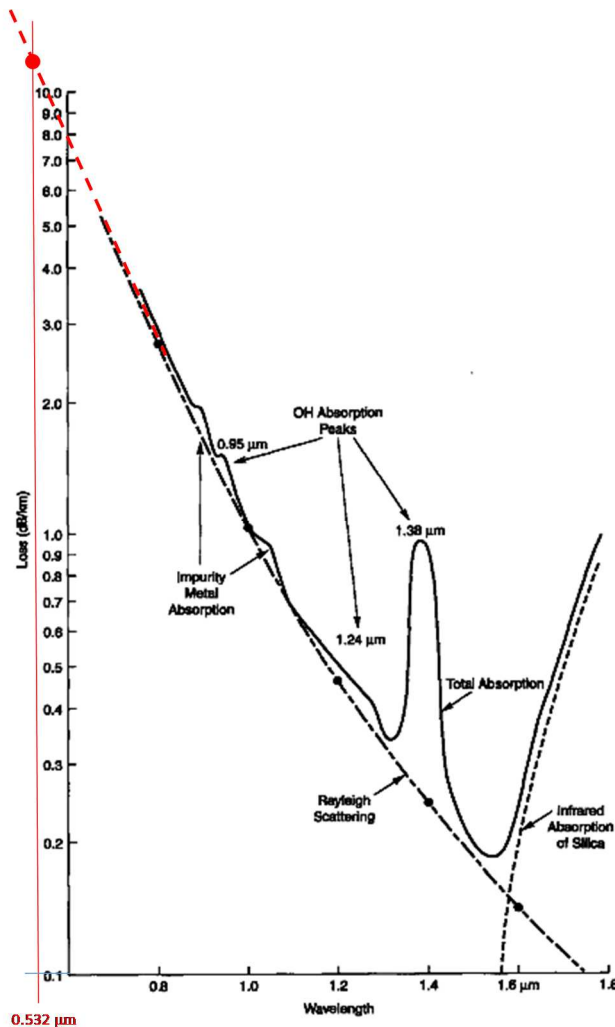


Figure 5-23 Typical fused silica fibre optic losses (basic picture from Ref. [44] with added projection at 532 nm)

On the market are available good products of silica glass material as example reported in Ref. [45] but with a loss higher than 12 dB/km.

5.4.1 Development needs

The appropriate selection and characterization of the fibre optic is an important step in the development of the experiment. Based on the considerations reported in the previous paragraph, during the early detailed definition of the experiment, some development and performance assessment activities are appropriate in the following areas:

- detailed thermal design of the spool (and its support) and early breadboarding and test of the complete open loop length compensation to check the effectiveness;
- assessment of the attenuation level at short wavelength for the candidate fibres.

5.5 Single Photon Detectors

True Single Photon detectors are necessary for the experiment and the general performances are identified by the following types of parameters:

- Quantum Efficiency (QE);
- Dark Count Rate (DCR);
- After-pulse probability;
- Gating features;
- Timing features;
- (Active) thermal stabilization.

Appropriate QE combined with low DCR and low after-pulse probability are pre-requisite. Gating is used in order to activate the counting only during time windows of interest so to exclude spurious counting as much as possible. In this application, the pulses transmission from ground is periodic and controlled by a selected repetition rate. This combined with a good achievable timing synchronization between the Ground Station and the Spacecraft would allow gating implementation.

Active solid state thermal stabilization is a definitively desirable feature especially in view of the detectors installation in a Spacecraft environment. Detectors already embedding such feature are preferable.

An example of product interesting for the application is a PDM series Single Photon Detector from MPD (Micro Photon Devices) given in Ref. [46] and some of its characteristics are summarized in Figure 5-24.

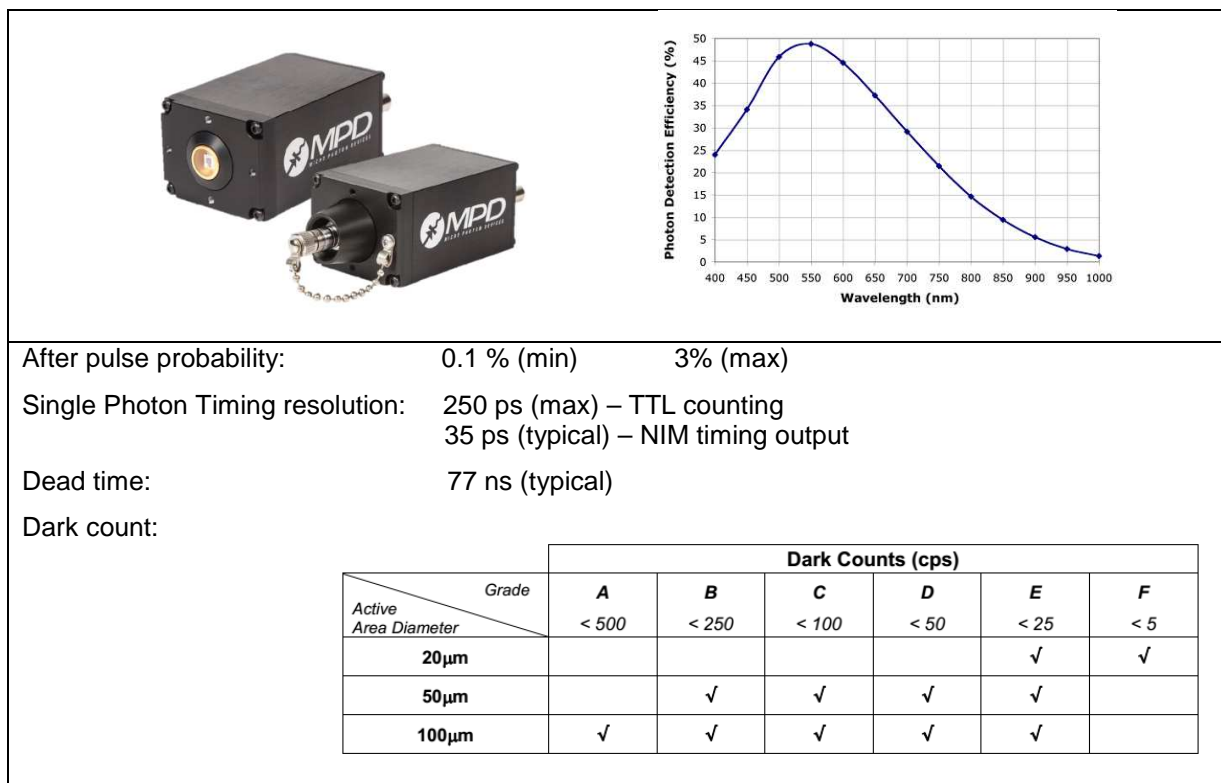


Figure 5-24 Some features of the PDM-MPD Single Photon Detector (synthesis from Ref. [46])

5.5.1 Development needs

In general, for a space application, flying equipment need to pass appropriate development and qualification tests whatever technology/product is selected. The equipment (in this case a Single Photon Detector) need to guarantee the foreseen performances after severe environmental condition and in particular:

- Launch vibration;
- Thermal Vacuum cycling;
- Radiation.

In this respect some early verification are appropriate.

For the subsequent simulation purposes the following average characteristics are considered:

- Quantum Efficiency = 45 %
- Dark Count Rate = 25 count/s
- After-pulse probability = 3 %

5.6 Some issues on Corner Cube Retro-Reflectors

The implementation of many 'small' retro-reflectors on-board, like in many existing Spacecrafts, give raise to *superposition effects* on the return beam (reflections from different locations at different distances and with different view cross section). This is of concern if the if Doppler compensation has also to be compatible via a 'double measurement scheme'). The utilization of a single 'wide' retro-reflector could be more appropriate.

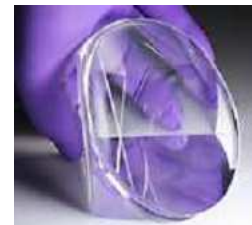


(on Bei-Dou S/Cs)

Figure 5-25 Some examples in-flight retro-reflector



(on Lageos)



(picture from Zygo data sheet (Ref.[47]))

Figure 5-26 Examples wide area retro-reflector

5.6.1 Development needs

Design and characterization of corner cube retro-reflector(s) assembly (use of one single 'wide' device or study an appropriate surface layout).

(Page Intentionally Left Blank)

6 OVERAL EXPECTED PERFORMANCES

6.1 Model updating based on photon counting

So far the programs utilized (including the last 'cowsim292moddephaseBN' implementing the 'Modulus $N \cdot \lambda$ ' compensation) all had the key objectives to determine the de-phasing induced by the metric part effects and therefore the probability to detect the photon at one sensor or the other. Basically was assumed to 'ride the photon that leave the ground interferometer and reaches the space based interferometer'. The implicit assumption has been therefore to observe/deal with phenomena occurring at single photon level.

A final version of simulation program (cowsim292moddephaseBNFIN1) then has been implemented with the objective to perform photon counting at the detectors taking into account a more complete experimental configuration. The key points characterizing the development of this last program are summarized as follows (see also schematics in Figure 6-1):

- photon pulses, with due energy and repetition rate, are generated by the ground laser source;
- at generation the number of photons associated to each single pulse is very high;
- during the from the ground station to the spacecraft three types of attenuation will reduce the number of photons present per pulse:
 - attenuation in the optical circuits (on ground and after on board);
 - atmospheric attenuation;
 - free space attenuation;
- the average number of photons per pulse reaching the spacecraft (following a Poissonian distribution) is expected, by design, much less than one in average so that everything observed at S/C level is, with high probability, at single photon level and with much less probability at two or more photons level;
- each photon reaching the detectors will then be counted based of the characteristics of the detectors including spurious or unwanted counts (quantum efficiency, after-pulse, dark counting);
- the counting's at the two detectors, carried out for duly sized observation windows, allows to re-construct measured probabilities and then the associated de-phasing.

The re-constructed de-phasing is then the key scientific data return for the mission experiment.

The results obtained from simulation when considering the various sources of errors and uncertainties are then compared against the expected nominal results when no errors and uncertainties are present. This allows to have both an indication on the level of accuracy achievable as well as sensitivity indications against critical parameters.

Clearly if the experiment were performed then the simulated results (both nominal and the perturbed ones) can directly be compared against the real flight data.

As far as the pulses *repetition rate*, *attenuation* and *single photon detectors gating*, they deserve some more clarifications as here-below reported.

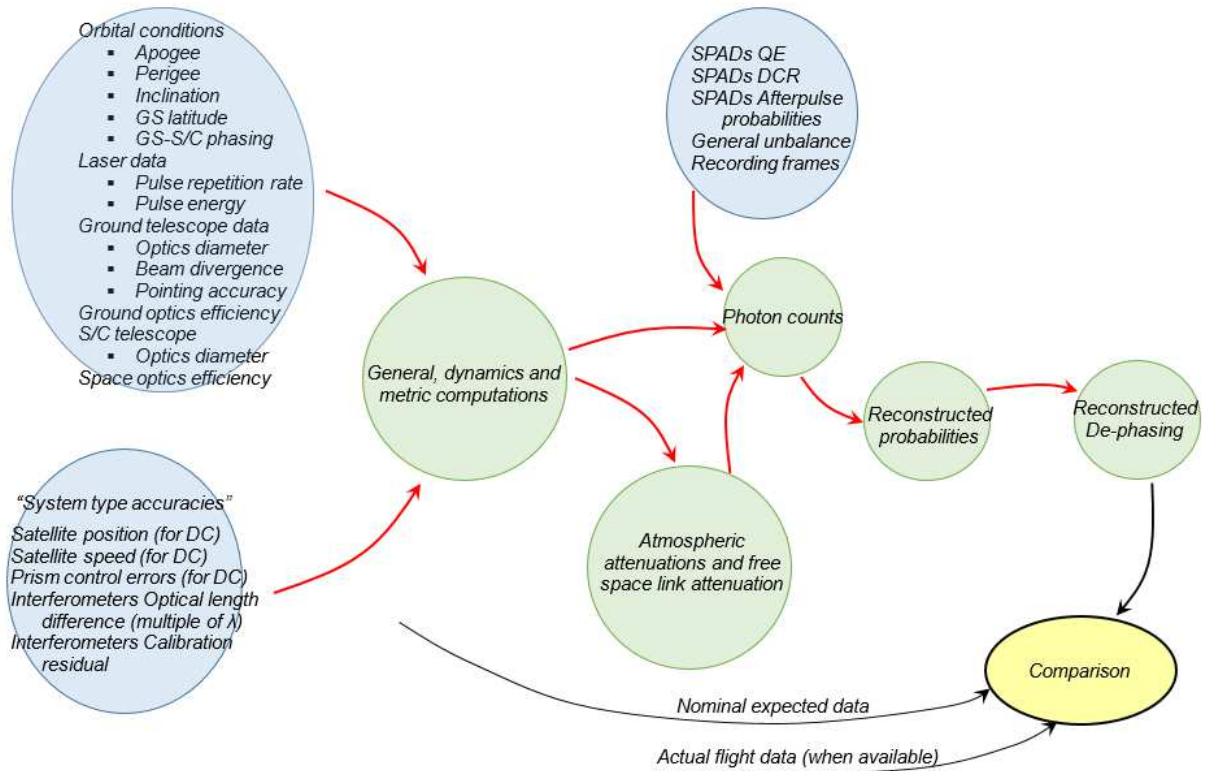


Figure 6-1 Structure (flow) schematics of the final version of experiment simulation program

6.1.1 Photon pulses repetition rate

The repetition rate needs be limited in order to guarantee that no more than one pulse at a time is present in the interferometers. This will avoid any possible cross interference between photons belonging to subsequent pulses. As an example, for interferometers length of 400 m, the maximum repetition rate shall therefore not exceed c/L (c = speed of light, L = Interferometer imbalance length). For a 400 m interferometer therefore repetition rate < 750 kHz.

6.1.2 Attenuations

In the following, rather than utilizing attenuations, transmission is considered. For the total transmission, three contributions are foreseen:

- Atmospheric transmission;
- Free space link transmission.
- Optics efficiency (on ground and on board).

The total transmission takes then the form:

$$T_{TOT} = \frac{\text{Number of photons reaching the detectors}}{\text{Number of photons emitted by the source}} = \eta_G \cdot T_{atm} \cdot T_{free\ space} \cdot \eta_S \quad (6.1)$$

where:

η_G = Overall ground optics efficiency
 η_S = Overall space based optics efficiency
 T_{atm} = Atmospheric transmission
 $T_{free\ space}$ = Free 'space link' transmission

➤ Atmospheric Transmission

Atmospheric transmission T_{atm} depends on factors such as wavelength, elevation of observation and general reference conditions taken for the atmosphere. In Figure 6-2 is reported a profile of atmospheric transmission taken from Ref. [48] in reference conditions of clear sky and 2 cm of precipitable water vapour. In general it is: $T_{atm} = T_A(\lambda, \vartheta_{zen})$

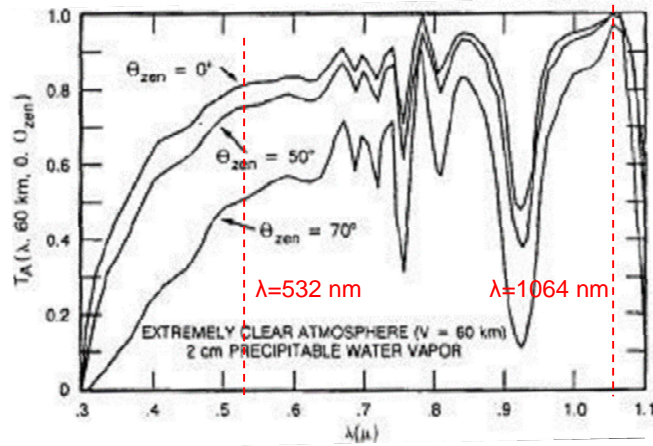


Figure 6-2 Atmospheric transmission (T_A) as a function of wavelength and of angular displacement from zenith (picture taken from Ref. [45])

➤ Free space transmission

The free space transmission can be computed via equations derived from the so called 'radar link equation' (see for example Ref. [49] and Ref. [20]).

The one way (from ground to satellite) link equation, in the specific case considered, can be written as:

$$T_{Free\ Space} = \frac{N_{Photons\ (received\ per\ pulse)}}{N_{Photons\ (transmitted\ per\ pulse)}} = G_t \frac{1}{4\pi D^2} \pi r_o^2 \quad (6.2)$$

where:

D = Distance (slant) between the ground telescope and the space telescope
 r_o = Objective radius of the space telescope

$G_t = \frac{8}{\vartheta_t^2} \exp \left[-2 \left(\frac{\vartheta_p}{\vartheta_t} \right)^2 \right]$ = Ground optical transmission gain
 ϑ_t = Ground telescope divergence

ϑ_p = Ground telescope pointing error

➤ Optics efficiency

Optics efficiency (both on ground optics and on board optics, here interpreted as transmissivity) can be determined based on the optical elements present, including the fibre optics forming the 'long arm' of the Mach-Zender interferometers.

As discussed in previous paragraph, attenuations a short wavelength utilizing fused silica (silica glass), can be in the order of -12 dB/km.

Assuming not to make any specific optimization on fibre development/selection, a 400 m loop (long arm) would then present an attenuation of approximately -4.8 dB (transmissivity of 0.33 linear scale). Furthermore, in order to have a balanced condition (between the superimposed modes) an equivalent attenuation could be inserted into the short arm (by means of e.g. neutral disk attenuator).

As far as the number-types-topology of the optical elements, this will depend on the specific design chosen; however in order to derive an order of magnitude (for the attenuations), preliminary layouts shown in Figure 6-3 and in can be considered for the ground and space optics respectively.

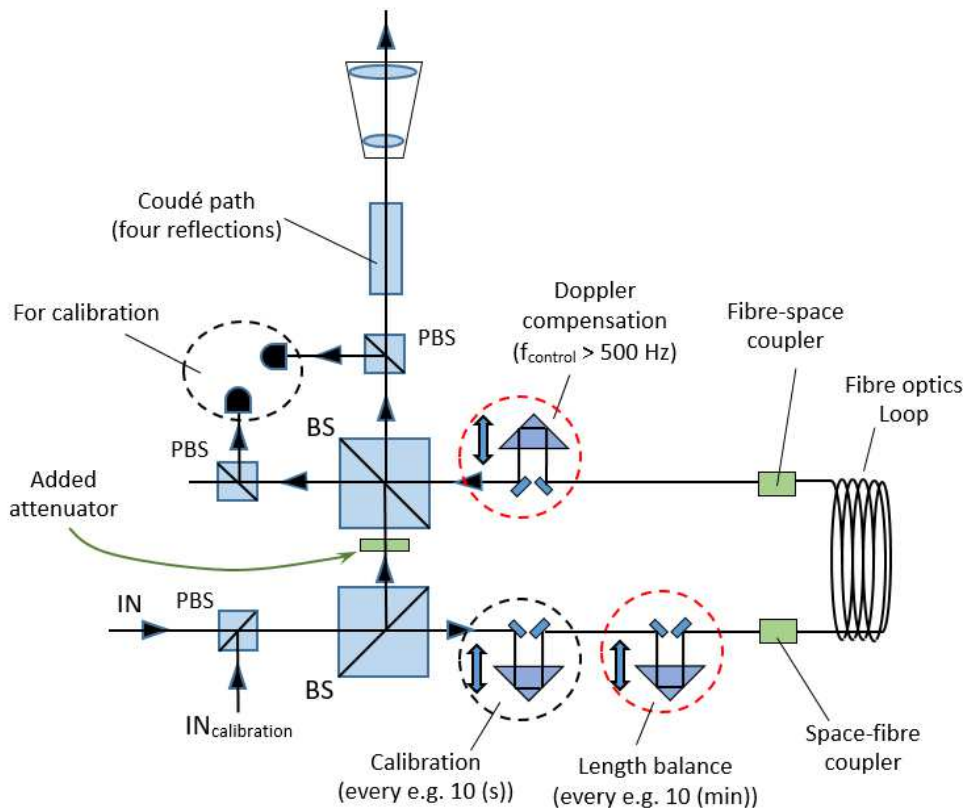


Figure 6-3 Schematics of ground optics (only for attenuation estimate)

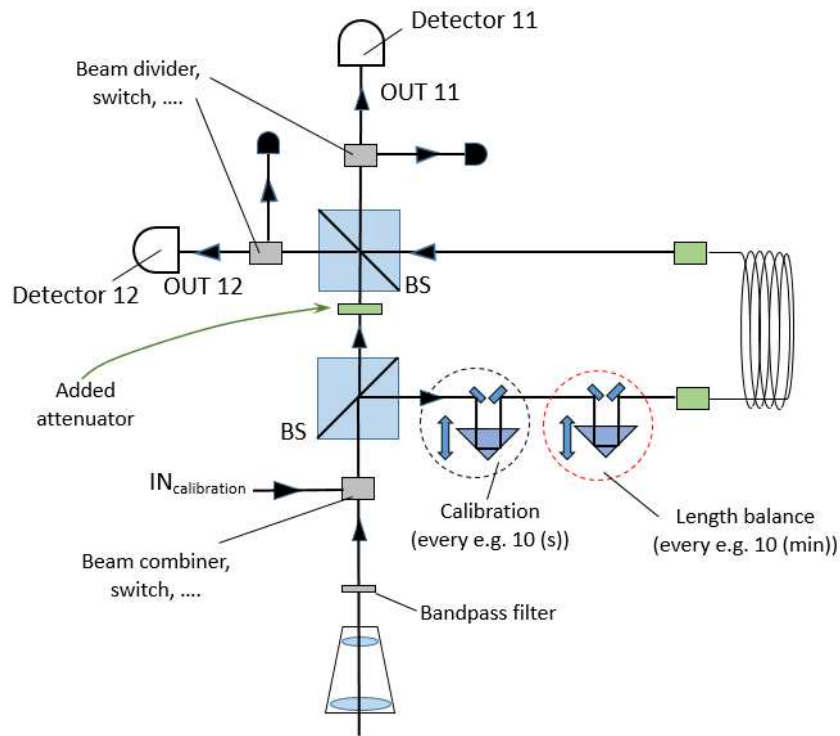


Figure 6-4 Schematics of spacecraft optics (only for attenuation estimate)

For the ground optics approximately 24 reflections/refractions are expected while for the Spacecraft optics a total of 17 are expected. In summary the optics efficiency (inclusive of fibre optics) can be assumed as:

$$\eta_G = (0.96)^{24} \cdot 0.33 \cdot \frac{1}{2} \sim 0.06 \quad (\text{ground optics efficiency})$$

$$\eta_S = (0.96)^{17} \cdot 0.33 \sim 0.16 \quad (\text{space based optics efficiency})$$

where an average reflection/refraction process efficiency of 0.96 has been assumed.

6.1.3 Single Photon detectors (features and gating)

True Single Photon detectors are necessary for the experiment and their general level of performances are identified in terms of Quantum Efficiency (QE), Dark Count Rate (DCR), after-pulse probability. Since two detectors are used, a slight asymmetry is inevitable and the following parameters are assumed for the purposes of simulation:

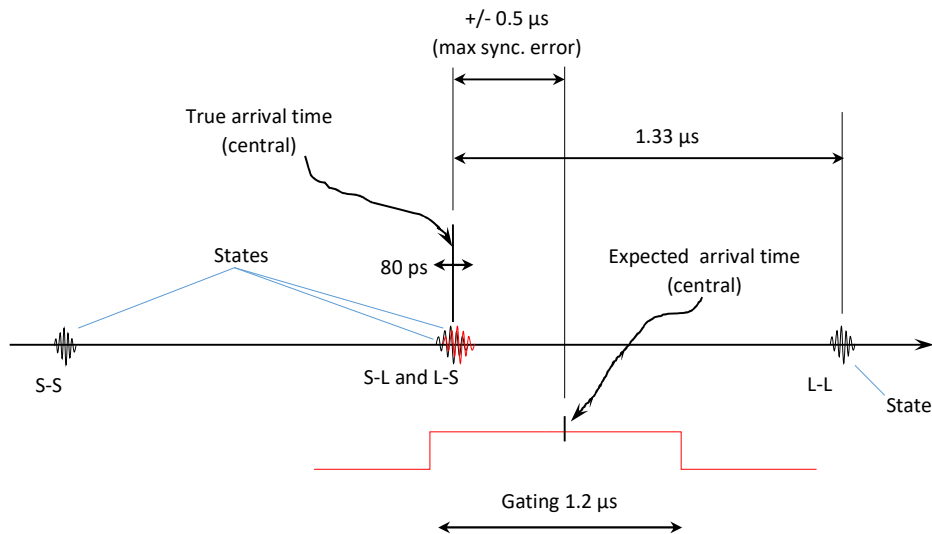
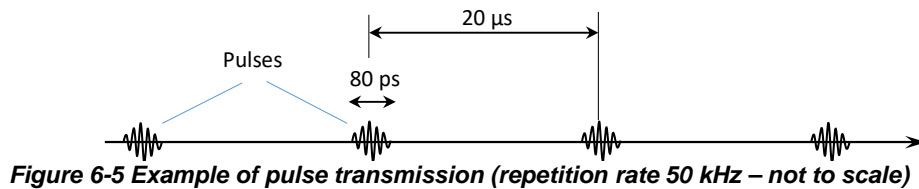
SPAD11	SPAD12
▪ Quantum Efficiency = 45 %	▪ Quantum Efficiency = 47 %
▪ Dark Count Rate = 25 count/s	▪ Dark Count Rate = 22 count/s
▪ After-pulse probability = 3 %	▪ After-pulse probability = 2 %

The purpose of gating is to enable photon detection only for the minimum time needed thus reducing the influence of spurious effects like dark count rate. It is noted that the pulses transmission from ground are periodic and controlled by a selected repetition rate (see for example Figure 6-5 for a pulse repetition rate of 50 kHz). Each pulse, arriving at the Spacecraft,

since duly attenuated, can carry one photon in superposition of states; the gating objective is to enable the photon acquisition by the detector only for the states S-L and L-S arriving indistinguishable at the 'central window' (see for example Figure 6-6). The width of the gate (ideally to be kept to a minimum) depend on:

- coherence time of the photon;
- time synchronization accuracy between the S/C and the GS;
- time separation between subsequent pulses (repetition time);
- interferometer unbalance.

In the example of Figure 6-6 the gating time has been tentatively set to $1.2\ \mu\text{s}$, compatible with repetition time of $20\ \mu\text{s}$, coherence time of $80\ \text{ps}$, interferometer unbalance of $400\ \text{m}$ (which induce states separation of about $1.33\ \mu\text{s}$) and a synchronisation accuracy (between S/C and GS) as bad as $\pm 0.5\ \mu\text{s}$.



Concerning time synchronization error between Ground Station and Spacecraft, the utilization of Oscillators/GPS disciplined units can be considered (since GPS signals are available, for large portions of time, to S/C in LEO, MEO up to GEO). These units can provide synchronization accuracies in the *order of tens of nanoseconds* (see for example Ref. [50]). In case of GPS signal loss, these disciplined systems can hold a good synchronization for long time. For example the Chip Scale Atomic Clock (CSAC) -GPS Disciplined Oscillator reported in Ref. [51], and recently available *off-the-shelf for space applications*, allows of $\pm 1\ \mu\text{s}$ accuracy after 24 hours of GPS loss ($\pm 0.5\ \mu\text{s}$ are certainly guaranteed after 12 hours of GPS loss).

6.2 Revised reference requirements

A tentative set of key requirements was already given in Table 4-3. However based on the technology considerations performed in Paragraph 5, some of the requirements can likely be revised or taken as goal, specifically:

- *Vbias*: Satellite speed (S/C-GS radial) measurement bias
- *Vnoise*: Satellite speed (S/C-GS radial) meas. noise
- *Pcbiasn*: Prism control bias error
- *Pcnoisen*: Prism control noise error
- δ L1ID: Perturbation (multiple w. l.) on Ideal length of GS interferometer
- δ L2ID: Perturbation (multiple w. l.) on Ideal length of S/C interferometer
- Interferometers calibration and stability

The revised set of key requirements is summarized in herebelow Table 6-1.

Requirement/Performance	Remark
<i>Rbias</i> : Satellite position knowledge bias.... = 5 m	
<i>Rnoise</i> : Satellite position knowledge noise (1 sigma).... = 1.5 m	
<i>Vbias</i> : Satellite speed (S/C-GS radial) measurement bias... = - 0.0004 m/s (for the reference trajectory..... = -0.0002 m/s	Paragraph 5.1
<i>Vnoise</i> : Satellite speed (S/C-GS radial) meas. noise (1 sigma)... = 0.0002 m/s (for the reference trajectory..... = 0.00015 m/s	Paragraph 5.1
<i>Pcbiasn</i> : Prism control bias error = 3 nm (development goal..... = 1 nm	Paragraph 5.2.3
<i>Pcnoisen</i> : Prism control noise error(1 sigma).....= 0.3 nm (development goal).....= 0.1 nm	Paragraph 5.2.3
δ L1ID: Perturbation (multiple w. l.) on Ideal length of GS interferometer = + 205 λ (= 400.00010906 m)	Assuming FS fibre L=400 m ΔT meas = 0.5 °
δ L2ID: Perturbation (multiple w. l.) on Ideal length of S/C interferometer = - 410 λ (= 399.99978188 m)	Assuming FS fibre L=400 m ΔT meas = 1 °
<i>Delta L2-L1</i> : Calibration-calibration and geometrical stability included = - 0.004 μ m (development goal)..... = -0.001 μ m	Paragraph 5.3

Table 6-1 Revised set of key requirements

6.3 Expected performance in selected orbital cases

6.3.1 Simulated cases

Four simulation cases are considered (Table 6-2): R1A, R1B, R1C, R1D and they refer to the same reference orbit R1 with variants in operative conditions and input parameters to assess the relevant performance variation.

Cases *R1-A* to *R1-B* investigate two wavelengths (532 and 1064 nm respectively) and both cases refer to conditions where prism control capability (used for Doppler compensation),

interferometers calibration/stability and S/C speed determination are assumed compatible with a short term dedicated development/verification activity. In passing from case R1-A to R1-B, the following input modifications have been considered (to support results comparison):

- The energy per pulse is halved in order to work with approximately the same number of photons per pulse injected into the ground interferometer (in the specific case approximately $2.676 \cdot 10^8$);
- The interferometers length associated to residual multiple wavelength is modifies so to be an exact multiple also for the new wavelength; specifically:
 - $\delta L1/D$: Perturbation (multiple w. l.) on Ideal length of GS interferometer = $+ 103 \lambda$ ($= 400.000109592 \text{ m}$)
 - $\delta L2/D$: Perturbation (multiple w. l.) on Ideal length of S/C interferometer = $- 205 \lambda$ ($= 399.99978188 \text{ m}$)
 -
- Assuming the same wavelength be utilized for both the experiment and the interferometers calibration, then the following feature has been taken for the 1063 nm case:
 - *Delta L2-L1: Calibration-calibration and geometrical stability included* = $- 0.008 \mu\text{m}$
- The accuracies achievable in prism positioning do not change with the wavelength and the same parameters of bias and noise are maintained;
- The new attenuations are automatically updated;
- The NMOD parameter for the 'NA' type compensation is halved in order to refer to the same prism actuator stroke.

Cases R1-C and R1-D consider a basic frequency of 532 nm and refer to *enhanced capability* (R1-D being goal) as far as prism control (for Doppler compensation), interferometers calibration/stability and S/C speed determination.

Case	Orbit data	Pulses	Ground station	Remarks
R1-A	P=8000 km A=22000 km i=28°	$\lambda = 532 \text{ nm}$ Energy = $0.1 \cdot 10^{-9} \text{ J}$ PRR = 50000 Hz	Matera	R1=Reference trajectory (see paragraph 4.1)
R1-B	P=8000 km A=22000 km i=28°	$\lambda = 1064$ Energy = $0.05 \cdot 10^{-9} \text{ J}$ PRR = 50000 Hz	Matera	R1=Reference trajectory (see paragraph 4.1)
R1-C	P=8000 km A=22000 km i=28°	$\lambda = 532 \text{ nm}$ Energy = $0.1 \cdot 10^{-9} \text{ J}$ PRR = 50000 Hz	Matera	R1=Reference trajectory (see paragraph 4.1) Prism control features (bias and noise) as per goal requirements Interferometers calibration matching as per goal requirements
R1-D	P=8000 km A=22000 km i=28°	$\lambda = 532 \text{ nm}$ Energy = $0.1 \cdot 10^{-9} \text{ J}$ PRR = 50000 Hz	Matera	R1=Reference trajectory (see paragraph 4.1) Prism control features (bias and noise) as per goal requirements Interferometers calibration matching as per goal requirements Spacecraft speed accuracy determination as per reference trajectory

Table 6-2 Simulated reference cases

For all cases the following apply:

- the complete list of input conditions is given (including all disturbances/perturbations, assumed data for detectors, optics efficiency, laser pulses data,.....);
- disturbances/perturbations are superimposed in worst case combination;
- the experimentation is considered to be carried out at elevations $\geq 20^\circ$;
- the *reconstructed probabilities* and *reconstructed de-phasing (modulus 2π)* are plot superimposed to the *nominal* expected one (code: cowsim292moddephaseB). For the phases, two bands at $+0.1$ and -0.1 radians around the nominal are added;
- the actual visibility and nominal visibility plots are superimposed.

As far as the GS, Matera MLRO is considered and the relevant coordinates are recalled:

- Radius = 6370 km
- Latitude = 40.65° N
- Longitude= 16.70° E
- Beam divergence = 30 arcsec (assumed-compatible)
- Pointing error = 5 arcsec (assumed-compatible)

The number of photons per pulse available at the detectors input depend on the number of injected photons and on the overall link transmissibility, from the entrance port of the ground interferometer to the exit port of the S/C based interferometer. As mentioned, this encompass attenuation in the ground optics, the atmosphere, the free space propagation and the S/C based optics. As example for case R1-A the link total transmissibility results as shown in Figure 6-7.

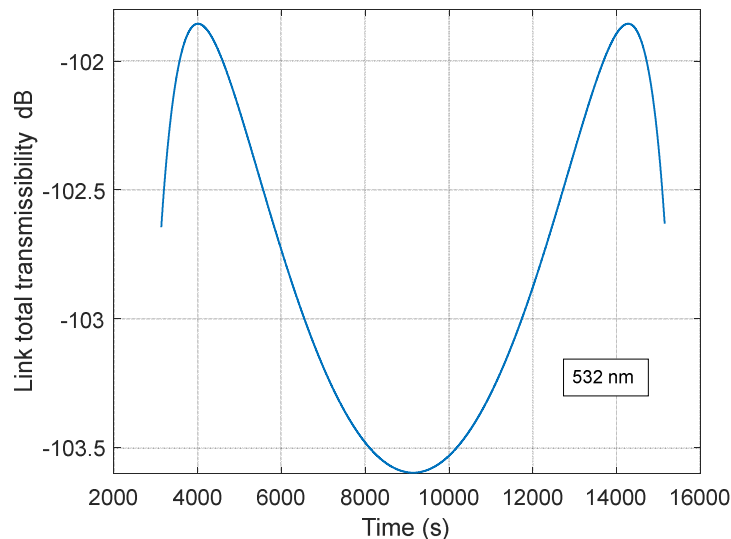


Figure 6-7 Example of total link transmissibility (case R1-A)

The obtained simulation results for the four given cases (R1-A, R1-B, R1-C and R1-D) are reported in Figure 6-8 through Figure 6-16.

6.3.2 Simulation results

Case R1-A

BB – Satellite PERIGEE or APOGEE (w.r.t. e. c.)...=8000000 m AA – Satellite APOGEE o PERIGEE (w.r.t. e.c.)...=22000000 m INCLD – Orbit inclination.....=28 deg Orbital period TT = 1.828328566550028e+04 s Half orbital period HOP = 9.141642832750142e+03 s LAMBDA GS – Latitude of GS.....=40.65 deg RGS – Ground Station altitude (w.r.t. e. c.)=6370000 m LONGIGS0 – Initial long. Of GS (@ t=0)...=- HOP*OMEGAGS rad TIN = 0 s TFIN – Final simulation time.....=18283.285 s DDTT – Satellite trajectory simulation step=0.001 s DT – Output simulation step (> DDTT – in 10 x multiples)....=1 s rbias – Satellite POSITION measurement bias.....=5 m moise – Satellite POSITION meas. noise (1 sigma)....=1.5 m vbias – Satellite SPEED meas. bias.....= - 0.0004 m/s vnoise – Satellite SPEED meas. noise (1 sigma).....=0.0002 m/s pcbiasn – Prism control bias error=3 nm pcnoisen – Prism control noise error(1 sigma).....=0.3 nm LAMBDA L – Laser wavelength= 532 nm TAUCP – Coherence time.....=80 ps L1ID – Ideal length of ground interferometer.....=400.00010906 m L2ID – Ideal length of space interferometer.....=399.99978188 m Delta L2-L1 cal-cal and thermomech. stability DELTAL2TMM = - 0.004 μ m	Feed Back DL1: (YES=1, NO=0)=1 Prism DISTURBANCES activation: (YES=1, NO=0)=1 NMOD*lambda type compensation (e.g. 40)..... (#)=10 EONG – Efficiency On Ground Optics (Source excluded).....=0.06 TTDAAS – Tx Telescope Divergence angle=30 arcsec PEGTAS – Pointing Error Ground Telescope=5 arcsec DOOT – Diameter Objective On Board Optics=0.25 m EONB – Efficiency On Board Optics (SPADs excluded).....=0.16 Laser data FLIM-Preferred maxi. Of Laser Pulse Frequency....= 7.5e+05 Hz Laser Pulse Frequency (106easurmen < FLIM).....=50000 Hz Laser Sigle Pulse Energy=0.0000000001 J End Laser data QUEFF11-SPAD11 Quantum Efficiency=0.45 DCR11-SPAD11 Dark Count Rate=25 counts/s AFTPU11-Afterpulse Probability 11(percentage)=0.03 QUEFF12-SPAD12 Quantum Efficiency=0.47 DCR12-SPAD12 Dark Count Rate=22 counts/s AFTPU12-Afterpulse Probability 12(percentage)=0.02 GATINGmicros-SPADS gating interval=1.2 μ s OPTICALUNB-Optical unbalance to the two sensors (%)....=0.01 EXPWF-Experimental windows frame duration=10 s
--	---

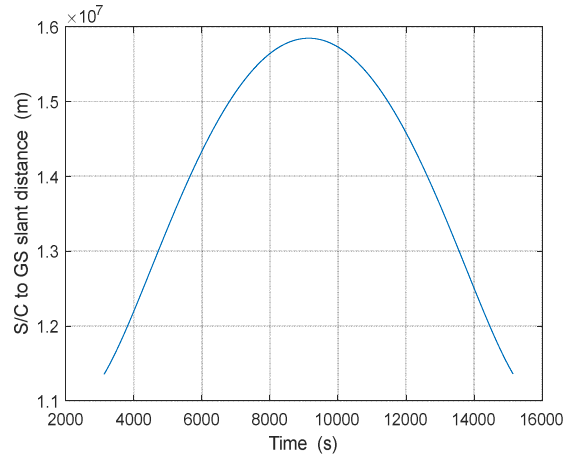
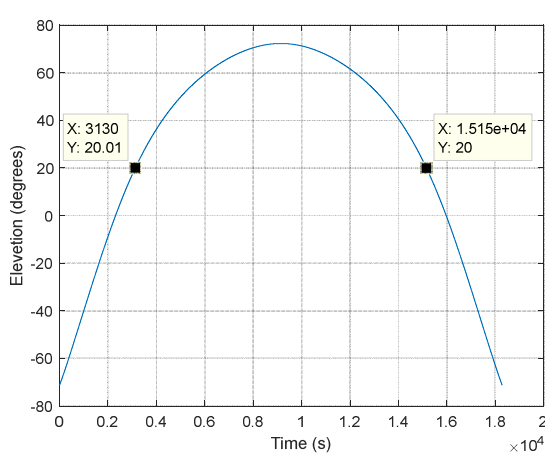


Figure 6-8 Case R1-A: Elevation (left) and slant distance (right)

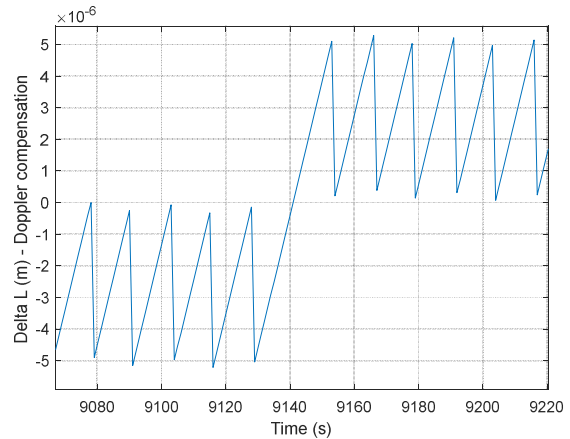
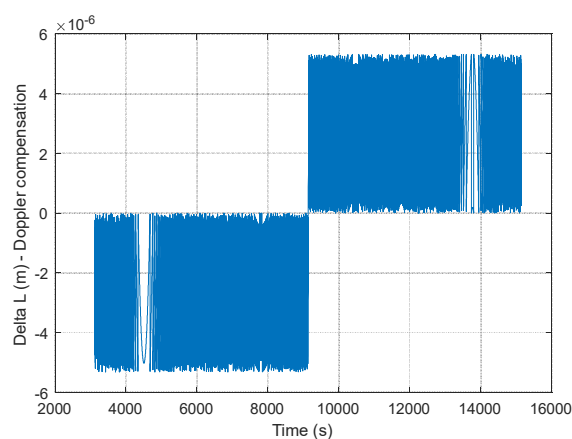


Figure 6-9 Case R1A: Delta L for Doppler compensation (left) and a time expanded view (right)

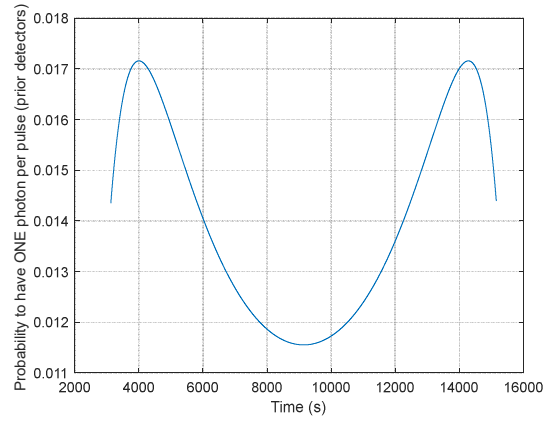
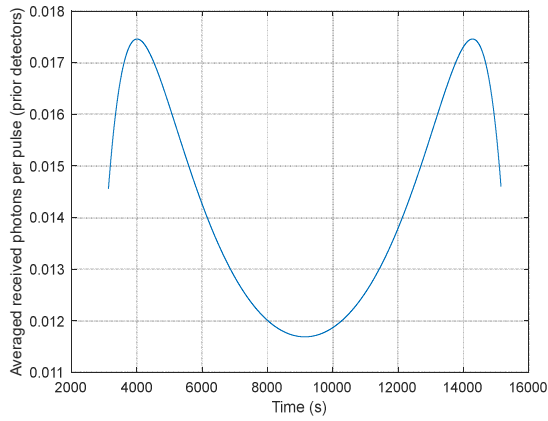


Figure 6-10 Case R1-A: Received average number of photons per pulse (left), probability to have ONE received photon per pulse (right)

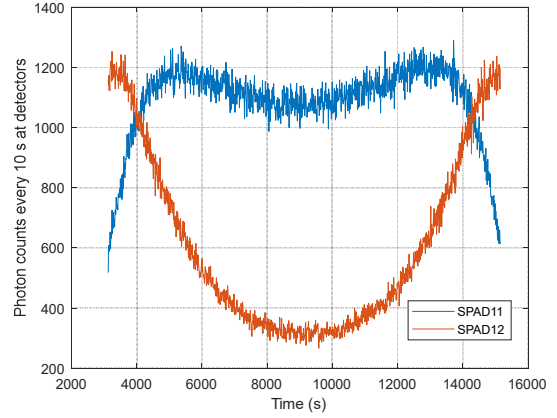
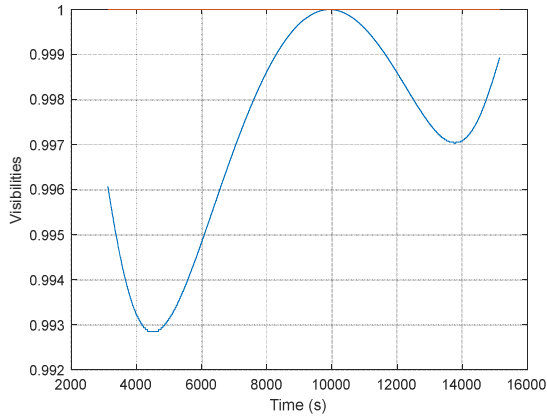


Figure 6-11 Case R1-A: Visibilities (left), total photons counting at detectors in 10 seconds moving windows (right)

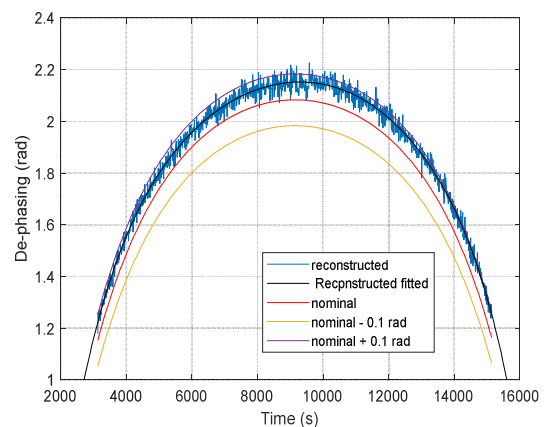
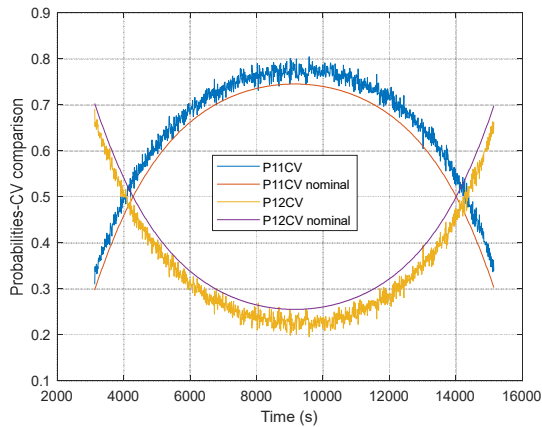


Figure 6-12 Case R1-A: Reconstructed probabilities of detecting photons in central window vs. nominal probabilities (left), reconstructed de-phasing vs. nominal de-phasing (right)

Case R1-B

BB – Satellite PERIGEE or APOGEE (w.r.t. e. c.)...=8000000 m
 AA – Satellite APOGEE o PERIGEE (w.r.t. e.c.)...=22000000 m
 INCLD – Orbit inclination.....=28 deg
 Orbital period TT = 1.828328566550028e+04 s
 Half orbital period HOP = 9.141642832750142e+03 s
 LAMBDA GS – Latitude of GS.....=40.65 deg
 RGS – Ground Station altitude (w.r.t. e. c.)=6370000 m
 LONGIGS0 – Initial long. Of GS (@ t=0)...=- HOP*OMEGAGS rad
 TIN = 0 s
 TFIN – Final simulation time.....=18283.285 s
 DDTT – Satellite trajectory simulation step=0.001 s
 DT – Output simulation step (> DDTT – in 10 x multiples)....=1 s
 r bias – Satellite POSITION measurement bias.....=5 m
 m noise – Satellite POSITION meas. noise (1 sigma)....=1.5 m
 v bias – Satellite SPEED meas. bias.....= - 0.0004 m/s
 v noise – Satellite SPEED meas. noise (1 sigma).....=0.0002 m/s
 pcbiasn – Prism control bias error=3 nm
 pnoise – Prism control noise error(1 sigma).....=0.3 nm
 LAMBDA L – Laser wavelength= 1064 nm
 TAUCP – Coherence time.....=80 ps
 L1ID – Ideal length of ground interferometer.....= 400.000109592 m
 L2ID – Ideal length of space interferometer.....=399.99978188 m
 Delta L2-L1 cal-cal and thermomech. stability DELTAL2TMMM
 = - 0.008 μ m

Feed Back DL1: (YES=1, NO=0)=1
 Prism DISTURBANCES activation: (YES=1, NO=0)=1
 NMOD*lambda type compensation (e.g. 40)..... (#)=5
 EONG – Efficiency On Ground Optics (Source excluded).....=0.06
 TTDAAS – Tx Telescope Divergence angle=30 arcsec
 PEGTAS – Pointing Error Ground Telescope.....=5 arcsec
 DOOT – Diameter Objective On Board Optics.....=0.25 m
 EONB – Efficiency On Board Optics (SPADs excluded).....=0.16
 Laser data
 FLIM-Preferred maxi. Of Laser Pulse Frequency.....= 7.5e+05 Hz
 Laser Pulse Frequency (108easuremen < FLIM).....=50000 Hz
 Laser Sigle Pulse Energy=0.00000000005 J
 End Laser data
 QUEFF11-SPAD11 Quantum Efficiency=0.45
 DCR11-SPAD11 Dark Count Rate=25 counts/s
 AFTPU11-Afterpulse Probability 11(percentage)=0.03
 QUEFF12-SPAD12 Quantum Efficiency=0.47
 DCR12-SPAD12 Dark Count Rate=22 counts/s
 AFTPU12-Afterpulse Probability 12(percentage)=0.02
 GATINGmicros-SPADS gating interval=1.2 μ s
 OPTICALUNB-Optical unbalance to the two sensors (%).....=0.01
 EXPWF-Experimental windows frame duration=10 s

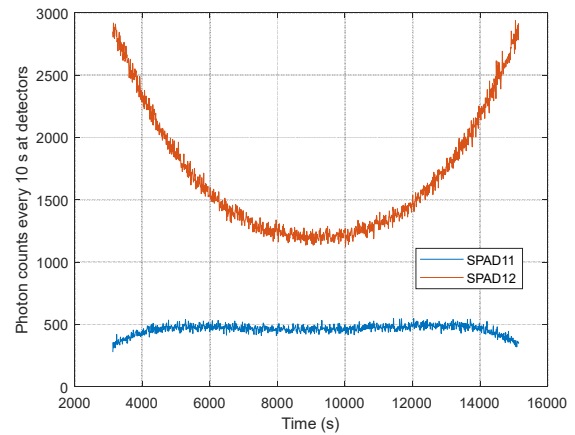
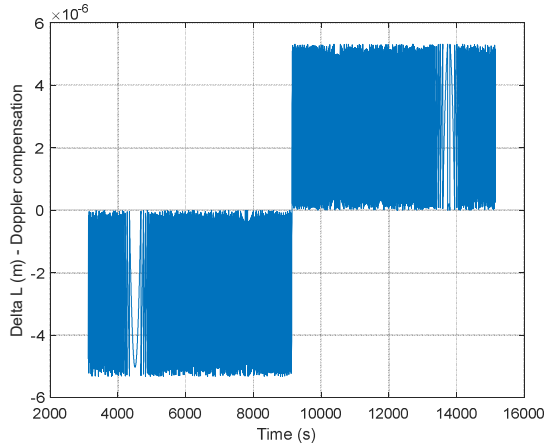


Figure 6-13 Case R1-B: Delta-L for Doppler compensation (left), total photons counting at detectors in 10 seconds moving windows (right)

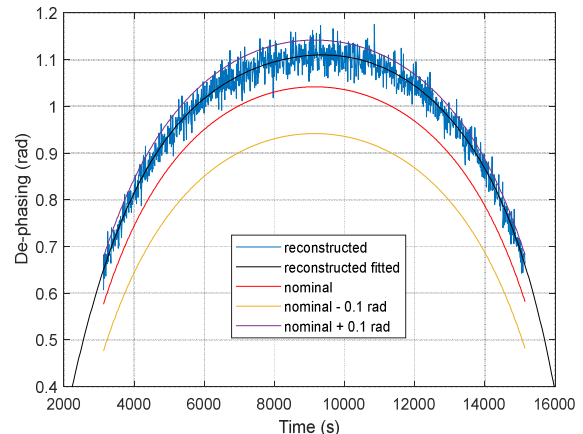
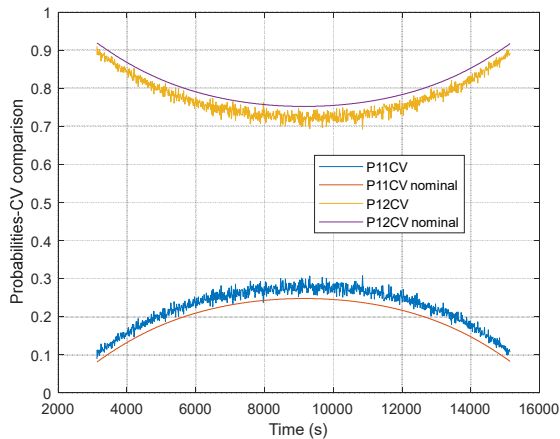


Figure 6-14 Case R1-B: Reconstructed probabilities of detecting photons in central window vs. nominal probabilities (left), reconstructed de-phasing vs. nominal de-phasing (right)

Case R1-C

BB – Satellite PERIGEE or APOGEE (w.r.t. e. c.)...=8000000 m AA – Satellite APOGEE o PERIGEE (w.r.t. e.c.)...=22000000 m INCLD – Orbit inclination.....=28 deg Orbital period TT = 1.828328566550028e+04 s Half orbital period HOP = 9.141642832750142e+03 s LAMBDA GS – Latitude of GS.....=40.65 deg RGS – Ground Station altitude (w.r.t. e. c.)=6370000 m LONGIGS0 – Initial long. Of GS (@ t=0)...=- HOP*OMEGAGS rad TIN = 0 s TFIN – Final simulation time..... =18283.285 s DDTT – Satellite trajectory simulation step =0.001 s DT – Output simulation step (> DDTT – in 10 x multiples).... =1 s rbias – Satellite POSITION measurement bias..... =5 m noise – Satellite POSITION meas. noise (1 sigma).... =1.5 m vbias – Satellite SPEED meas. bias..... = - 0.0004 m/s vnoise – Satellite SPEED meas. noise (1 sigma)..... =0.0002 m/s pcbiasn – Prism control bias error(1 sigma)..... =1 nm pcnoisen – Prism control noise error(1 sigma)..... =0.1 nm LAMBDA L – Laser wavelength = 532 nm TAUCP – Coherence time..... =80 ps L1ID – Ideal length of ground interferometer..... =400.00010906 m L2ID – Ideal length of space interferometer..... =399.99978188 m Delta L2-L1 cal-cal and thermomech. stability DELTA L2TMMM = - 0.001 μm	Feed Back DL1: (YES=1, NO=0) =1 Prism DISTURBANCES activation: (YES=1, NO=0) =1 NMOD*lambda type compensation (e.g. 40)..... (#) =10 EONG – Efficiency On Ground Optics (Source excluded)..... =0.06 TTDAAS – Tx Telescope Divergence angle=30 arcsec PEGTAS – Pointing Error Ground Telescope=5 arcsec DOOT – Diameter Objective On Board Optics =0.25 m EONB – Efficiency On Board Optics (SPADs excluded)..... =0.16 Laser data FLIM-Preferred maxi. Of Laser Pulse Frequency.....= 7.5e+05 Hz Laser Pulse Frequency (109easuremen < FLIM).....=50000 Hz Laser Sigle Pulse Energy=0.0000000001 J End Laser data QUEFF11-SPAD11 Quantum Efficiency=0.45 DCR11-SPAD11 Dark Count Rate=25 counts/s AFTPU11-Afterpulse Probability 11(percentage)=0.03 QUEFF12-SPAD12 Quantum Efficiency=0.47 DCR12-SPAD12 Dark Count Rate=22 counts/s AFTPU12-Afterpulse Probability 12(percentage)=0.02 GATINGmicros-SPADS gating interval=1.2 μ s OPTICALUNB-Optical unbalance to the two sensors (%).....=0.01 EXPWF-Experimental windows frame duration=10 s
---	--

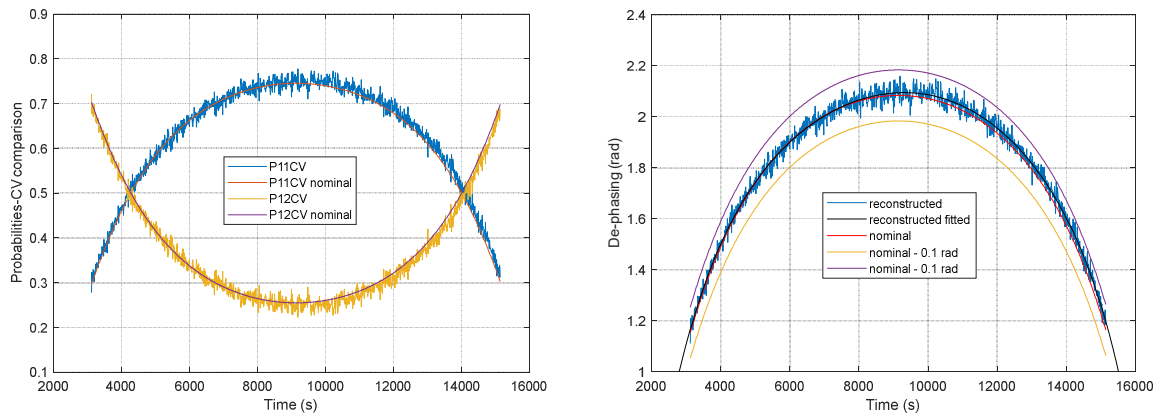


Figure 6-15 Case R1-C: Reconstructed probabilities of detecting photons in central window vs. nominal probabilities (left), reconstructed de-phasing vs. nominal de-phasing (right)

Case R1-D

BB – Satellite PERIGEE or APOGEE (w.r.t. e. c.)...=8000000 m
 AA – Satellite APOGEE o PERIGEE (w.r.t. e.c.)...=22000000 m
 INCLD – Orbit inclination.....=28 deg
 Orbital period TT = 1.828328566550028e+04 s
 Half orbital period HOP = 9.141642832750142e+03 s
 LAMBDAGS – Latitude of GS.....=40.65 deg
 RGS – Ground Station altitude (w.r.t. e. c.)=6370000 m
 LONGIGS0 – Initial long. Of GS (@ t=0)...=- HOP*OMEGAGS rad
 TIN = 0 s
 TFIN – Final simulation time.....=18283.285 s
 DDTT – Satellite trajectory simulation step=0.001 s
 DT – Output simulation step (> DDTT – in 10 x multiples)....=1 s
 rbias – Satellite POSITION measurement bias.....=5 m
 noise – Satellite POSITION meas. noise (1 sigma)....=1.5 m
vbias – Satellite SPEED meas. bias.....= - 0.0002 m/s
vnoise – Satellite SPEED meas. noise (1 sigma).....=0.00015 m/s
pcbiasn – Prism control bias error=1 nm
pcnoisen – Prism control noise error(1 sigma).....=0.1 nm
 LAMBDA – Laser wavelength= 532 nm
 TAUCP – Coherence time.....=80 ps
 L1ID – Ideal length of ground interferometer.....=400.00010906 m
 L2ID – Ideal length of space interferometer.....=399.99978188 m
Delta L2-L1 cal-cal and thermomech. stability DELTAL2TMMM
= - 0.001 μ m

Feed Back DL1: (YES=1, NO=0)=1
 Prism DISTURBANCES activation: (YES=1, NO=0)=1
 NMOD*lambda type compensation (e.g. 40)..... (#)=10
 EONG – Efficiency On Ground Optics (Source excluded).....=0.06
 TTDAAS – Tx Telescope Divergence angle=30 arcsec
 PEGTAS – Pointing Error Ground Telescope=5 arcsec
 DOOT – Diameter Objective On Board Optics=0.25 m
 EONB – Efficiency On Board Optics (SPADs excluded).....=0.16
 Laser data
 FLIM-Preferred maxi. Of Laser Pulse Frequency.....= 7.5e+05 Hz
 Laser Pulse Frequency (110easuremen < FLIM).....=50000 Hz
 Laser Sigle Pulse Energy=0.0000000001 J
 End Laser data
 QUEFF11-SPAD11 Quantum Efficiency=0.45
 DCR11-SPAD11 Dark Count Rate=25 counts/s
 AFTPU11-Afterpulse Probability 11(percentage)=0.03
 QUEFF12-SPAD12 Quantum Efficiency=0.47
 DCR12-SPAD12 Dark Count Rate=22 counts/s
 AFTPU12-Afterpulse Probability 12(percentage)=0.02
 GATINGmicros-SPADS gating interval=1.2 μ s
 OPTICALUNB-Optical unbalance to the two sensors (%).....=0.01
 EXPWF-Experimental windows frame duration=10 s

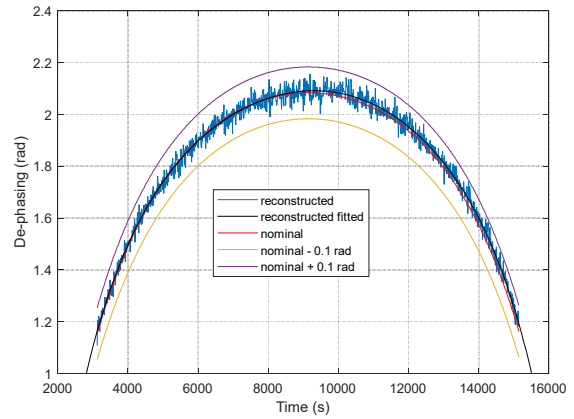
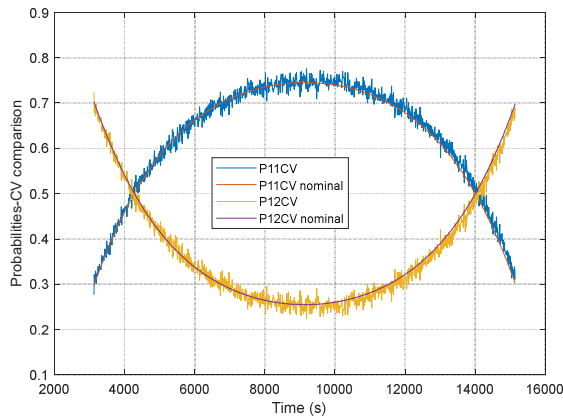


Figure 6-16 Case R1-D: Reconstructed probabilities of detecting photons in central window vs. nominal probabilities (left), reconstructed de-phasing vs. nominal de-phasing (right)

6.3.3 Considerations on obtained results

The performance evaluation have been done taking as reference the conditions discussed in paragraphs 6.2 and 6.3.1. The maximum magnitude of the disturbances have been selected tentatively compatible with values considered achievable at this evaluation stage and as a goal reachable via a specific development activity. Concerning the sign (of the biases), they have been selected such as to add-up their perturbation effect on accuracy. Specifically:

- *parameters affecting directly de-phasing:*
 - satellite speed measurement bias
 - prism control bias error
 - interferometers calibration residual and stability
- *parameters affecting directly visibility (interferometers macroscopic length modifications as multiple of wavelength) :*
 - length modifications of ground interferometer
 - length modifications of space interferometer

In this respect *the obtained performances are somehow a worst case* since their combined effect on de-phasing, in actual conditions, can also decrease.

In Figure 6-17 through Figure 6-20 are reported the obtained De-phasing Errors (reconstructed – nominal) with fitting and average and the obtained Residuals (Error – Error fit) for the four cases R1-C, R1-D, R1-A and R1-B.

Cases R1-C and R1-D are the most performing and *can be considered as reference* assuming the support of an appropriate technology development activity; for case R1-D (goal):

- Fitted curve: the maximum de-phasing error for the fitted curves presents a value of $\approx +0.032$ rad made up by an 'average' of $\approx +0.01$ rad *plus* a slow waving in the order of $\approx \pm 0.022$ rad;
- Residual curves: a noise of about ≈ 0.02 rad is present (this can be suppressed off-line by filtering);

Cases R1-A and R1-B have the objective to compare two frequencies (with somehow relaxed requirements on technology):

- Fitted curves: the maximum de-phasing error for the fitted curves present an average of $\approx +0.08/0.09$ rad, addition of an 'average' plus a slow waving part. The performance for the case $\lambda=1064$ nm appears slightly better than the case $\lambda=532$ nm due to the relative modifications of the delta L2-L1 calibration residual (assumed depending on wavelength) and the keeping of the same prism control accuracy assumed independent on wavelength;
- Residual curves: the standard deviation is ≈ 0.02 rad for both $\lambda=532$ and $\lambda=1064$ cases; indeed the number of photons involved is the same for the two since the orbit geometry and distances are the same and the energy per pulse have been halved for the longer wavelength.

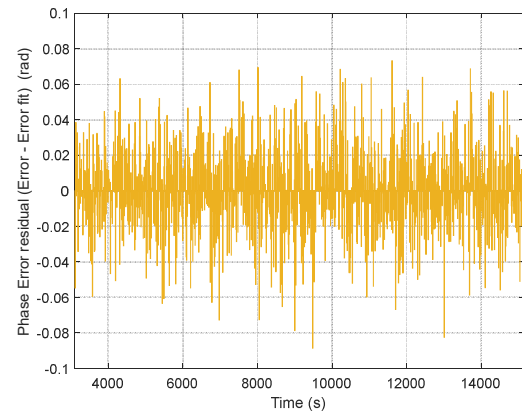
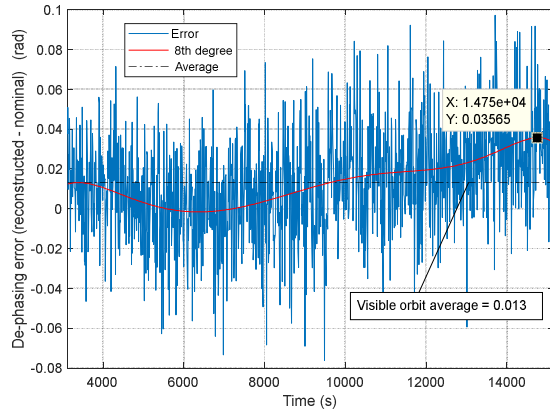


Figure 6-17 Case R-1C: De-phasing error and residual

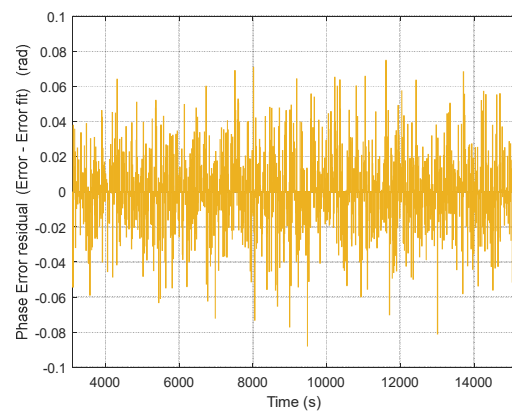
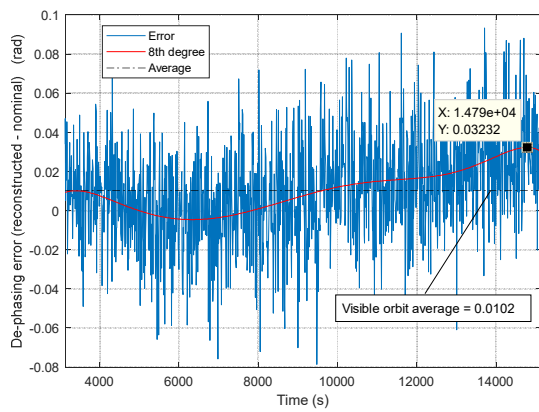


Figure 6-18 Case 1D: De-phasing error and residual

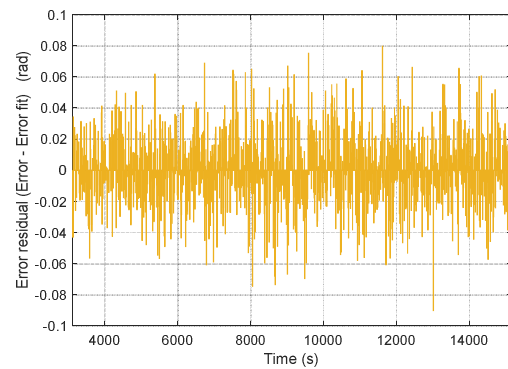
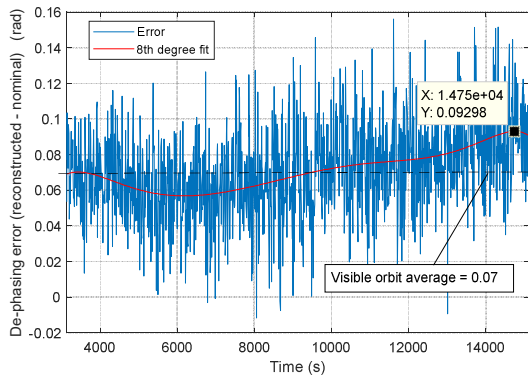


Figure 6-19 Case 1A: De-phasing error and residual

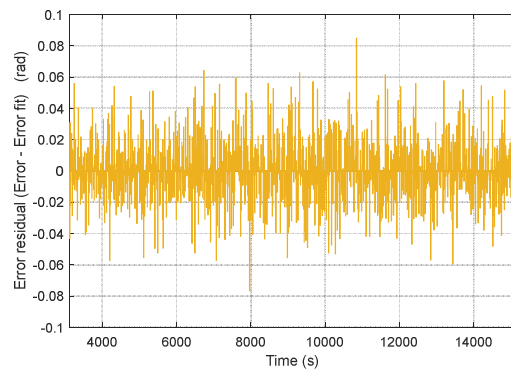
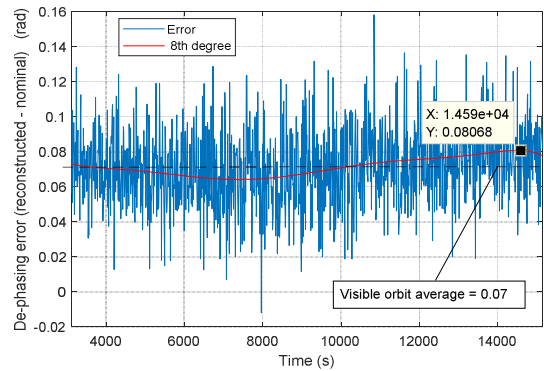


Figure 6-20 Case 1B: De-phasing error and residual

As already mentioned, the real performances are expected somehow better than the ones above illustrated since the likely occurrence of the five key influencing parameters may mediate their effects. Furthermore, depending on the stability of input perturbation parameters, the 'average' part of de-phasing error during orbit might be partly compensated.

In summary, until a next step of feasibility study, the following approximate performances ('round' numbers only slightly better than the above presented to avoid being too optimistic) could be taken as reference for de-phasing reconstruction after photons counting:

- maximum absolute error (for the fitted curve) ≈ 0.03 rad decomposed as
 - 'average' error ≈ 0.01 rad
 - slowly varying fluctuations (superposed to 'average') ≈ 0.02 rad
- Noise of residual (rms) ≈ 0.02 rad removable by filtering

(Page Intentionally Left Blank)

7 SUMMARY AND CONCLUSIONS

The main subject of this PhD research has been to discuss the effects played by gravity on single photon interference in cases where photon propagation is over long distances (thousands or tens of thousands kilometres) with large variation of General Relativistic metric tensor. In particular space-time curvature theoretically affects phase coherence of photons wave packets propagating in quantum superposition along trajectories at different gravitational potential. Measurable interferometric effects should therefore arise with fringes and visibility characteristics depending on the specific experimental conditions. Gravitational 'red-shift', 'time dilation', 'photon trajectory bending' and 'classical observer-source relative motion (classical Doppler effect)' all contribute, at a different degree, to phase shift accumulation and 'which-way' information building-up shaping the measured interferograms.

Interferometric effects are strongly related to frequency variations induced by the experimental conditions and space-time curvature. Specifically frequency variation caused by the so-called 'gravitational red-shift' and 'photon trajectory bending' can be derived in curved space time by considering the geodesic motion of light (null geodesic) in the assumed metric. It is however noted that this effect can also be partly explained in a semi-classical approach; for photons this imply assuming a 'gravitational mass' equal to the photon energy divided by the square of the speed of light. As far as 'time dilation' effects, involved by pseudo Euclidean signatures, they cannot be explained semi-classically and the metric embedded in the fundamental tensor is needed.

Frequency variations caused by classical 'observer-source relative motion' generates very large frequency Doppler effects and wave packets phase variations which mask and 'confuse' the relativistic effects: the classical Doppler effect has to be *removed to a high degree of precision* in order to distinguish the ones related to metric.

Sufficiently large de-phasing (exceeding coherence of utilized photons) may in principle lead to know 'which-way' the photon has taken possibly causing wave packets to be distinguishable with consequent modifications of interferometric effects. To generate a full 'distinguishability' under *practical experimental conditions*, gravity fields much higher than the one generated by Earth are needed (e.g. some thousands times higher).

It is evidenced that the first measurements related to gravity induced quantum interference has been performed by Colella-Overhauser-Werner (COW) in 1975 utilizing a Neutron Interferometer implementing quantum superposition along separate trajectories in a laboratory set-up; indeed it was a phase shift measurement on matter-waves. The experiment has been subsequently repeated several times during the years, always utilizing Neutrons.

In this Research Thesis has been studied the detection of gravity induced quantum interference directly employing photons in schematics utilizing both ground elements and space platform: this approach is sometimes named 'optical COW' and has already been suggested by other researchers. Single photon conditions at the detecting interferometer are approximated, in the considered cases, by means of laser short pulses duly attenuated along the optical link (crossing the atmosphere and propagating over a long free-space distance).

Three experimental configurations have been evaluated and they differ in terms of potential scientific return and cost/complexity:

- 'Oneway' based utilization of two interferometers, one at the GS one on-board the S/C
- 'Twoways' based on utilization of one interferometer only which is placed on board the S/C
- 'Twoways' based on utilization of one interferometer only placed at the GS

The configurations have been first analysed in terms of single photon interference at the two receiving detectors, interference modulated by the experimental conditions and in particular by

the space-time curvature. Total order of magnitude of de-phasing induced by gravity (and consequent probability at detectors) have been estimated based on a reference Spacecraft trajectory. The potential scientific return of the 'oneway' configuration resulted overwhelming with respect the 'twoway' configurations and despite the higher complexity-cost, the 'oneway' configuration has been chosen for further evaluations.

The classical Doppler compensation approach considered for the analysis of the selected configuration has been based on *ground interferometer length control* driven by GS-S/C relative speed measurement. It is however noted that the compensation technique is an important point and, should the experimentation be pursued in the future, further evaluations on the issue are important.

Several factors affects the overall experiment performances and, in order to quantify the perturbations, a thorough sensitivity analysis have been performed for the selected oneway configuration. Among the parameters considered are:

- interferometers length mismatch (due to calibration residuals and stability mismatch);
- errors in knowledge of Spacecraft position and speed;
- control errors in the implementation of the Doppler compensation via interferometer length control (prism displacement control).

This analysis allowed to derive a first set of requirements.

Some key technological aspects have then been analysed in more detail and specifically: critical aspects for the classical Doppler compensation (relative speed measurement accuracy and actuation of Ground Interferometer length control), interferometers calibration, Single Photon sensors characteristics, thermal stability considerations and attenuation on fibre optics. This allowed to preliminary identify specific development needs and to revise some the initial assumed requirements.

A second type of analysis has then been performed (always for the selected configuration) going down to photon counting at the two detectors over selectable (moving) observation windows. This second type of analysis accounted also for:

- laser pulses characteristics (repetition rate, pulse energy, pulse duration);
- attenuation of the atmospheric-optical link (as a function of Spacecraft and Ground Station relative position, observation elevation and efficiencies);
- characteristics of the Single Photon Detectors (Quantum Efficiency, Dark Count Rate, after-pulse probability).

The (simulated) photon counting, allows to reconstruct the probability curves at the two detectors and then to *reconstruct the de-phasing curve*. This can be compared against *the nominally expected curves* in order to derive overall performance figures. The analysis has been carried out based on selected Ground Station/Spacecraft configurations.

Under the assumption, to be confirmed by actual experimentation, that superposition is maintained over the conditions and geometries considered (e.g. 8000/22000 km orbits, 532 nm, inaccuracies superimposed,) then the reconstructed de-phasing curves could be characterized by:

- overall de-phase excursion ≈ 1 rad
- maximum absolute error (for the fitted curve) ≈ 0.03 rad
- noise of residual (rms) ≈ 0.02 rad – removable by filtering

If, in the future, actual experiment data were available then the simulated performances could be compared to the actual measured performances (for confirmation of interference presence, actual photons counts, associated probabilities and associated de-phasing).

Should the experiment be of interest to the Agencies and actually be pursued then a detailed feasibility study, involving both Universities and Industries, is necessary. The objective would be to confirm the final configuration (including the choice of the Doppler compensation approach), identify a detailed development plan aiming at confirming feasibility (and improvements on achievable performances) and in general to verify the experiment compatibility with medium size Spacecraft's (e.g. 500-600 kg) and small launchers (e.g. Vega C) in order to limit the costs.

(Page Intentionally Left Blank)

8 ANNEXES

8.1 Annex-A: Estimation of frequency perturbations caused by light trajectory bending

In this annex is evaluated the *contribution to frequency shift only due to light trajectory deflection*; the evaluation is performed by utilizing the solution to the null geodesic equations available in literature in an assumed Schwarzschild metric and is carried out in a simplified geometric configuration where light trajectory and experimenters velocity all lay on the same plane. This is done in order to perceive the effect from a direct physical/geometrical point of view as well as to get an order of magnitude of the shift contribution from the bending of light trajectory. In the Doppler formulation utilized, computation of terms of the following type are needed (see Figure 8-1):

$$\mathbf{V} \cdot \mathbf{k}$$

where \mathbf{k} is the local wave vector.

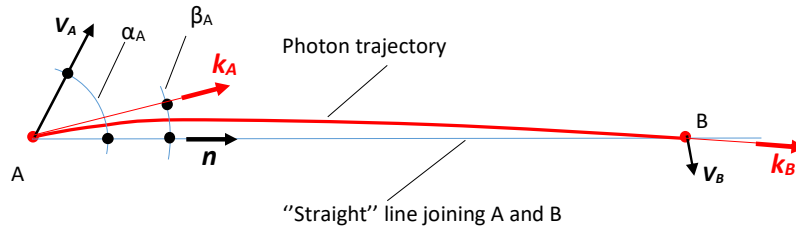


Figure 8-1 General scheme for illustration of the approximation used (Not to Scale)

The projections of the speeds of A and B along the respective wave vector directions can first be computed as:

$$\left\{ \begin{array}{l} V_{A//} = V_A \cos(\alpha_A - \beta_A) \sim V_A \cos(\alpha_A) - V_A \sin(\alpha_A) \cdot \beta_A \quad \text{where} \quad V_A = |V_A| \\ V_{B//} = V_B \cos(\alpha_B - \beta_B) \sim V_B \cos(\alpha_B) - V_B \sin(\alpha_B) \cdot \beta_B \quad \text{where} \quad V_B = |V_B| \\ \beta \ll \pi/2 \end{array} \right. \quad (8.1)$$

Taking in consideration the relation linking the transmitted angular frequency (by A) to the received angular frequency (by B), the contributions to the *angular frequency variations* just due to the presence of non-null β_A and β_B angles lead to the following:

$$\left\{ \begin{array}{l} \frac{\delta \omega}{\omega} \sim -V_{B\perp} \frac{\beta_B}{c} + V_{A\perp} \frac{\beta_A}{c} \\ V_{B\perp} = V_B \sin(\alpha_B) \\ V_{A\perp} = V_A \sin(\alpha_A) \end{array} \right. \quad (8.2)$$

So the estimation of β_A and β_B is needed. To perform the computation the general scheme and formula for light deflection around and external to the Schwarzschild radius of a massive body, as shown in here below Figure 8-2, is utilized (see Ref. [10]).

$$\left\{ \begin{array}{l} X = b - \frac{GM}{bC^2} \cdot \frac{X^2 + 2Y^2}{\sqrt{X^2 + Y^2}} \\ X_0 = \frac{b}{1 + \frac{GM}{bC^2}} \\ \delta_\infty = 2 \frac{GM}{bC^2} \end{array} \right. \quad (8.3)$$

$M \sim 5.97 \cdot 10^{24} \text{ (kg)} = \text{Earth mass}$

$G \sim 6.67 \cdot 10^{-11} \frac{\text{m}^3}{\text{kg s}^2} = \text{Gravitational constant}$

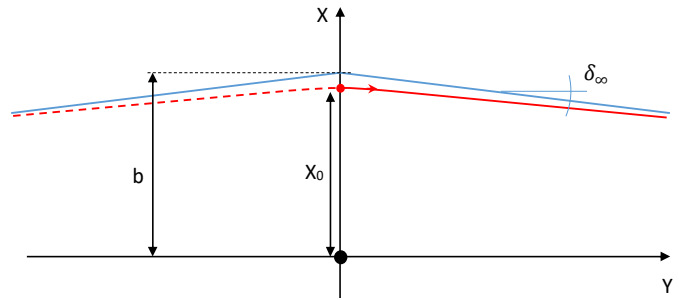


Figure 8-2 General equations and light bending scheme (see Ref[10])-Not to Scale

Based on above equation a specific simulation has been performed aiming at computing β_A and β_B as a function of the separation distance between A (GS) and B (S/C) for any given elevation observation elevation angle as schematized in Figure 8-3.

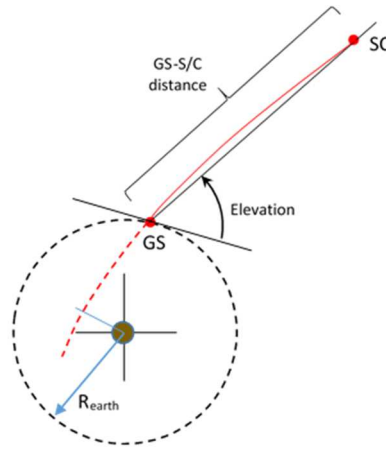


Figure 8-3 Schematics for β angle computation (generic positions shown) – Highly distorted scale

Maximum of deflections will occur when elevation approach zero (observation around local horizon) while deflections will be zero when elevation approaches 90° (in vertical). Generic elevations present intermediate deflections: indeed it is noted that as elevation increases, although parameters b or X_0 decrease, the maximum of bending build up would virtually occur in the part of photon trajectory 'inside the radius R_{earth} ' (outside R_{earth} the photon trajectory would be 'more straight').

To have an order of magnitude of the angular frequency shift contribution from the trajectory bending, a GS (A) and S/C (B) reference orbital configuration has been simulated with the characteristics given in Table 8-1.

S/C orbit type (elliptical)	GS location	Interferometers length	Passage type
<input type="checkbox"/> A = 32582 km <input type="checkbox"/> P = 23372 km <input type="checkbox"/> I = 0°	<input type="checkbox"/> R = 6372 km <input type="checkbox"/> Latitude = 0°	<input type="checkbox"/> L1=L2= 6000 m	<input type="checkbox"/> Apogee

Table 8-1 General characteristics of the GS and S/C orbital configuration used for estimation purposes

The β_{GS} and β_{SC} and the relative angular frequency shift $\frac{\delta\omega}{\omega}$ have then been computed at different elevation conditions (0°, 30°, 60° and 88° in ascending sequence). In Figure 8-4 are reported, as an example, the trends of β_{GS} and β_{SC} at 30° elevation while the overall results are summarized in Table 8-2.

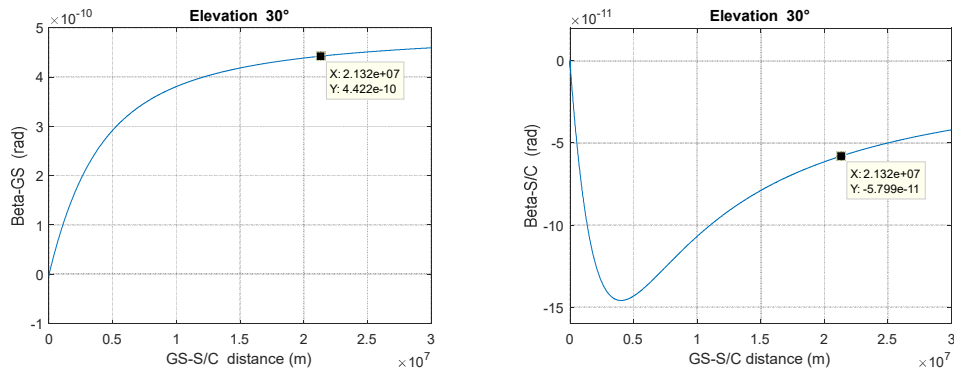


Figure 8-4 Trends of β_{GS} and β_{SC} at 30° elevation (as example)

Elevation (degrees)	GS-S/C distance (m)	β_{GS} (rad)	$\beta_{S/C}$ (rad)	$\frac{\delta\omega}{\omega}$
0	22590000	$1.195 * 10^{-9}$	$-1.92 * 10^{-10}$	$+2.76 * 10^{-15}$
30	21320000	$4.422 * 10^{-10}$	$-5.799 * 10^{-11}$	$+1.146 * 10^{-15}$
60	22900000	$6.464 * 10^{-11}$	$-6.714 * 10^{-12}$	$+1.69 * 10^{-16}$
88	26180000	$2.038 * 10^{-14}$	$-1.752 * 10^{-15}$	$+5 * 10^{-20}$

Table 8-2 Angular frequency shift obtained at different elevation

8.2 Annex-B: Coordinate speeds vs. physical speeds: effects on frequency perturbations

For the purposes of the experiment considered the coordinate speeds are speeds evaluated in a Schwarzschild frame while physical speeds are speeds measured by a local observers. In general the discrepancy between the (variation of) coordinate speeds and the (variation of) physical speeds is, as order of magnitude, in the order of (see Ref.[16]):

$$\mu = -\frac{GM}{c^2 r_{observer}} \quad (8.4)$$

$$\left| \delta \left(\frac{V_{coord}}{c} \right) \right| = |2\mu| \cdot \left| \left(\frac{V_{phys}}{c} \right) \right| \quad (8.5)$$

$r_{observer}$ being the position (distance from earth centre) from where the local observer perform the measurement.

The effect on frequency variation estimation can then be evaluated with reference to the general frequency relationship already previously introduced:

$$\omega_{SCRX}(t1) \cong \underbrace{\left[\left(1 - \frac{2GM}{c^2 r_g(t)} \right) - \beta_{\phi,g}^2(t) \right]^{\frac{1}{2}} \left[\left(1 - \frac{2GM}{c^2 r_s(t1)} \right) - \left(1 - \frac{2GM}{c^2 r_s(t1)} \right)^{-1} \beta_{r,s}^2(t1) - \beta_{\theta,s}^2(t1) - \beta_{\phi,s}^2(t1) \right]}_{\text{Metric part}} * \underbrace{\left[\frac{1 - \frac{V_{SC//f}(t1)}{c}}{1 - \frac{V_{GS//f}(t)}{c}} \right]}_{\text{'Doppler part'}} * \omega_{GSTX}(t) \quad (8.6)$$

As far as the *metric part* the frequency uncertainty introduced by assuming the coordinate speeds equal to the physical speeds can be estimated as order of magnitude:

$$\left| \frac{\delta\omega}{\omega} \right| \approx 10^{-19}$$

As far as the *'Doppler part'*, assuming for example to measure a $V_{//}$ in the order of 1000 m/s, the frequency uncertainty can be estimated as order of magnitude:

$$\left| \frac{\delta\omega}{\omega} \right| \approx 4 \cdot 10^{-15}$$

9 REFERENCES

- [1] H. Colella, A. W. Overhauser, S. A. Werner, "Observation of Gravitationally Induced Quantum Interference", Volume 34, Number 23, Physical Review Letters, 9 June 1975
- [2] S. Werner, "Neutron Interferometry", Lectures, Fundamental Neutron Physics Workshop, The University of Washington, May 3-4 2007
- [3] D. Rideout et al. "Fundamental quantum optics experiments conceivable with satellites reaching relativistic distances and velocities", Published 18 October 2012, Classical and Quantum Gravity, Volume 29, Number 22
- [4] "Italian Space Agency perspective on Small Satellites", Agenzia Spaziale Italiana (ASI), CIRA, 10 February 2016
- [5] G. Vallone, P. Villoresi et al. "Quantum interference along satellite-ground channels", arXiv:1509.07855v1 [quant-ph], 25 Sep 2015
- [6] B. Finzi, M. Pastore, "Calcolo Tensoriale e Applicazioni", Seconda edizione, Zanichelli Bologna, 1971
- [7] J. L. Synge, "Relativity: The General Theory", School of Theoretical Physics, Dublin Institute for Advanced Studies, North Holland Publishing Co., 1976
- [8] D. R. Terno, F. Vedovato, M. Schiavon, A. R. H. Smith, P. Magnani, G. Vallone, P. Villoresi, "Proposal for an Optical Test of the Einstein Equivalence Principle", arXiv:1811.04835v2 [gr-qc] 24 Jan 2019
- [9] D. Kleppner et al., "An orbiting clock experiment to determine the gravitational red-shift", Astrophysics and Space Science 6 (1970) 13-32
- [10] V. Barone, "Relatività – Principi e applicazioni (lo spostamento verso il rosso paragraph 11.10)", Bollati Boringhieri 2004
- [11] Angelo Bassi, "Models of spontaneous wave function collapse: what they are, and how they can be tested", J. Phys.: Conf. Ser. 701 012012, 2016
- [12] A. Bassi, K. Lochan, S. Satin, T. P. Singh, H. Ulbricht, 'Models of Wave-function Collapse, Underlying Theories, and Experimental Tests', Review of Modern Physics 85(2), April 2012
- [13] R. Trebino, "Ultrashort Laser Pulses I", Georgia Tech. University, www.frog.gatech.edu
- [14] R. P. Feynman, R. B. Leighton, and M. Sands, "The Feynman Lectures on Physics", Addison-Wesley, Reading 1965, Vol. 3, p. 1-1
- [15] E. J. Galvez, C. H. Holbrow et al., "Interference with correlated photons: Five quantum mechanics experiments for undergraduates", American Journal of Physics 73 (2), February 2005
- [16] L. D. Landau, E. M. Lifshitz, "The Classical Theory of Fields", Institute for Physical Problems, Academy of Sciences of the U.S.S.R.
- [17] M. Zych, F. Costa, I. Pikovski, C. Brukner, "Quantum interferometric visibility as a witness of general relativistic proper time", Nature Communications, 2(1):505 · October 2011
- [18] M. Zych, F. Costa et al., "General relativistic effects in quantum interference of photons", Classical and Quantum Gravity, 29:22401 · November 2012

- [19] D. R. Terno, F. Vedovato, M. Schiavon, A. R. H. Smith, P. Magnani, G. Vallone, P. Villoresi, "Proposal for an Optical Test of the Einstein Equivalence Principle", arXiv:1811.04835v3 [gr-qc] 14 Nov 2019
- [20] G. Vallone, D. Bacco, D. Dequal, S. Gaiarin, V. Luceri, G. Bianco, P. Villoresi, "Experimental Satellite Quantum Communications", Physical Review Letters, 115(4)- June 2014
- [21] D. Dequal, G. Vallone, D. Bacco, S. Gaiarin, V. Luceri, G. Bianco, P. Villoresi, "Experimental single photon exchange along a space link of 7000 km", Physical Review A, Volume 93.010301, September 2015
- [22] VEGA C User's Manual, Issue 0 Revision 0, May 2018
- [23] Silverbird Astronautics, <http://silverbirdastronautics.com/LVperform.html>
- [24] International Laser Ranging, <https://ilrs.cddis.eosdis.nasa.gov/index.html>
- [25] Robert Wolf, "Satellite Orbit and Ephemeris Determination using Inter Satellite Links", Grades eines Doktors der Ingenieurwissenschaften, Universitat der Bundeswehr Munchen zur Erlangung, 2000
- [26] Physic Instrument Q-521 Q-Motion® Miniature Linear Stage- Product data – (<https://www.physikinstrumente.com/en/products/>)
- [27] Smaract – SLC 1720-Product data – (<http://www.smaract.com/products/>)
- [28] Physic Instrument – LISA actuator linear stage P 753.1CD – (<https://www.Physikinstrumente.Com/en/products/>)
- [29] Mad City Lab – MCL Nano-MET 10-Product data – (<http://www.madcitylabs.com/nanopositioners>)
- [30] Aerotech – QNPHD30L 10-Product data (<https://www.aerotech.com/product-catalog/piezo-nanopositioners>)
- [31] ORS Ultrastable Laser, from MenloSystem (www.menlosystem.com)
- [32] SLS-INT-1550-200-1 Hz-Level Rack Mounted Laser System, from Stable Laser System (stablelasers.com)
- [33] J. Alnis, A. Matveev, N. Kolachevsky, T. Wilken, Th. Udem, T.W. Hänsch, "Sub-Hz line width diode lasers by stabilization to vibrationally and thermally compensated ULE FabryPerot cavities", Max-Planck-Institut für Quantenoptik (Garching, Germany) and P.N. Lebedev Physics Institute (Moscow, Russia)
- [34] ULE® Corning Ultra Low Expansion Glass (<https://www.corning.com/>)
- [35] B. Argence et al., "Prototype of an ultra-stable optical cavity for space applications", 5 November 2012 / Vol. 20, No. 23 / OPTICS EXPRESS 25409
- [36] NPL – Optical Reference Cavity for Space (npl.co.uk/qmi)
- [37] P. Gill, "Ultra-stable lasers, Clocks and CO2-filled hollow core fibre frequency references for Space science", Workshop on Quantum Technology Implementations for Space, ESTEC, 20th November 2018
- [38] Stable Laser System – Fabry Perot cavities – (<http://stablelasers.com/fabry-perot-cavities/>)
- [39] Stable Laser System – Choosing a cavities – (<http://stablelasers.com/choosing-cavity/>)
- [40] E. Black, "Notes on the Pound-Drever-Hall technique", Technical Note LIGO-T980045-00-D 4/16/98, CALTEC – MIT

- [41] Vescent Photonics, "Pound-Drever-Hall Locking of a Chip External Cavity Laser to a High Finesse Cavity Using Vescent Photonics Lasers & Locking Electronics", VDN00116 rev. 1
- [42] Pound-Drever-Hall technique – Interned available data – Wikipedia
- [43] C. Francese, M. Bisi, P. Cordiale, "Laser Frequency Stabilization for Aerospace Applications", INRIM (To-Italy), Proceedings of the euspen International Conference – Delft – June 2010
- [44] FOSCO Fiber Optics, "Optical Fiber Loss and Attenuation"
- [45] Thorlab – Single Mode Fibre S405-XP Product data (www.thorlab.com)
- [46] MPD – PDM Series Photon Counting Detectors, Product data (www.micro-photon-devices.com)
- [47] ZYGO – Corner Cube Retro-reflectors, Product data (www.zygo.com)
- [48] John J. Degnan, "Millemeter Accuracy SatelliteLaser Ranging: a Review", Space Geodesy and Altimetry Projects Office, NASA/GSFC, USA
- [49] P Villoresi, T Jennewein et al, "Experimental verification of the feasibility of a quantum channel between space and Earth", New Journal of Physics 10 (2008) 033038 (12pp)
- [50] TSync Time Code Processors – Orolia (www.orolia.com)
- [51] CSAC GPS Disciplined Oscillator – Symmetricom (www.symmetricom.com)

(Page Intentionally Left Blank)

10 LIST OF ACRONYMS

ASI	Agenzia Spaziale Italiana
BS	Beam Splitter
CCR	Corner Cube Reflector
COW	Colella-Overhauser-Werner
CSAC	Chip Scale Atomic Clock
CTE	Coefficient of Thermal Expansion
DCR	Dark Count Rate
ECEF	Earth Centered Earth Fixed frame
EOM	Electro Optical Modulator
FS	Fused Silica
FSR	(cavity) Free Spectral Range
FWHM	Full Width Half Maximum
GPS	Global Positioning System
GR	General Relativity
GS	Ground Station
LEO	Low Earth Orbit
MEO	Medium Earth Orbit
MLRO	Matera Laser Ranging Observatory
MPD	Micro Photon Devices
MZI	Mach Zender Interferometer
PD	Photo Diode
PDH	Pound Drever Hall
PRR	Pulse Repetition Rate
QE	Quantum Efficiency
S/C	Spacecraft
SPAD	Single Photon Avalanche Detector
SR	Special Relativity
TRT	Time Round Trip
ULE	Ultra Low Expansion (material)